PROCESSING AND CHARACTERIZATION OF CARBON FIBER REINFORCED SILICON CARBIDE (C/C-SiC) MATRIX COMPOSITES

A THESIS SUBMITTED TO
THE GRADUATE SCHOOL OF NATURAL AND APPLIED SCIENCES
OF
MIDDLE EAST TECHNICAL UNIVERSITY

BY

SİMGE TÜLBEZ

IN PARTIAL FULFILLMENT OF THE REQUIREMENTS
FOR
THE DEGREE OF MASTER OF SCIENCE
IN
METALLURGICAL AND MATERIALS ENGINEERING

JULY 2015

Approval of the thesis:

PROCESSING AND CHARACTERIZATION OF CARBON FIBER REINFORCED SILICON CARBIDE (C/C-SiC) MATRIX COMPOSITES

submitted by **SİMGE TÜLBEZ** in partial fulfillment of the requirements for the degree of **Master of Science in Metallurgical and Materials Engineering Department, Middle East Technical University** by,

Prof. Dr. Gülbin Dural Ünver _____
Dean, Graduate School of **Natural and Applied Science**

Prof. Dr. C. Hakan Gür _____
Head of Department, **Metallurgical and Materials Engineering**

Assoc. Prof. Dr. Arcan F. Dericioğlu _____
Supervisor, **Metallurgical and Materials Eng. Dept., METU**

Assoc. Prof. Dr. Ziya Esen _____
Co-supervisor, **Materials Science and Eng. Dept., Çankaya Uni.**

Examining Committee Members:

Prof. Dr. Cevdet Kaynak _____
Metallurgical and Materials Engineering Dept., METU

Assoc. Prof. Dr. Arcan F. Dericioğlu _____
Metallurgical and Materials Engineering Dept., METU

Prof. Dr. Caner Durucan _____
Metallurgical and Materials Engineering Dept., METU

Assoc. Prof. Dr. Ziya Esen _____
Materials Science and Eng. Dept., Çankaya Uni.

Assist. Prof. Dr. Mert Efe _____
Metallurgical and Materials Engineering Dept., METU

Date: 22.07.2015

I hereby declare that all information in this document has been obtained and presented in accordance with academic rules and ethical conduct. I also declare that, as required by these rules and conduct, I have fully cited and referenced all material and results that are not original to this work.

Name, Last name: Simge Tülbez

Signature :

ABSTRACT

PROCESSING AND CHARACTERIZATION OF CARBON FIBER REINFORCED SILICON CARBIDE (C/C-SiC) MATRIX COMPOSITES

Tülbez, Simge

M.S., Department of Metallurgical and Materials Engineering

Supervisor: Assoc. Prof. Dr. Arcan F. Dericioğlu

Co-Supervisor: Assoc. Prof. Dr. Ziya Esen

July 2015, 121 pages

The current study was undertaken to investigate the production and characterization of Carbon Fiber Reinforced Silicon Carbide (C/C-SiC) Matrix Composites. Liquid silicon infiltration (LSI) method was utilized to produce the C/C-SiC composites. Processing of these composites via LSI process composed of three main stages. CFRP production, pyrolysis and liquid silicon infiltration. Each production stage has an important effect on the efficiency of the LSI process, therefore present study investigates the effect of the corresponding parameters on the silicon infiltration process by comparing the properties of the C/C preforms and resulting C/C-SiC composites obtained by various processing conditions. Application of pyrolysis experiments at varying temperatures and TGA of the matrix material revealed that phenolic resin completely converts to turbostratic carbon above the dehydrogenization temperature of the cured phenolic resin. Moreover, increasing pyrolysis temperature

results in decreasing density, increasing porosity content and increasing crack opening of the C/C preform which directly affect the efficiency of the LSI process. Taking into consideration of all of the parameters directly affect the efficiency of the LSI process, comparison of density, microstructure and flexural strength of the resulting C/C-SiC composites revealed that pyrolysis should be applied at 1000 °C and following silicon infiltration of the C/C preforms should be conducted at 1650 °C under vacuum.

Impregnation of carbon nanotube (CNT) to the C/C preforms as matrix additive enhances the efficiency of liquid silicon infiltration resulting in composite having higher density and strength. Moreover, microcrystalline cellulose, CNT and nano-SiC powders added to the carbon derived from the phenolic resin enhances the SiC formation kinetics.

Keywords: Ceramic Matrix Composites, Microstructure, Pyrolysis, Liquid Silicon Infiltration, Matrix Additive.

ÖZ

KARBON FİBER TAKVİYELİ SİLİSYUM KARBÜR SERAMİK MATRİSLİ (C/C-SiC) KOMPOZİTLERİN ÜRETİMİ VE KARAKTERİZASYONU

Tülbez, Simge

Yüksel Lisans, Metalurji ve Malzeme Mühendisliği Bölümü

Tez Yöneticisi: Doç. Dr. Arcan F. Dericioğlu

Ortak Tez Yöneticisi: Doç. Dr. Ziya Esen

Temmuz 2015, 121 sayfa

Bu çalışma, Karbon Fiber Takviyeli Seramik Matrisli (C/C-SiC) Kompozitlerin üretimi ve karakterizasyonunu ele almıştır. C/C-SiC kompozitler sıvı silisyum emdirme (LSI) methodu ile üretilmiştir. Bu malzemelerin üretim prosesi elyaf takviyeli polimer matrisli kompozit (CFRP) üretimi ile başlar. Daha sonra sırasıyla piroliz ve sıvı silisyum emdirme işlemleri uygulanır. Her bir üretim aşamasının sıvı silisyum emdirme işleminin verimliliği üzerine büyük etkileri vardır, bu nedenle bu çalışma üretim aşamalarındaki değişken parametlerin karbon/karbon önkalıp ve nihai ürün olan C/C-SiC kompozitlere olan etkisini araştırmaktır. Farklı sıcaklıklarda uygulanan piroliz işlemi ve matris malzemesinin TGA sonuçlarına göre, fenolik reçine dehidrojenasyon sıcaklığının üstündeki sıcaklıklarda turbostratik karbona dönüşmektedir. Ayrıca artan piroliz sıcaklığıyla birlikte sıvı silisyum emdirme işleminin verimliliğini doğrudan etkileyen yoğunluğun azaldığı, gözenek miktarı ve çatlak boyutunun arttığı gözlenmiştir. Sıvı silisyum emdirme işleminin verimliliğini etkileyen tüm parametler göz önünde bulundurularak, üretilen C/C-SiC kompozitlerin

yoğunluk ve bükülme dayançları karşılaştırıldığında, piroliz 1000 °C, sıvı silisyum endirme işleminin ise 1650°C sıcaklık ve vakum altında uygulanmalıdır.

Karbon/karbon önkalıplara matris katkı malzemesi olarak karbon nanotüp (CNT) ekleyerek sıvı silisyum emdirilen kompozitlerin yoğunluk ve bükülme dayançlarında artış gözlenmiştir. Ayrıca, mikrokristalin selüloz, karbon nanotüp ve nano-SiC malzemeleri toz halinde fenolik reçineden elde edilen karbona eklendiğinde SiC oluşum kinetiğini hızlandırdığı gözlenmiştir.

Anahtar Kelimeler: Seramik Matris Kompozit, Mikroyapı, Piroliz, Sıvı Silisyum Emdirme, Matris Katkı Malzemesi.

To My Beloved Family

ACKNOWLEDGEMENTS

My sincere thanks goes to my remarkable supervisor Assoc. Prof. Dr. Arcan F. Dericioğlu for his continuous encouragement to begin my graduate study. I am indebted to him for leading me to the field of research and shaping my academic vision and background with his endless academic experience. His guidance helped me in all the time of my research. I would not have imagined writing this thesis without his motivation.

I would like to tell my sincere gratitude to Assoc. Prof. Dr. Ziya Esen for his guidance, support and patience throughout the whole time of this thesis study.

I am grateful to all the staff of the Department of Metallurgical and Materials Engineering, my previous and current lab mates Selen Gürbüz, Güney Daloğlu, Aylin Güneş, Sıla Ece Atabay and Güney Mert Bilgin who have been patient about my silly and aggressive mood. I am so lucky to have such a great lab mates.

I appreciate to my friends, Mertcan Başkan, Mustafa Can Kutsal, Ezgi Bütev, Erkan Aşık, Fatih Sıkan, Aylin Sevimli, Semih Pençereci and Ecem Cankurt for their helps, and never ending support.

I would like also to express my deep appreciation to my family; Şaziye, Mehmet and Tunay Tülbez who have been patient through thesis writing period.

I am also grateful to my sweet heart Gamze Karaman for her valuable support and encouragement. There may be distance, but I know you are not so far.

I specially thank to Damla Alptekin, Ali İbrahim Bostancıoğlu and Efecan Bozulu, for their understanding, endless support and their lovely friendship. I must also acknowledge ‘Semiconductor Group’ for sharing good and bad times through thesis writing period.

TABLE OF CONTENTS

LIST OF TABLES

TABLES

LIST OF FIGURES

FIGURES

CHAPTER 1

INTRODUCTION

Materials are the base for the technology and progress in technology requires advance in materials, especially for aerospace and military applications. In recent years, usage of carbon fiber-reinforced silicon carbide (C/C-SiC) matrix ceramic composites instead of monolithic ceramics and traditional refractory materials has increased considerably due to their superior properties. Because of their relatively low densities and high temperature mechanical properties as well as erosion and thermal shock resistance compared to their counterparts, C/C-SiC ceramic composites are being used as high temperature structural materials in applications such as components in thrust providing parts of rocket/missile systems and thermal protection systems of the nose cap of the reentering space crafts. Besides these practices, C/C-SiC composites are also utilized in high performance brake pad and clutch applications. Considering the great combinations of excellent wear resistance and lightweight, high and stable coefficient of friction, it is not surprising that C/C-SiC composites have been used as a first choice for friction applications.

By improving their manufacturing processes, these existing application areas may be expanded, and novel application areas could be aroused in the near future. Besides the possible improvements in manufacturing techniques, increase in material properties such as mechanical strength and environmental stability which directly affect the material's performance, by reliable, repeatable and cost feasible methods must be considered. Among the currently available techniques, liquid silicon infiltration (LSI) method was chosen for the production of C/C-SiC composites in this study considering

all these requirements. The basic advantage of the LSI process is that it leads to near net shaping composite manufacturing providing lower fabrication time and cost.

Processing of the C/C-SiC composites via LSI method starts with the production of carbon fiber reinforced polymer matrix (CFRP) composite part. This part is pyrolized in a high temperature furnace under inert atmopshere to burn out its polymeric binder and to convert its polymer matrix into a carbon resulting in a porous C/C preform. In the following stage, carbon matrix is converted into SiC matrix by melt infiltration of liquid silicon and formation of the ceramic end product termed as C/C-SiC composite. It can be stated that the properties of the final composite depend on both CFRP and C/C preform characteristics, the raw materials used together with the applied processing steps and their parameters. Although extensive research has been carried out on the production of C/C-SiC composites, no detailed study is available which adequately covers the effects of the production step parameters on the properties of the final composite.

In this regard, the present study firstly investigates the effect of different pyrolysis temperatures on the microstructure and resulting properties of the C/C preforms obtained from the initial CFRP. Liquid silicon infiltrates into the C/C preform via capillary forces, therefore, microstructure and properties of C/C preform have an important effect on the subsequent silicon infiltration process. Additionally, apart from the characteristics of the C/C preform, understanding the transformation of the polymer matrix into carbon during pyrolysis is very important, and hence this study also covers the pyrolysis behavior of the phenolic resin.

To the best of our knowledge, the effect of temperature and protective atmosphere utilized during the LSI process on the characteristics of the resulting C/C-SiC composites has not been reported in literature in a comprehensive manner. In this regard, present study discusses the effect of these parameters on the densification behavior by comparing the properties of the C/C-SiC composites obtained by various processing conditions. Therefore, optimum LSI parameters were investigated through the production of C/C-SiC composites in order to obtain final products with high density and enhanced strength.

Moreover, as a novel contribution to the literature, in order to increase the efficiency of the liquid silicon infiltration, matrix additives such as carbon nanotubes (CNT) and nano-SiC particles were impragnated into C/C preforms, and effect of usage of these additives on the characteristics of LSI processed C/C-SiC composites were investigated throughout this study. Finally, alternative matrix material combinations in powder form were let to react with liquid silicon using predetermined optimum process parameters to get insight about the reactivity of the candidate matrix material.

This thesis consists of five main chapters that give information about the topics covered in the study. Chapter 2 is subdivided into various parts to present a detailed background about the main components of the study. First of all, properties of C/C-SiC composites and the requirements for engineering applications as well as their comparison with other structural materials were explained, basically. Additionally, production techniques of C/C-SiC composites, their advantages and disadvantages were discussed, where specific attention was paid to the liquid silicon infiltration method. Apart from these, application areas of C/C-SiC composites and properties required by the applications were also presented in Chapter 2. In Chapter 3, materials used in the current study and details of liquid silicon infiltration method utilized in the production of the C/C-SiC composites were explained in detail. Moreover, this chapter also contained the brief information about characterization techniques used in the current study. Chapter 4 presents the experimental results which include preliminary pyrolysis experiments using phenolic resin in powder form conducted prior to the pyrolysis of CFRP composites containing both carbon fiber fabrics and resin matrix in order to determine the effect of pyrolysis temperature on the conversion of the phenolic polymer matrix into carbon along with the results of the experiments conducted to understand the optimum liquid silicon infiltration parameters. Furthermore, results and discussions on the effect of both nano-SiC powder and carbon nano tube usage as matrix additives in the C/C preforms on the silicon infiltration behavior was presented. Effect of using alternative matrix material combinations on the reaction and C/C-SiC composite formation kinetics has been also discussed in Chapter 4. Finally, conclusions together with the future works are given in Chapter 5.

CHAPTER 2

“

LITERATURE REVIEW

In this chapter, basically general information about carbon fiber reinforced silicon carbide matrix composites (C/C-SiC) and applications areas will be presented, and their properties will be compared with other structural materials as well. Additionally, production techniques of C/C-SiC composites will be introduced by focusing on liquid silicon infiltration methods.

2.1 Composite Materials

Composite materials are manufactured to obtain a new material, which has characteristics different from the individual components, by combining physical and chemical properties of each component. Engineering materials should be light, strong, stiff, tough, and have high wear and corrosion resistance. All of the desired properties cannot be met by metals, ceramics and polymers in their monolithic form. Therefore, the solution is the production of composite materials. Composite era is started in 1960’s; however, this was not a new idea because composite materials was used first by nature and then, by ancient engineers. For example, wood is composed of lignin and cellulose fibers; bone contains hydroxyl apatite and collagen fibers and straw brick includes mud and straw pieces.

For the formation of composite material at least two different constituents must exist. The criteria for the engineering point of view, both constituents have to present in reasonable amounts (> 5%); otherwise there will be no significant improvement in material property. Additionally, constituent phases must have different properties to get properties that are different from that of each constituent. Accordingly, the composite material must be produced by mixing and combining constituents,

otherwise, in the case of the reaction and phase transformation, there will be no composite material formation.

Composite materials contain mainly three constituents, namely, matrix, reinforcement material and interface (between matrix and reinforcement). Continuous matrix material is the primary phase and often presents greater in quantity. Classification of the composites is done according to type of matrix material as polymer matrix composites (PMC), ceramic matrix composites (CMC) and metal matrix composites (MMC). Reinforcement material, on the other hand, is the secondary phase that may present in one or more than one type in the form of fibrous and/or particulate shape. It is usually harder, stronger and stiffer than the matrix and thus, enhances mechanical or other properties of the matrix phase. The third constituent, the interface region or interphase, is present between matrix and reinforcement and transfers the applied load from matrix to reinforcement.

2.2 Ceramic Matrix Composites (CMC)

Engineering and industrial applications require advanced materials that must have high temperature resistance, stable surfaces, dimensional stability, wear and corrosion resistance. It is known that ceramics have high temperature resistance and better high temperature mechanical properties than those of metals and polymers [1]. Monolitic ceramics (Al_2O_3 , Si_3N_4 , SiC , ZrO_2), ceramic coatings like thermal barrier coatings (TBC), environmental barrier coatings (EBC) and ceramic matrix composites are some of the examples for high temperature ceramic materials that can be classified as advanced materials. Although monolithic ceramics possess desirable properties such as high strength, high temperature resistance, chemical inertness, wear and erosion resistance and low density, they do not show any plasticity and exhibits brittle behavior under thermal and mechanical loading conditions. In order to overcome this drawback, reinforcements in the form of fibers, particulates and whiskers are used to increase toughness of the ceramic materials. CMC have been developed to obtain a damage tolerant quasi-ductile fracture behavior and to maintain all other advantages of monolithic ceramics at elevated temperature conditions. Comparison of stress-strain

curve in monolithic ceramics and ceramic matrix composites is shown in Figure 2.1. As area under the stress-strain curve is directly related to the toughness of the material, it is clear that high toughness in a ceramic based material can be obtained by manufacturing ceramic matrix composites instead of monolithic ceramics.

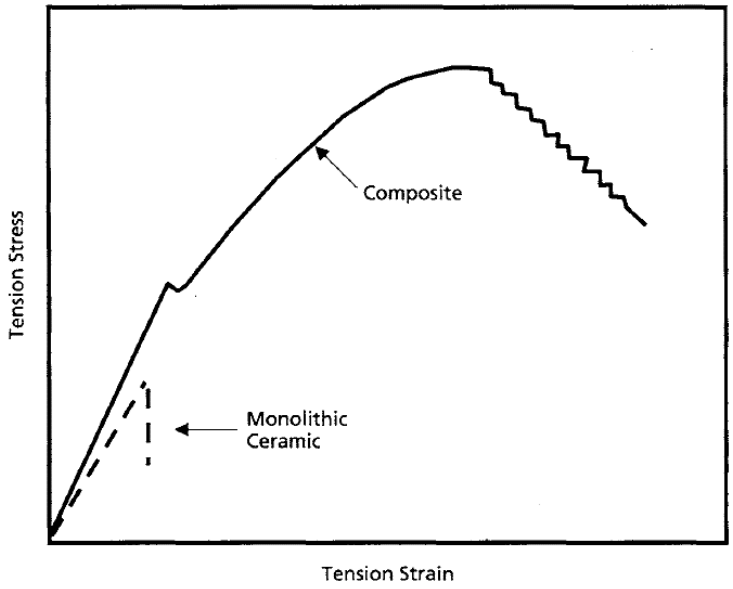

Figure 2. 1 Stress-strain curves for monolithic ceramics and ceramic matrix composites [2].

There are many different subgroups of CMC which are designated in terms of fiber and matrix materials that are separated by a slash. For example, C/SiC is a ceramic matrix composite that is composed of carbon fiber and silicon carbide matrix. Reinforcement materials for ceramic matrix composites may be oxide fibers such as alumina, mullite and silica or titanium diboride, silicon nitride as well as the non-oxide carbon and silicon carbide fibers. Matrix materials, on the other hand, contain glasses, glass-ceramics and ceramics such as carbon, silicon carbide, silicon nitride, aluminides and oxides. Generally oxide fibers in the composites are combined with oxide matrices

and likewise, non-oxide fibers with non-oxide matrices. C/C, C/SiC, C/C-SiC, SiC/SiC and Ox/Ox, (‘’Ox’’ represents one of the oxide materials) are some of the examples of CMC’s.

2.3 C/C-SiC Composite

Compared to other engineering materials, non-oxide fiber reinforced ceramic matrix composites present the highest specific strength (Figure 2.2) at high temperatures, therefore, C/SiC composites are essential materials for lightweight structures and components that are exposed to high mechanical and thermal loads. C/C-SiC composites are widely preferred in structural parts instead of monolithic ceramics due to their superior mechanical properties, oxidation and wear resistance, and pseudo-ductility [3] [4].

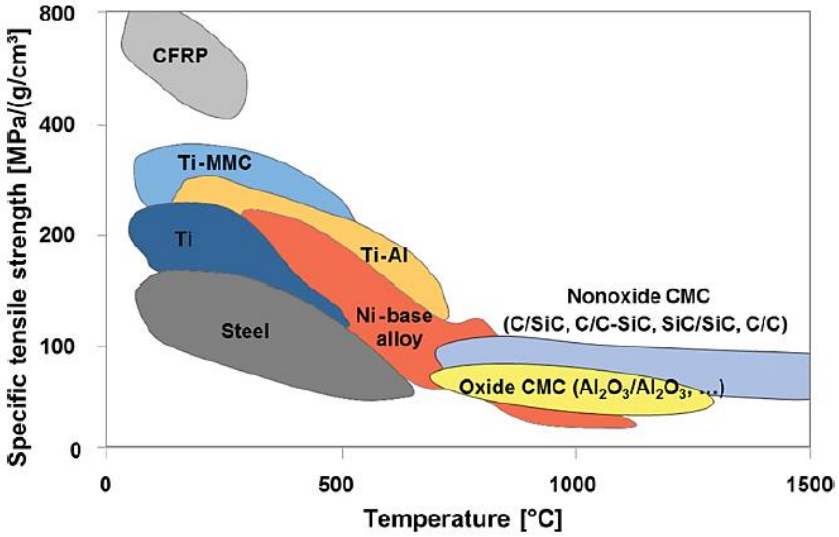

Figure 2. 2 Specific strength of materials as a function of temperature [5].

Although reinforcement materials in PMC’s increase the strength and stiffness of the composite, carbon reinforcement in C/SiC composites results in only slight increment of strength or it may even cause a decrease in strength in melt infiltrated components. However, fibers contribute the toughness increment by energy dissipating mechanisms

such as crack deflection, debonding, fiber bridging and fiber pullout (Figure 2.3) [6] [7].

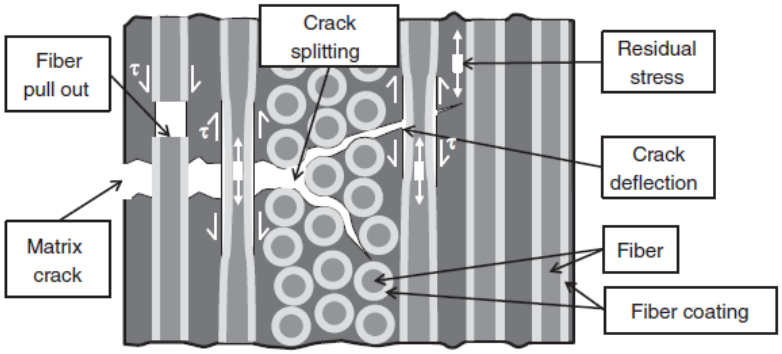

Figure 2. 3 Schematic illustration of energy dissipating mechanism in CMC [7].

Advancing cracks that are bridged by fibers, Figure 2.4, makes composites less brittle and damage tolerant by resulting in high tensile strength strength (σ_{UTS} > 3500 MPa) and elongation at failure (ε_f > 1.5%), which are significantly higher than that of bulk ceramics (SiC: σ_{UTS} = 400 MPa, ε_f < 0.05%).

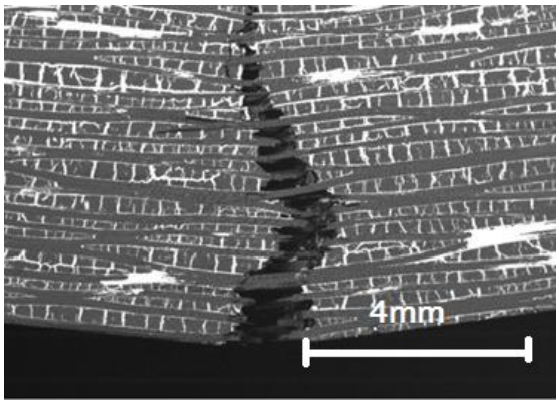

Figure 2. 4 Quasi-ductile fracture behavior of C/C-SiC showing crack deflection, fiber bridging and pull out of fibers and C/C bundles.

2.3.1 Composition and Microstructure

C/C-SiC composites are composed of carbon fibers and β-SiC matrix and depending on the manufacturing techniques, residual carbon matrix and residual silicon may exist. Composite composition and microstructure depend on the manufacturing methods, manufacturing atmosphere, composition of the raw materials, and type, quantity and arrangement of fiber preform. For example, CVI (Chemical vapor infiltration) method leads to stoichiometric SiC formation, whereas in the PIP (Polymer infiltration and pyrolysis) process conversion of the matrix into SiC depends on preceramic precursor. Generally, CVI and PIP result in C/SiC composites containing carbon fibers embedded in SiC matrix, whereas LSI (Liquid silicon infiltration) method leads to C/C-SiC materials in which the carbon fibers primarily are in C matrix, leading to dense C/C bundles embedded in SiC or SiC – residual Si mixture, Figure 2.5.

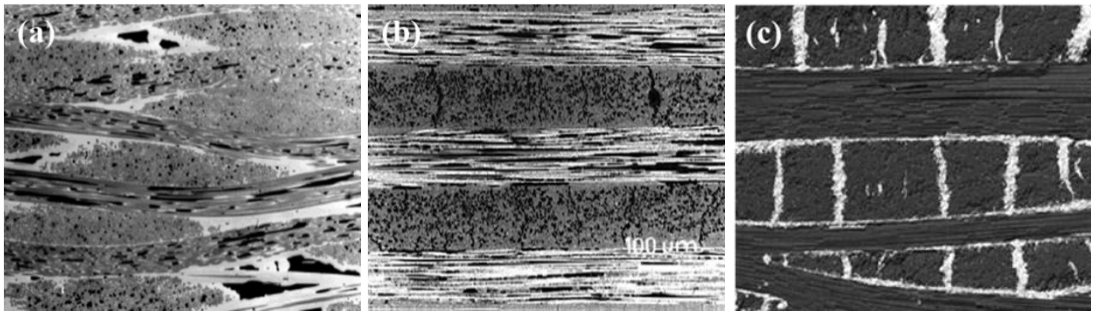

Figure 2. 5 Typical microstructures of carbon fiber reinforced SiC matrix composites (a) C/SiC composite manufactured via CVI containing carbon fiber filaments (dark gray), SiC matrix (light gray) and porosity (dark), (b) C/SiC material manufactured by PIP, (c) C/C-SiC composite manufactured by LSI containing dense C/C bundles (dark gray) embedded in Si-SiC matrix (light gray).

Open porosity content of the C/C-SiC composites also depends on method utilized during manufacturing. Composites that are produced by CVI method have usually residual porosity contents around 8-12 %, whereas in PIP method porosity is decreased

down to 6-10%. On the other hand, in LSI process it is possible to obtain C/C-SiC composites with open porosity contents as low as 1-4 %. As mentioned C/SiC composites are low density (1.8–2.4 g/cm^3) materials with slightly higher densities than CFRP (1.5 g/cm^3). For example, LSI composite, which contains approximately 60 vol. % carbon fiber and residual carbon matrix, have low density nearly 1.9 g/cm^3 with low amount of open porosity content.

2.3.2 Mechanical and Thermal Properties

Mechanical and thermal properties of C/SiC composites are directly related with microstructure of the composite and properties of the raw materials used in the composite (Table 2.1). Depending on the fiber architecture, C/SiC composites may behave as highly anisotropic material, therefore, simple rule of mixture may not work during calculation of the strength, thermal conductivity and co-efficient of thermal expansion (CTE). Mechanical properties not only depends on manufacturing method of the composite but also are related with type, volume content and architecture of the fibers.

Table 2. 1 Typical Properties of C Fibers, SiC and Silicon.

Property	**Carbon Fibers**	**SiC**	**Si**
Density (g/cm^3)	1.76	3.21	2.33-2.5
Tensile Strength (MPa)	3950	-	113
Strain to failure (%)	1.7	-	-
Young's Modulus (GPa)	238	461	112
Compression Strength (MPa)	-	-	-
Flexural Strength (MPa)	-	415-575	300
CTE (10^{-6} K^{-1})	-0.1	2.2-4.0	2.6
Thermal Conductivity W/(m.K)	10	300-63	156
T_{melt}/T_{max}	-	2700	1414

The mechanical properties of C/C-SiC composites manufactured by various methods are given in Table 2.2. As seen in Table 2.2, composites that are produced via LSI process have lower mechanical properties than that of composites manufactured by CVI and PIP methods. In CVI and PIP methods, applied fiber coatings minimize the reaction between fiber and the matrix, whereas in LSI some amount of carbon fibers may be converted to SiC as a result of reaction between fibers and the matrix. Since fiber content is an important parameter for mechanical strength, a decrease in its content as a result of such reactions affects the final composite behavior.

Table 2. 2 Mechanical and Thermal properties of C/SiC composites manufactured by various methods [8-11].

Property	**CVI**	**PIP**	**MI**
Fiber Architecture	2D fabrics	2D fabrics	2D fabrics
Fiber Content (vol%)	42-47	50	60
Density (g/cm^3)	2.1-2.2	1.8	>1.8
Porosity	10-15	8	2
Tensile Strength (MPa)	300-320	260	110
Strain to failure (%)	0.6-0.9	0.53	0.25-0.3
Young's Modulus (GPa)	90-100	110	50-55
Flexural Strength (MPa)	450-500	240	80-140
Thermal Conductivity (W/m.K)	14	14	28-33
$CTE_{\perp}$ (10^{-6} K^{-1})	5	5	6-6.5
$CTE_{\parallel}$ (10^{-6} K^{-1})	3	2	1.0-1.5

2.3.3 Oxidation and Wear Resistance

Although under inert conditions C/C composites are thermally stable temperatures up to 2700 °C, in an oxidizing environment, they may lose their mechanical strength due to oxidation of carbon fibers and carbon matrix. In C/C-SiC composites, conversion

of carbon matrix into silicon carbide results in a good oxygen barrier due to reduction of the carbon surface. Therefore, due to this barrier layer C/C-SiC composites have lower mass loss values than C/C composites at elevated temperatures.

Moreover, C/C-SiC composites present superior tribological properties and have high thermal stabilities and low specific masses. Monolithic SiC has low wear rates and high friction coefficient. However, especially for friction applications these monolithic ceramics show catastrophic behavior due to their high brittleness. Therefore, in such applications monolithic ceramics are replaced by their C/SiC composite counterparts, which contain carbon fibers with a high damage tolerance and SiC matrix with stable friction coefficient.

2.4 Processing Routes of C/C-SiC Composites

In order to obtain C/C-SiC composite materials carbon reinforcement fibers must be embedded to SiC ceramic matrix; however, production of the C/C-SiC composites is not a single step technique. Firstly carbon fibers are embedded into preforms then the preform matrix is converted to SiC by different methods. In nature, SiC (Moissanite) is a rare material and it can be found in meteorites and volcanic kimberlite [12]. On the contrary, man-made SiC which is also called carborondum, can be manufactured by CVD, liquid phase sintering (LPSSiC), or reaction bonding (RBSiC) [13]. For the manufacture of C/C-SiC materials, the processes based on CVD, pyrolysis of preceramic polymers, and reaction bonding have been adapted for the manufacturing of SiC matrices in fibrous preforms, leading to three different manufacturing methods such as polymer infiltration and pyrolysis, chemical vapor infiltration and liquid silicon infiltration, Figure 2.6.

All of the C/C-SiC composite manufacturing processes contain three main steps:

1- Production of the carbon fiber preform,
2- Building up a weak fiber/matrix interface,
3- Production of SiC matrix.

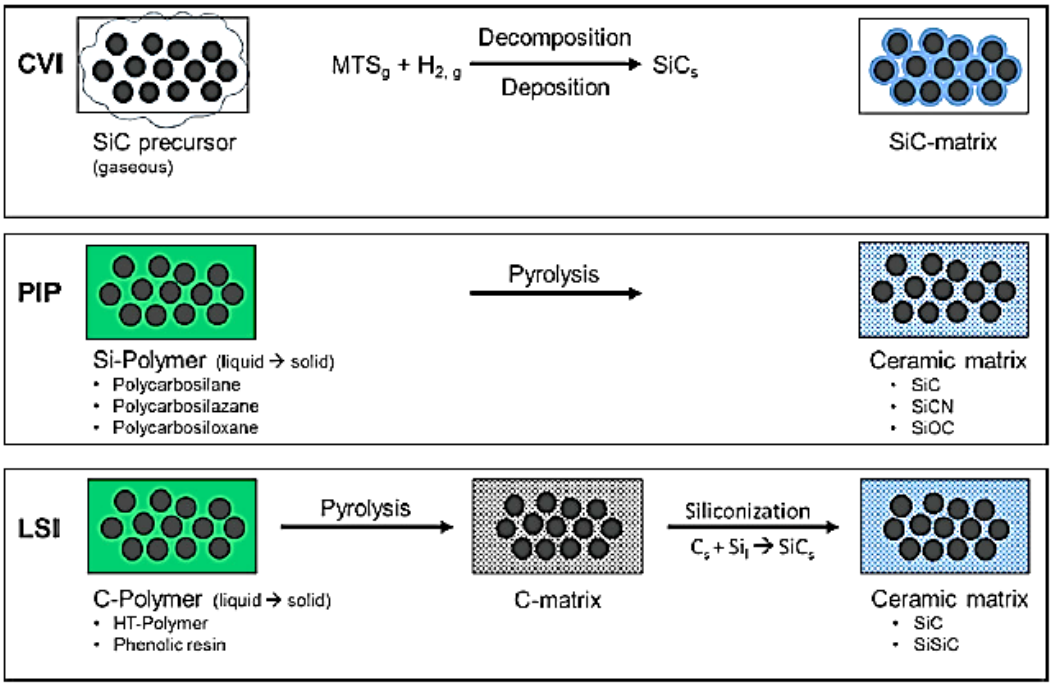

Figure 2. 6 Schematic overview of the different methods used for manufacturing of C/C-SiC Composites.

2.4.1 Polymer Infiltration and Pyrolysis (PIP)

Polymer infiltration and pyrolysis (PIP) process can be defined as the conversion of the preceramic precursor (organometallic compounds) into ceramic matrix via thermal decomposition [14]. It is known that these silicon based preceramic precursors such as polycarbosilanes, polymethylsilane and allhydridopolycarbosilane have been used for the production of bulk ceramics, ceramic matrices, ceramic fibers and coatings [15]. PIP process contains four different steps:

i. Deposition of fiber coating,
ii. Manufacture of CFRP preform,
iii. Pyrolysis of the CFRP preform,
iv. Densification via repeated polymer infiltration and pyrolysis (Figure 2.7).

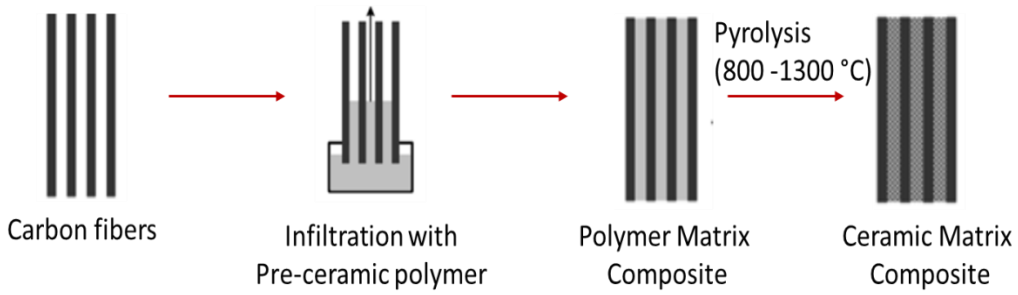

Figure 2. 7 Steps of polymer infiltration and pyrolysis process.

Firstly, in order to achieve weak fiber-matrix interphase the carbon fiber or fiber preforms are coated via continuous or discontinuous CVD or CVI processes. Thickness of the pyrolytic carbon (pyC) layer may change between 0.1–0.3 μm. The second step is manufacturing of a CFRP preform via wet filament winding, vacuum assisted polymer (VAP), or resin transfer molding (RTM). These techniques are very common for ordinary polymer matrix composites; however, usage of the preceramic precursors necessitates higher curing temperatures and inert atmosphere for elimination of oxidation during curing [16]. In the third step, CFRP preform is pyrolyzed in inert gas atmosphere. During pyrolysis, organic compounds are eliminated, the network of the polymer is decomposed and it turns into amorphous ceramic matrix. The percentage of the resultant ceramic depends on the type of preceramic polymer utilized and the pyrolysis atmosphere. The last step is the ceramization by pyrolysis which is applied at high temperature under vacuum or in inert atmosphere. Re-infiltration and pyrolysis steps are done 5-8 times in order to decrease residual porosity and increase the density of the matrix material and to obtain crystalline SiC [17], Figure 2.8.

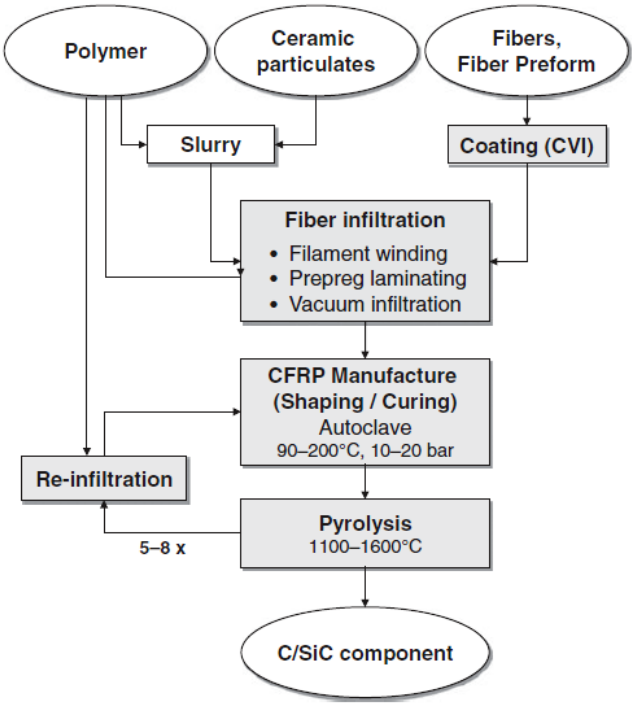

Figure 2. 8 Polymer infiltration and pyrolysis process [5].

Possibility of controllable matrix build-up and elimination of excess silicon are the main advantages of the PIP process. Additionally, pyrolysis temperature for conversion of the matrix is low, the fibers are not damaged during densification, therefore, high mechanical composite properties may be obtained. It is also possible to produce large sized and complex as well as thin walled, high temperature structures by this way. Compared to multistage CVI process, it is simple one-step process and more feasible economically. However, high shrinkage and low SiC yield may be observed due to conversion of the pre-ceramic polymer material into the ceramic matrix material. Moreover, because of high number of re-infiltration and pyrolysis steps matrix cracking may occur in the system.

2.4.2 Chemical Vapor Infiltration (CVI)

This manufacturing technique is very similar to chemical vapor deposition (CVD). It starts with converting the fibers into desired shape, called preform. In an infiltration chamber fiber preform is subjected to gas mixture. In order to prevent possible chemical reaction between matrix material and the fiber and to obtain a weak interphase between the fibers and the matrix, fiber coating is necessary. CH_4 gas is introduced into the preform to obtain carbon as the interlayer between fiber and the matrix. Pyrolytic carbon thickness in the process must be in the range of 0.1 -0.3 μm. In order to deposit SiC as a matrix material, a gas mixture of hydrogen and methyl - trichloro - silan) is exposed to carbon fiber preform in an infiltration furnace at temperatures approximately 800-1000 °C under the pressure of 1 kPa [18], Figure 2.9.

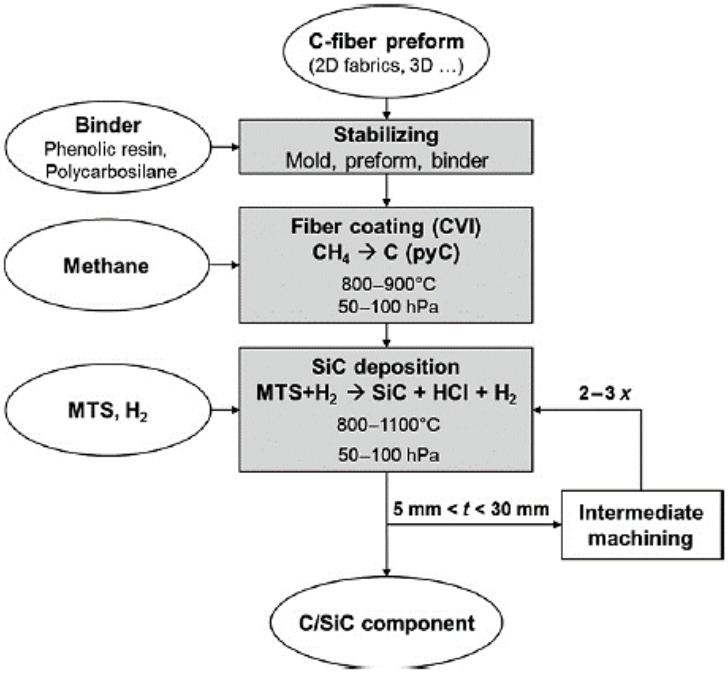

Figure 2. 9 Schematic view of CVI process [19].

Chemistry of the process is described by the following reaction:

$$CH_3\,SiCl_3\,(g) + H_2 \rightarrow SiC\,(s) + 3\,HCl$$

Hydrogen acts as a catalyst and at the end of the process beta-SiC is produced. To obtain the better quality of SiC matrix three parameters, namely, pressure, temperature and volume ratio of hydrogen and MTS have to be taken into consideration [19].
CVI method is suitable to produce not only for the simple plates but also for very large and complex structure since it is possible to form a carbon fiber preform in complex shape. For example, one of the largest C/SiC components in the world was manufactured by CVI method. This is the body flat for X38 with external dimensions of 1.5 x 1.5 x 0.15 m^3, Figure 2.10 [20]. For the industrial manufacture of C/SiC components, CVI is used by Herakles, France, MT Aerospace (MT), Germany, General Electric (GE), Goodrich (now UTC), and Surface Transforms PLC, UK [5].

Figure 2. 10 C/ SiC structures for X38 Spacecraft body flap (2 flaps, each 1600 mm x 1400 mm x 150 mm, t= 5-15 mm, m= 68 kg.

In the process, use of low temperature and pressure conditions gives less damage to fibers and thus, complex shapes can be produced. Moreover, by controlling the composition of the gases, pure and uniform fine grained SiC matrix which directly

affects the mechanical properties of the composite can be obtained. The main drawback of the CVI process is that slow matrix deposition rate which leads long cycle times for densification process. Moreover this long cycle times gives rise to high manufacturing cost.

2.4.3 Liquid Silicon Infiltration (LSI) or Melt Infiltration Process (MI)

The liquid silicon infiltration process, which is one of the manufacturing process of C/C-SiC composites, is applied by infiltration of liquid silicon into the porous C/C preform to obtain C/C-SiC composite. The oxidation and wear resistant of the C/C preform is increased by silicon infiltration which results in SiC/C zone [21]. Considering the disadvantages of polymer infiltration process and reaction bonding of Si-SiC materials, liquid silicon infiltration process is derived from both processes. It has been used since the 1970s and it was developed by German Aerospace Research Establishment [22]. Nowadays, MI-derived C/C-SiC materials produced via liquid silicon infiltration are industrially manufactured by Brembo SGL Carbon Ceramic Brakes (BSCCB), SGL Group (SGL), Schunk Kohlenstofftechnik GmbH (SKT),Ultramet, and Nammo Raufoss AS (Nammo). All of them have licensed the LSI process from DLR, Germany, to produce C/C-SiC friction pads, rocket motor components and other structural parts, respectively [18].

Processing of C/C-SiC composites via liquid silicon infiltration contains three main steps (Figure 2.11):

i. Production of carbon fiber reinforced polymer matrix composites (CFRP),
ii. Pyrolysis of CRRP to C/C preform,
iii. Liquid silicon infiltration of C/C preform.

Composites manufactured by LSI contain lower amount of porosities which results in higher shear strength and thermal conductivity. It is a near net shaping process and its main advantage is its in-situ joining capability and the possibility of manufacturing large and complex shape components with the help of near net shaping. Moreover, this

process has lower component fabrication time and thus, manufacturing cost is reduced considerably compared to other manufacturing techniques [23].

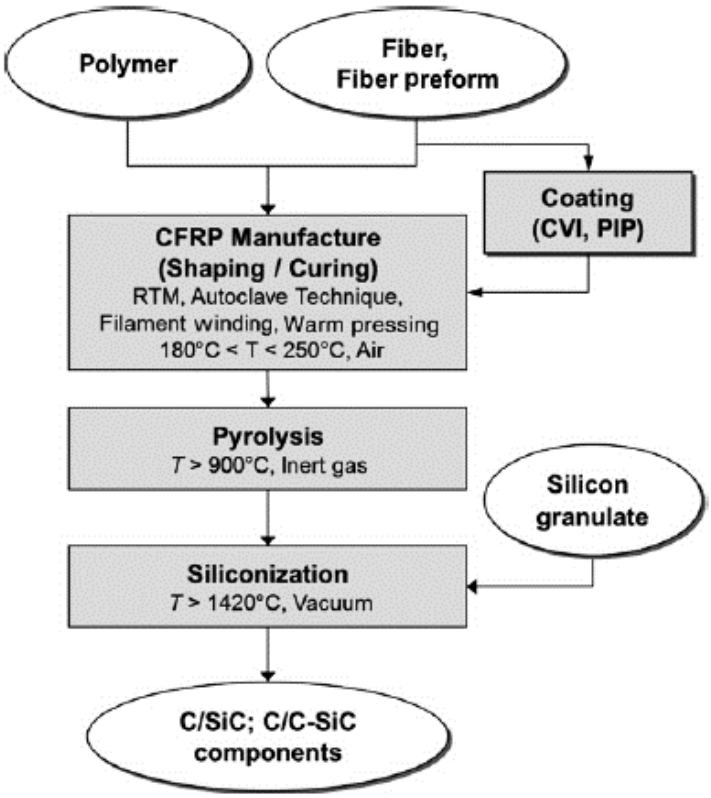

Figure 2. 11 Schematic overview of the manufacture of C/SiC materials via LSI.

2.4.3.1 Manufacture of CFRP Composites

CFRP composites are made by combining of reinforcement carbon fibers with thermoset or thermoplastic polymers as a matrix material. Resin transfer molding (RTM), autoclave technique, warm pressing and wet filament winding are the commonly used methods to produce CFRP composites [24].

In the RTM process, dry preforms stacked as 2D fabrics or 1D cross plies are pressure infiltrated with the liquid precursor. In order to avoid fiber displacement and to obtain better infiltration properties, the viscosity of the matrix material and the infiltration

pressure should be as low as possible. Therefore, infiltration pressure may change between 0.03–0.08 MPa and the temperature must be nearly 200◦C for the curing of the matrix material effectively [25].

The autoclave technique is used for the manufacture of large, complex-shaped CFRP preforms, for example, for nose caps of spacecraft [24]. Prepregs that are composed of phenolic precursors and 2D fabrics are used as raw materials. Firstly, the prepreg plies are placed into a mold with predefined fiber orientations. Then, the laminate is covered by an airtight, flexible foil and is consolidated by applying vacuum between the mold and the foil. Finally, prepregs are cured at a maximum pressure and temperature of about 1 MPa and 200◦C, respectively [26].

Warm pressing is used for manufacturing of very complex-shaped CFRP preforms, based on randomly oriented short fibers, such as internally ventilated brake discs or flat plates based on 2D fabric prepregs [27]. As a matrix material phenolic resins in liquid or powder form can be used. Moreover, similar to autoclave technique, prepregs that are composed of phenolic precursors and 2D fabrics can be used. Pressure and temperature in the process may change between 2–5 MPa and 200-250 ◦C, respectively [28].

Wet filament winding, on the other hand, is generally preferred for manufacturing of rotationally symmetric compounds such as tubes, integral combustion chambers and nozzle extensions [29]. Fibers are infiltrated with the phenolic precursor and wound on a turning mandrel in order to reach predefined angle or fiber orientation. After finishing the filament-winding process, curing is applied at ambient pressure or consolidation is done by a vacuum bag [30].

2.4.3.2 Pyrolysis of CFRP to C/C preform

The second step in the production of C/C-SiC composites involves converting the polymer matrix into amorphous carbon that will react with the liquid silicon at the final step. Polymer matrix to carbon conversion is applied by pyrolysis of CFRP under the inert atmosphere at temperatures above 900 ◦C. The pyrolysis of CFRP is the most

critical step for the densification of the C/C preforms because conversion of the polymer matrix into amorphous carbon may result in evolution of gas products, mass loss of about 36–40% and a volume contraction of about 50–60%. Since the carbon fibers have higher thermal stability than the matrix material the shape of the CFRP does not change considerably. However, internal stresses in the CFRP and tension stresses in the matrix give rise to formation of cracks, (Figure 2.12).

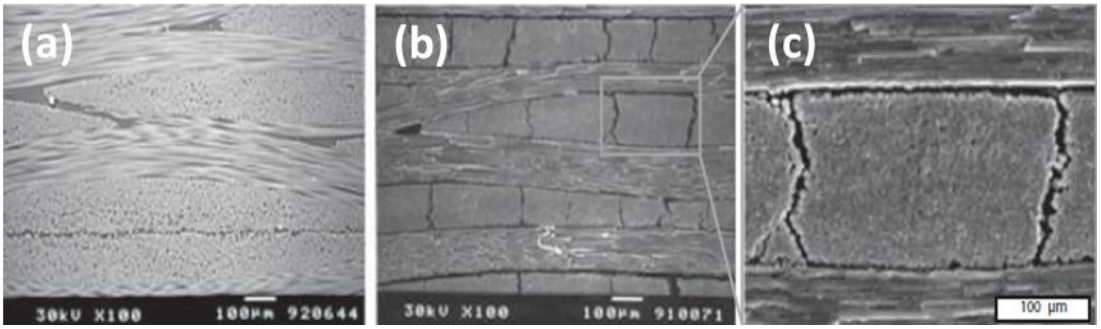

Figure 2. 12 SEM micrographs of CFRP composites (a) before pyrolysis, (b) and (c) after pyrolysis.

When polymers are subjected to heat under an inert atmosphere, reactions occurs within the C/C chain and they lose their non-carbon species by the formation of gaseous products and finally, they change to form carbon. This process is called carbonization. Intermolecular reactions during the process may take place in three ways:

i) The chains may decompose into small molecules and evolving gas products leave some carbon behind. An example of this type of polymer is polyethylene.

ii) The chains may be separated to aromatic lamellae and the material transforms to the plastic state from spherulitic liquid crystals. The transformation results with a crystalline anisotropic coke. An example of this condition is poly-vinly chloride.

iii) The chains do not decompose into smaller molecules, besides, coalesce with other chains. There is no condition for forming plastic state. The final char's condition about being isotropic or anisotropic depends on type of precursor material.

Carbon is produced only from cases (ii) and (iii) that have very different properties. In the case of the CFRP pyrolysis there must be no plastic state formation, therefore, case (iii) is operative during the process. Phenol resins and other furfuryalcohol-polyimide, polyphenylen- and polyphenylenoxide-based resins can be used for this type of carbonization [31]. When polymers belong to type (iii), their pyrolysis contains four main steps as follows:

i) The Precarbonization stage (Post Curing): Monomers and solvents begin to remove and additional crosslinking takes place. At the end of the precarbonization stage material is still polymeric.

ii) The carbonization stage (Main pyrolysis): Polymer matrix is mainly converted to carbon in this stage. Rapid weight loss and high shrinkage give rise to "ladder structure", where the carbon domains are linked by hydrogen bonds.

iii) Dehydrogenization: At the end of the main pyrolysis there exist one hydrogen atom for every two carbon atoms. Removing remaining hydrogen atoms results in linearly conjugated carbon atoms, in other words, turbostratic carbon structure is obtained.

iv) Annealing (Defect healing): Pyrolysis temperatures above 1200 ◦C mainly cause removal of crystal defects. The material stays hard, amorphous and turbostratic even after pyrolysed at 3000 ◦C [31-34].

Nature of the carbonization depends on the chemical structure of the matrix material. Thermal decomposition rate of the components depends on its size, free radical formation capability and the presence of the substituents in aromatic rings.

2.4.3.3 Silicon Infiltration and SiC Ceramic Matrix Build-up

In the last process step, C/C preform is infiltrated with molten silicon, at temperatures above the melting point of Si (1420 °C), Table 2.3. In order to obtain effective silicon infiltration and to prevent oxidation, infiltration is applied under vacuum by the help of capillary forces. During infiltration, silicon reacts with the carbon present in the preform and forms SiC matrix. The chemical reaction between solid carbon and molten silicon is an exothermic reaction and shown as follows:

$$Si(l) + C(s) \rightarrow SiC(s) \quad [\Delta H = -68\ kJ/mol]\ [35]$$

Table 2. 3 Physical properties of silicon.

Physical Properties	**Unit**	**Value**
Density, ρ	g/ cm^3	2.33 – 2.34 (20 ° C)
Melting temperature, T_m	°C	1414 – 1420
Surface Stress, σ	Nm^{-1}	0.72 – 0.75 (1550 ° C in Vacuum)
Wetting Angle, θ	Degrees,°	30 – 41 (compared to SiC in Vacuum)
Dynamic Viscosity, η	10^{-4} Pas	5.10 – 7.65 (1440 ° C)

Liquid silicon has low viscosity comparable to water, good wettability to carbon and SiC and high surface tension, therefore, a fast infiltration even into large C/C preforms is possible. The infiltration behavior can be analyzed by the capillary theory of Gibb and Darcy's law, which explains the motion of the liquid silicon in a capillary by considering the effects of the capillary and reaction forces, initial porosity and capillary diameter [36]. Analytical calculation models for infiltration of silicon based on Navier Stokes Equation [37] indicate that infiltration time is in the range of minutes for an infiltration height up to 500 mm (Figure 2.13). It can be said that less time is necessary for the infiltration and the complex shapes that contain sufficient amount of pores and microcracks may also be infiltrated.

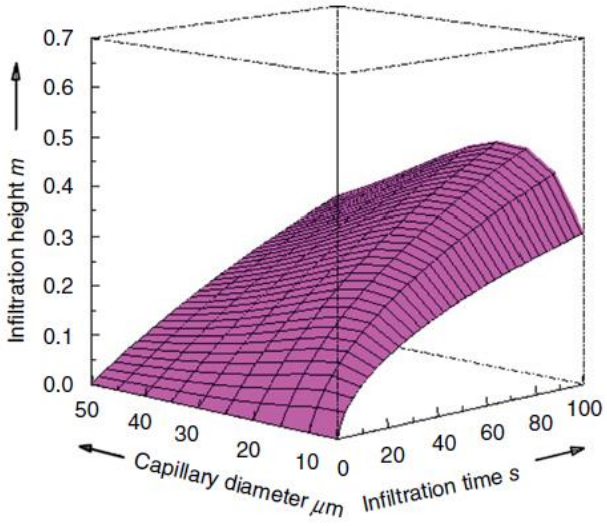

Figure 2. 13 Calculated infiltration height of a single capillary in a C/C preform in dependence of infiltration time and capillary diameter [37].

At the same time of infiltration, silicon reacts with the carbon in the contact areas and forms the SiC matrix. Infiltration may close completely the open pores and micro cracks of C/C composite and form dense C/C-SiC composite because transformation of carbon matrix to SiC ceramic matrix causes a volume increase of 91% that ensures the complete filling of the pores and micro cracks [37]. Depending on the microstructure, crack size and porosity content of the C/C preform infiltrated silicon may not be completely transformed to SiC, therefore, unreacted residual silicon may remain in the microstructure.

Liquid silicon infiltration is known as a near net shape technique because both pyrolysis and infiltration steps have low contraction rates, in other words, there is no significant change in size and geometry of the component.

2.4.3.3.1 Mechanism of SiC Formation during Siliconization

Silicon carbide formation is a high temperature solid-liquid reaction that contains two different materials, one of them has higher melting point than the other, therefore, chemical reaction takes place at the interfacial region [38]. At the end of the reaction, the final ceramic material has higher melting point than that of both reactants. Similarly, refractory carbides and borides can be obtained by these reactions. For SiC formation, reaction between carbon which has a sublimation temperature greater than 3000 °C and silicon whose melting temperature is 1414 °C takes place [39].

For the infiltration process, there are two different mechanisms operative during the formation of SiC [40]:

i) Diffusion limited silicon carbide formation: Diffusion of carbon and silicon through the SiC is the limiting step. This mechanism contains two steps. First one is nucleation of SiC and the second one is growth of nucleated SiC and formation of continuous polycrystalline SiC layer (Figure 2.14(b)). On the other hand, chemical reaction between solid carbon and silicon vapor results in formation of nanocrystalline porous SiC. In the growth stage of the SiC layer diffusion takes place among reactants (Figure 2.14(c)).

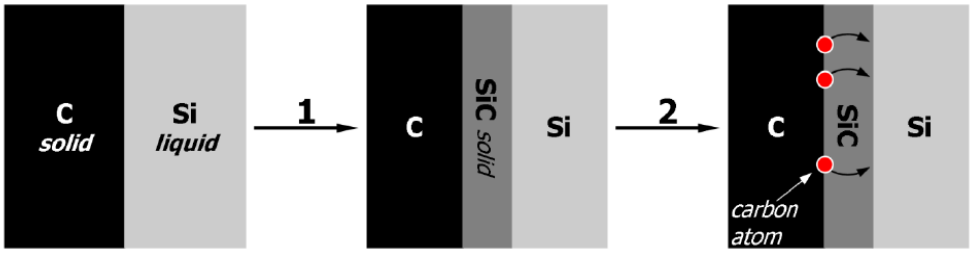

(a) (b) (c)

Figure 2. 14 Reaction at the interface between liquid silicon and carbon, (a) Initial C/Si interface, (b) nucleation of a SiC at the interface and (c) SiC growth by carbon diffusion through interface [40,41].

There basically exists two different approaches about diffusion. Gern and Kochendorfer state that SiC growth depends on diffusivity of silicon atoms. On the other hand, Hon and Davis have shown that the diffusion coefficient of carbon in SiC is 50–100 times higher than the diffusion of silicon through SiC. Therefore, SiC growth occurs by the diffusion of carbon atoms through the SiC and the reaction at the SiC/Si interface. This contradiction was solved by Schulte-Fischedick who studied the SiC layer near the carbon fibers and showed the existance of nanocrystals between C/C region and larger grains. Based on the nanocrystal SiC detected in transmission electron microscopy, Figure 2.15, it is proposed that reaction starts immediately by forming this nanocrystalline layer and grain growth initiates from these nanolayers by diffusion of carbon through the nanosized porous SiC.

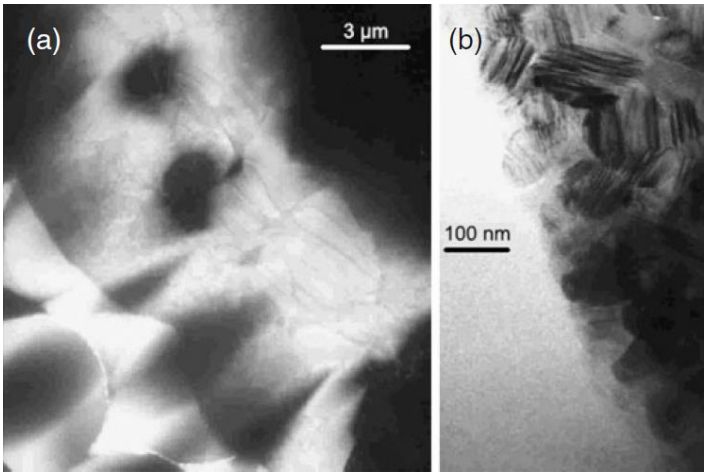

Figure 2. 15 TEM images showing a nanocrystalline layer of SiC at interface C–SiC [42].

ii) Solution-precipitation mechanism: Pampuch stated that SiC formation occurs by the solution–precipitation mechanism. In this approach, firstly carbon dissolves in silicon and then, SiC precipitates occur when supersaturated liquid solution is obtained. The rate of formation is higher than the rate obtained by diffusion mechanism. Dissolution of carbon is an exothermic reaction, therefore, at dissolution

regions temperature increases locally and accordingly, carbon solubility increases. The carbon diffuses to locally cooler sites, where it precipitates as SiC.
As mentioned above, literature contains two different mechanism for the formation of SiC; however, microstructural characterizations exhibit heterogeneous nucleation and growth of SiC by diffusion of carbon through the formed SiC layer.

2.4.3.3.2 Reaction between Liquid Silicon and Glassy Carbon at the Silicon Carbon Interface

Mathematical methods try to explain the effects of capillary forces on SiC formation during liquid silicon infiltration; however, they lack of the chemical reactions that occurs at the interface of liquid silicon and carbon. Diffusion is a time dependent process and measurements of the time-dependent silicon carbide layer thickness proves that SiC formation occurs by heteregenous nucleation and growth mechanism.

Diffusion limited silicon carbide formation is similar to the oxide layer formation of metal surfaces [42] at which the diffusion of oxygen through the oxide layers that exist at the interface between metal and the air. Actually, silicon carbide must contain enough concentration of lattice defects or electronic defects which enhance the diffusion of silicon and carbon through the silicon carbide. The diffusion of carbon is believed to be driven by an electric field across the silicon carbide layer, Figure 2.16. At the Si-SiC interface, silicon donates its electrons to silicon carbide, therefore, interface becomes positively charged. On the other hand, at the SiC-C interface electron donation from silicon carbide to carbon creates negative charges. Therefore, electric field is created and serves as the driving force for carbon diffusion.

The diffusion of silicon and carbon in β-SiC is attributed to a vacancy mechanism. The major lattice defects within silicon carbide are carbon and silicon Schottky defects. The diffusivity of carbon in silicon carbide is 2.90×10^{-7} $cm^2.s^{-1}$ at 1800ºC [44], and the diffusivity of silicon is 9.5×10^{-10} cm^2 s^{-1}., at the same temperature [45]. Therefore, considering the higher diffusivity of carbon compared to silicon, the effect of silicon diffusion in SiC formation may be ignored.

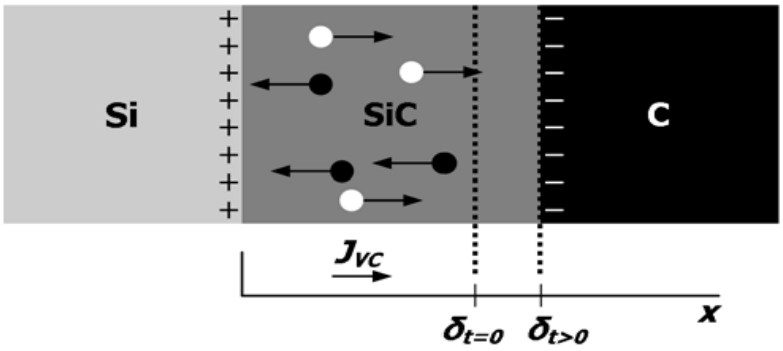

Figure 2. 16 SiC growth at the liquid silicon and carbon interface through carbon diffusion driven by an electric field.

2.4.3.3.3 Reactive Wetting of Glassy Carbon Surfaces by Liquid Silicon Droplets

Wetting behavior of carbon by liquid silicon depends on the degree of wetting which is related to contact angle and rate of wetting which can be defined as the velocity of the vapor-liquid-solid triple line [43], [45], [45]. Reactive wetting steps during process may be summarized as follows (Figure 2.17):

i) Reaction starts with the non-wetting condition, where the contact angle is 180º. Because first SiC nucleation occurs quickly, contact angle changes from 180º to 150º in a very short time.

ii) After the formation of SiC reactive wetting occurs over the entire contact area [46]. The contact angle maintains to decrease to the degrees of 50º and liquid silicon has a high spreading rate.

iii) During the terminal stage, the contact angle decreases at a much smaller rate and reaches a final value of approximately 35º. This corresponds to the wetting angle of liquid silicon on silicon carbide.

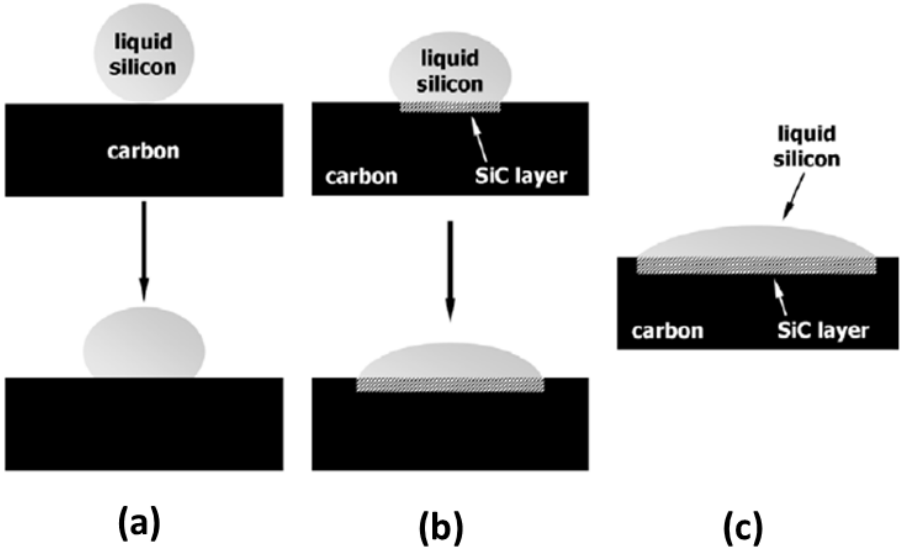

Figure 2. 17 Schematic illustration of the wetting of liquid silicon on glassy carbon surfaces, (a) non-reactive wetting, (b) reactive wetting, and (c) the terminal stage.

2.5 Applications of C/C-SiC Composites

C/C-SiC composites have superior thermal and mechanical properties with low density, high oxidation and erosion resistance compared to C/C composites or conventional metals. Therefore, they have numerous application areas depending on service temperature, time and atmosphere. They can maintain their thermal and mechanical properties at elevated temperatures due to high temperature stabilities of their reinforcement and matrix materials. Unlike the service temperature, service time is limited because of oxidation of carbon fiber at temperatures above 450◦C, and active oxidation of SiC above 1000–1900◦C depending on atmosphere. Therefore, while thermally loaded components like rocket propulsion systems may be used only for short term applications, long term stable components includes brake disks or satellites, which operates at moderate or low temperatures, Figure 2.18.

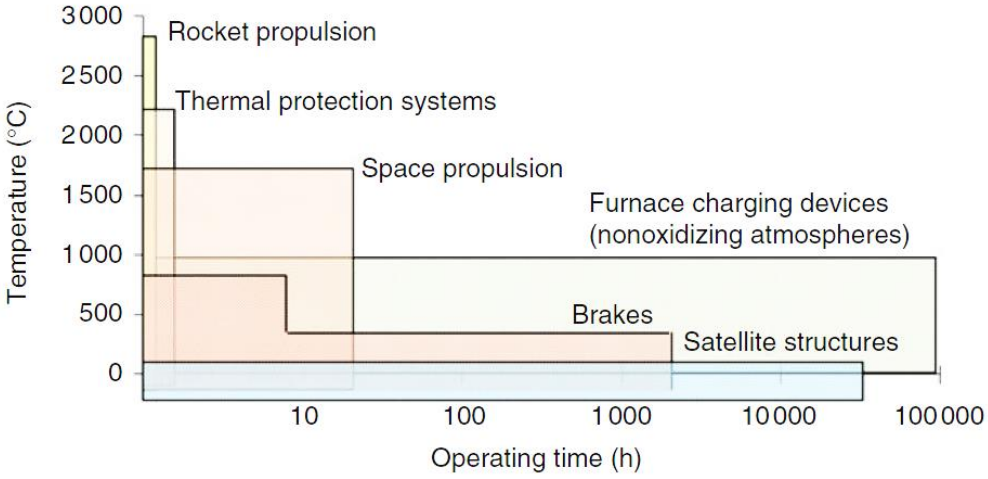

Figure 2. 18 Application areas of C/C-SiC composites which depend on service temperature and time.

2.5.1 Space Applications

Thermal protection system (TPS), which protects the space shuttle from the heat of atmospheric reentry [48], works under high thermal gradients and heating rates that are generated locally during the critical reentry phase, lasting up to 30 minutes. Maximum operation temperature of the system changes between 1600◦C and 2000◦C and TPS is exposed to highly oxidative environment. Traditional composite materials like carbon fiber reinforced polymers cannot withstand these extreme temperature conditions without oxidation. Therefore, in order to prevent this condition, C/C materials with oxidation protective coatings were introduced. However, to increase oxidation resistance C/C-SiC materials were used in NASA X-38 spacecraft (Figure 2.19), which is developed by DLR in the German TETRA program as nose cap due to its lightweight structure, high temperature resistivity and capability of near-net shape production [48].

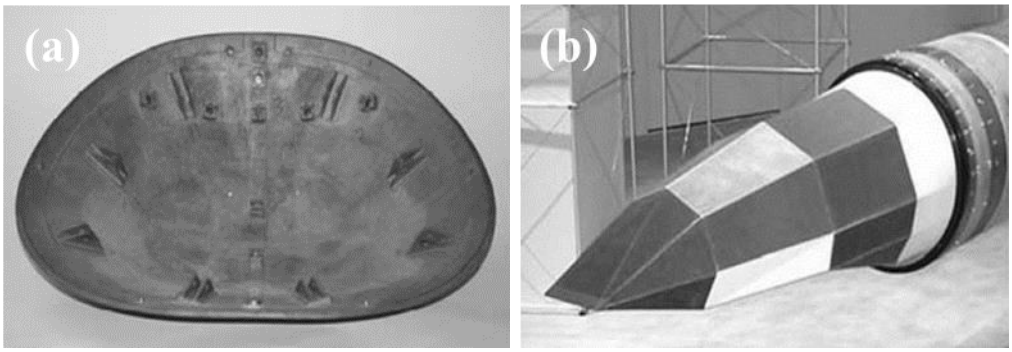

Figure 2. 19 C/C - SiC structural parts for TPS. (a) X 38, (b) Facetted TPS structure.

2.5.2 Short-Term Aeronautics-Jet Vanes

Thrust vector control systems are necessary for ballistic missile systems such as advanced fighters, research aircraft and tactile missiles in order to control the rocket thrust direction to steer the missile. For military rocket motors, by the help of the movable jet vanes which deflect the exhaust gases in the nozzles give rise to steer the missile [49]. Nearby the nozzle, there are four jet vanes exist, Figure 2.20, and they rotate according to commands from the missile guidance system to deflect the flame of the solid propellant. Material used in jet vane is very important because they are exposed to severe mechanical and thermal loads, therefore, they must withstand operation temperatures as high as 3000 K and velocities up to Mach 3.5. Moreover, use of aluminized solid propellant (blast of solid particles e.g. Al_2O_3) causes the erosion, which decreases the thrust vector control capability of the jet vane. Conventional jet vane materials are copper infiltrated tungsten (CIT) and heat treated 4340 steel. Compared to the metallic jet vanes, C/C-SiC materials have lower densities which enable weight saving in missile systems. Moreover, low thermal expansion coefficient and high thermal conductivity give rise to suitable thermal shock stability.

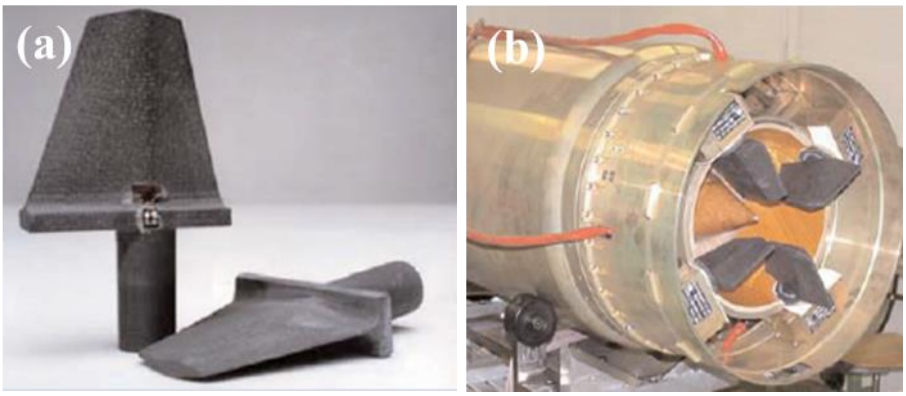

Figure 2. 20 C/C-SiC vane, b) jet vane assembly in the exhaust nozzle extension [18].

2.5.3 Satellite Structures

Laser communication terminals (LCTs) such as telescope structures are optical systems where laser beams are used for satellite communication to obtain data transmission. These structures have to be stable in the μm-scale for long operation times in space environment [50]. The low thermal expansion of C/SiC materials are suitable for LCT structures since deformation of the telescope, caused by thermal expansion due to solar irradiation, or by vibrations induced by different sources in the satellite may be prevented. For the telescope tube C/C-SiC materials are developed with a very low CTE ($0 \pm 0.1\times10^{-6}$ K^{-1}) in axial direction by the German TerraSAR-X and the US NFIRE using liquid silicon infiltration methods [51].

2.5.4 Friction systems

C/C composites and gray cast irons are being replaced by C/C-SiC composites in some applications such as brake disks and clutches. Although C/C composites are used for brake discs and clutches for racing cars, they have some disadvantages like high manufacturing cost, high wear that is caused by abrasion and oxidation, and a significant decrease of the COF at low temperature and in humid environments, Table

2.4. Moreover, compared to conventional materials like gray cast irons, C/SiC composites have lower densities which results in weight saving by reducing unsprung mass. Decreasing unsprung mass also leads to more driving comfort for automotive brake pad applications. In order to overcome these drawbacks C/C-SiC composites are developed using low cost phenolic resin precursors and short carbon fibers via LSI process. Visual appearance is also improved by using ceramic matrix materials because rusty metal disks and wheels heavily soiled with wear particles are avoided. Moreover, while metallic materials lose their mechanical and thermal properties at high temperatures, C-C/SiC materials retain their properties even at elevated temperatures [53-54].

Table 2. 4 Mechanical and thermophysical properties of carbon fiber reinforced silicon carbide (C/SiC) in comparison to a grey cast iron brake material GJS – 200 [18].

Property	**GJS - 200**	**C/SiC, SGL**	**C/C**
Density (g/ cm^3)	7.2	2.3	1.7-1.8
Tensile Strength (MPa)	150-250	20-40	-
Fracture Strain (%)	0.3	0.3-0.8	320
Young's Modulus (GPa)	90-100	30	50
Thermal Conductivity (W/mK)	54	40	25-30
Coefficient of Thermal Expansion	9; 12	1; 2	0.5

Brake systems of the modern cars must increase the safety of car not only in dry conditions but also in wet environment. They must possess high wear resistance, high braking comfort, high corrosion resistance and low weight.

C/SiC brake discs for the automobile market were presented by Daimler Benz in 1999 and Porsche at the International Motor Show (IAA) in Germany, and were used for the first time in Mercedes CL in 2000. Currently, the so-called PCCB (Porsche Ceramic

Composite Brake), Figure 2.21, is available for all Porsche models as an option and is a standard component for special edition cars. Furthermore, this type of ceramic pads are available for all sports cars.

Figure 2. 21 (a) Porsche Ceramic Brake (PCCB) with short fiber-based C/SiC brake disc rotor, manufactured via LSI. (b) Porsche Ceramic Composite Clutch (PCCC) based on carbon-fiber fabric-reinforced C/SiC.

Ceramic brake disks can be manufactured using combination of several different methods like reactive bonding + PIP, CVI + PIP and CVI + LSI; however, most widely used, economical and less time consuming method is liquid silicon infiltration method. As a reinforcement and matrix materials PAN based short carbon fibers and phenolic resin are used, respectively.

C/SiC composites are also used for brake pads for high performance elevators. These types of elevators are designed to withstand to high masses up to 45 tons and velocities of 10 m/s at elevated temperatures. If the speed of the elevator is more than the 10 m/s, emergency stop starts to work, in other words, brake pads must prevent free falling of elevator at the event of failure. At such working conditions metallic friction pads cannot be stable thermally and mechanically.

For the clutches applications, carbon/carbon materials are used widely. Racing and high performance clutches need minimum weight, low moment of inertia, maximum strength, optimal performance and maximum heat resistance [55] However, C/C materials do not provide these requirements because of their low wear resistance and

aggressive friction qualities. Moreover, although sintered metallic friction components have good friction behavior compared to C/C, as a drawback they have low heat resistance and high density. In order to overcome these drawbacks ceramic composite clutch is developed by Porsche [56]. In comparison to brake applications clutch disks must be more thin-walled and withstand higher mechanical loads. Therefore, unlike short fiber reinforced SiC matrix composites in brake disks, different layers of carbon fiber reinforcement is applied to obtain better strength.

2.5.5 Applications for High Temperature Treatment of Metals

C/C-SiC composites are important materials for high temperature treatment of metallic materials due to their low density and high heat capacity. They supply faster processes in terms of heating and cooling, therefore, lower energy consumption is achieved. Moreover, due to their high thermal stability they can be used for several years in service without any distortion and any shape change.

2.5.6 Light Armor

For the ballistic applications typical materials are armor steel, ceramic armors such as Al_2O_3, SiC and B_4C. Compared to the steel armors C/C-SiC composites takes advantages of lower density and use of these composites overcomes the high brittleness and low fracture toughness drawbacks seen in the monolithic ceramics. Moreover, since crack propagation rate is reduced by composite production C/C-SiC composites present multiple hit performance [51].

CHAPTER 3

EXPERIMENTAL PROCEDURE

3.1 Raw Materials

3.1.1 Phenolic Resin

Matrix material of carbon fiber reinforced polymer matrix (CFRP) composites was resole type phenol formaldehyde resin which was a thermoset and in oligomer condition. Phenolic resin was supplied from ROKETSAN A.Ş. in liquid form. For characterization the resin matrix in CFRP composites supplied resin was cured at 60 °C for 5 days in a removable mold and then, converted to powder form for XRD and TGA measurements.

3.1.2 Silicon Powders

In the present study, angular silicon powders (99.9 % purity), Figure 3.1(a), supplied from Aldrich were used as infiltration material to manufacture C/C-SiC composites. The average particle size of silicon powders was approximately 10 μm and the particle size was observed to change between 2 and 20 μm.

3.1.3 Microcrystalline Cellulose

Microcrystalline cellulose powders were used as alternative carbon precursor in order to understand the reaction kinetics of the matrix material. Cellulose powders were supplied from Alfa Aesar GmbH & Co KG. The average particle size of microcrystalline cellulose powders was approximately 35 μm and the particle size was observed to change between 15 and 50 μm, Figure 3.1(b).

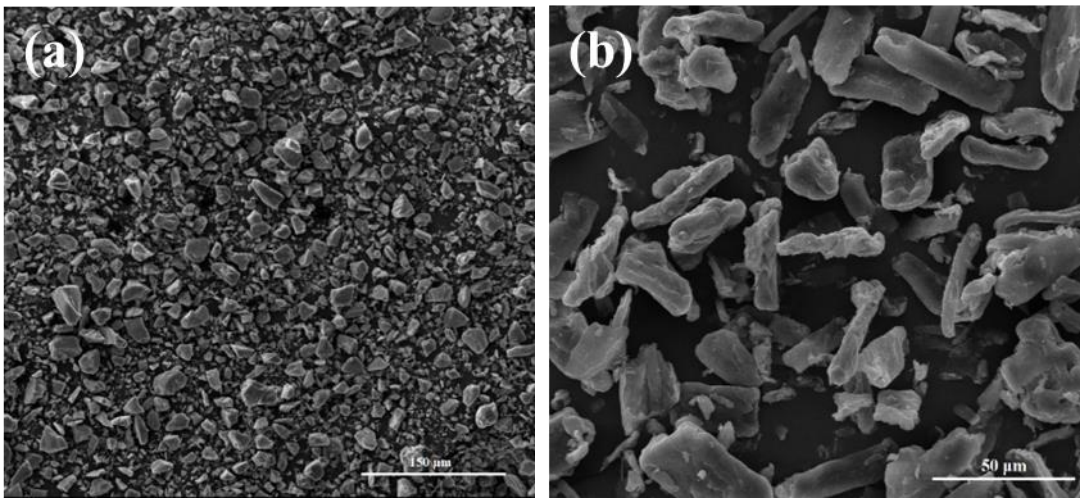

Figure 3. 1 Powders used in the study (a) Silicon and (b) Microcrystalline cellulose.

3.1.4 Beta Silicon Carbide Powders and Carbon Nano Tubes

SiC nano powders and carbon nano tubes were embedded into C/C preforms by ultrasonic method from alcohol-powder suspended solutions prior to liquid silicon infiltration to see the effect of nanoparticle addition on the infiltration process and composite formation.

Beta silicon nanopowders which were supplied from Alfa Aesar GmbH & Co KG had spherical shape and particle size between 100 and 200 nm, Figure 3.2(a). Carbon nanotubes were supplied from Nanografi Nanotechnology (NG01MW0101) was multiwall carbon nanotubes with purity higher than 95 % and outer diameter less than 7 nm, Figure 3.2(b).

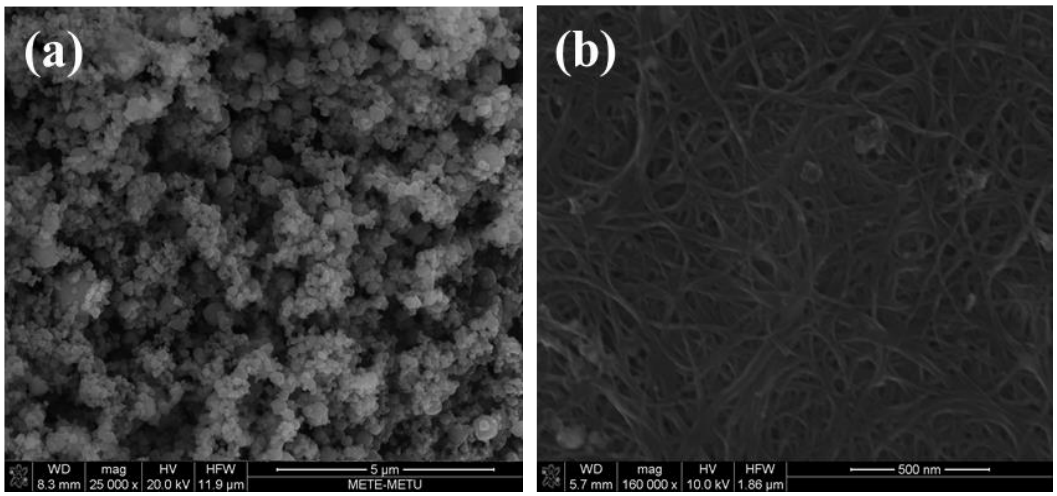

Figure 3. 2 Matrix additives used in this study (a) Beta nano silicon powders, (b) Carbon Nano tubes (CNT).

3.2. Pyrolysis and Production of Composites

3.2.1 Fabrication of Carbon Fiber Reinforced Polymer Matrix (CFRP) Composites

CFRP composites were fabricated in an autoclave by ROKETSAN A.Ş. using resol type phenol formaldehyde resin and carbon fibers as matrix and reinforcement materials, respectively. The resin, which was in oligomer condition, was used along with 40 vol % polyacrylonitrile (PAN) based 2D plain woven carbon fiber fabrics, Figure 3.3. The temperature and pressure inside the autoclave were maintained at 175 °C and 3-5 bar, respectively, during the holding time of 4 h.

Figure 3. 3 As-received Carbon Fiber Reinforced Polymer Matrix (CFRP) Composite

3.2.2 Investigation of Optimum Pyrolysis Temperature

3.2.2.1 Pyrolysis of Resin Matrix

Preliminary pyrolysis experiments were conducted using phenolic resin in powder form prior to pyrolysis of CFRP composites containing both carbon fiber fabrics and resin matrix in order to determine the effect of pyrolysis temperature on the conversion of the phenolic polymer matrix into carbon. Initially, cured phenolic resin was converted to powder form using alumina mortar. Particle size of the powder phenolic resin changed between 150 and 600 μm. Then, the powder resin was pyrolyzed for 3 h at various temperatures of 500, 600, 700, 800, 900 and 1000°C under flowing high purity nitrogen atmosphere, Figure 3.4.

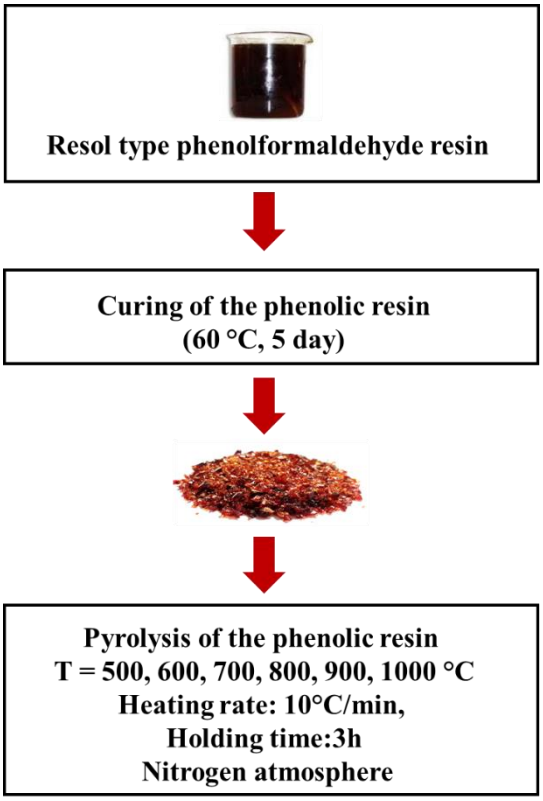

Figure 3. 4 Schematic flowchart showing pyrolysis steps of phenolic resin

3.2.2.2 Pyrolysis of CFRP to Form C/C Preforms

CFRP composites were pyrolyzed to obtain C/C composite preforms to be used in silicon infiltration studies. Carbonization of CFRP composites was performed at various temperatures with a constant heating rate of 10°C / min under flowing nitrogen atmosphere. In order to find out optimum pyrolysis temperature and to investigate the effect of the pyrolysis temperature on the microstructure and properties of CFRP composites, 6 different pyrolysis experiments were done for 3 h at temperatures of 500, 600, 700, 800, 900 and 1000 °C, Figure 3.5. After pyrolysis, the samples were allowed to cool slowly in the furnace under flowing nitrogen atmosphere in order to prevent excessive crack formation.

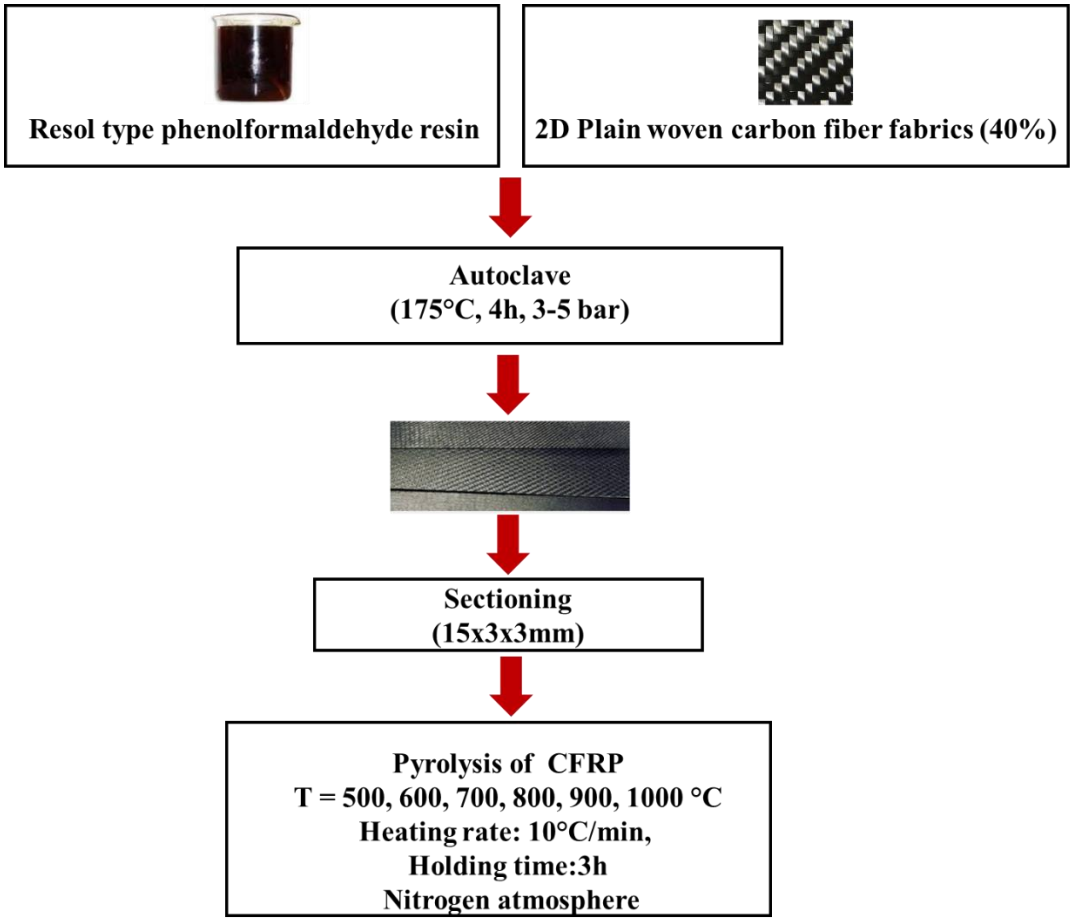

Figure 3. 5 Schematic flowchart showing production and pyrolysis steps of CFRP.

3.2.3 Nano-SiC or Carbon nanotube (CNT) Impregnation to C/C Preforms

Both Nano-SiC powders and carbon nano tubes were embedded into C/C preforms as matrix additives to compare and contrast silicon infiltration behavior and C/C-SiC composite formation in as-manufactured and nano particle added C/C preforms.

During preparation of nano SiC powder containing C/C preforms initially 15 ml ethanol and 0.5 g silicon carbide nano powders were mixed and kept in an ultrasonic disperser (UW 2070 BANDELIN, Berlin, Germany) for 10 minutes to obtain homogeneous suspension. After that, the C/C preforms were immersed into prepared

ethanol-SiC mixtures and hold in vacuum applied desiccators for 1 h in order to achieve complete penetration of mixtures into the pores of C/C preforms. Finally, the preforms were placed to a furnace kept at 50°C to remove the ethanol.

Likewise, carbon nano tubes were embedded into C/C preforms using the same method. Firstly, 0.01 g carbon nanotube and 5 ml propanol were mixed and kept in an ultrasonic disperser for 2 minutes and then, 2 ml homogeneous solution was transferred to another beaker which contains C/C preform and 8 ml propanol. Next, the suspension containing C/C preform was kept in an ultrasonic disperser for 10 minutes and placed in vacuum desiccators for 1 h to infiltrate suspension into porous structure successfully. At the last step, carbon nanotube embedded preforms were placed to a dryer at 50°C and hold for 1 h in order to remove the propanol from the C/C preforms.

3.2.4 Liquid Silicon Infiltration (LSI) of C/C Preforms

3.2.4.1 General

In this stage optimum process parameters were tried to be determined during infiltration of liquid silicon into C/C preforms manufactured via pyrolysis of CRFP composites. Mainly three types of preforms, namely, no additive, CNT impregnated and nano-SiC impregnated (Table 3.1), were utilized to examine the effect of initial preform condition on the infiltration of liquid silicon.

3.2.4.2 Infiltration

In order to apply liquid silicon infiltration process typical Lenton Tube laboratory furnace was initially converted to atmosphere/vacuum controlled tube furnace by designing and installing suitable flanges at the inlet and exist parts of the ceramic tubes including feed through thermocouple, sealing systems and gas/vacuum intake and outlet valves, Figure 3.6. Since employed temperatures were higher than the melting point of silicon (1414-1700 °C), B type 18% Rhodium- Platinum thermocouple with alumina protective coating was chosen. Excessive heating of the flanges at both sides

of the ceramic tubes was prevented by winding copper pipes around alumina tube and passing water at a constant temperature in the pipes throughout the experiments.

Figure 3. 6 Lenton Tube laboratory furnace converted to atmosphere/vacuum controlled tube furnace used in this study.

During infiltration process firstly around 1.6 g of Si powder was filled into graphite crucibles containing pyrolyzed C/C preforms as shown in Figure 3.7. Then, the crucibles were placed in the hot zone of the furnace with a molybdenum wire that has ability to resist high temperature conditions without getting any chemical reaction with liquid silicon.

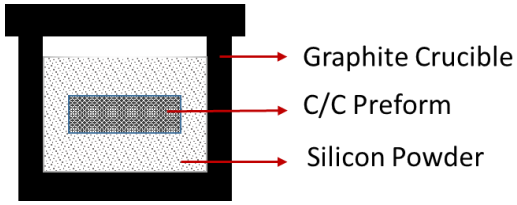

Figure 3. 7 Graphite crucible that containing pyrolyzed C/C preforms.

Before setting up the furnace, the furnace alumina tube was initially filled with Argon gas and then, vacuum was applied by a rotary pump to reduce the vacuum level at round 10^{-3} mbar, Table 3.1. Argon purging and vacuum degassing cycles were applied 3 times in order to ensure that the tube was free from air or any impurity gases. For infiltration process, the furnace was set up to desired temperature and heating rate was adjusted to 10°C / min. By the time furnace had reached to temperature 1300 °C, the samples were kept above the hot zone in order to prevent second pyrolysis of the C/C preforms. The samples which were initially in the cold zone of the furnace were placed slowly to a region of the furnace at which the temperature was approximately 900 °C to avoid excessive cracking due to rapid temperature change and the samples were hold at this region for 3 minutes for temperature equalization along the samples. Next, the samples were moved to the hot zone of the furnace and they were held for 1h at the test temperatures. Liquid silicon infiltration of porous C/C preforms was studied at various temperatures above the melting point of pure Si (1414 °C) both under flowing argon atmosphere and vacuum atmosphere of around 10^{-3} mbar. During the infiltration processes optimum process parameters were sought at which the complete reaction occurs between liquid silicon and free carbon in the C/C preform emerging from the phenolic matrix of the initial CFRP. Because complete reaction of Si with the free carbon to form SiC is known to result in a dense and homogenous composite containing C/C fibers separated from each other by SiC without any unreacted Si.

After infiltration, the furnace was switched off and the samples were allowed to cool in the furnace slowly under flowing argon atmosphere.

Table 3. 1 Classification of liquid silicon infiltration samples based on processing type and infiltration parameters.

Type of Processing	**Sample Code**	**Pyrolysis Temperature (°C)**	**Infiltration Temperature (°C)**	**Infiltration Atmosphere**
No-Additive	700P-1550LSI-A	700	1550	Argon
	800P-1550LSI-A	800	1550	Argon
	900P-1550LSI-A	900	1550	Argon
	1000P-1550LSI-A	1000	1550	Argon
	1000P-1550LSI-V	1000	1550	Vacuum
	1000P-1650LSI-V	1000	1650	Vacuum
Nano-SiC impregnated	Nano-SiC	1000	1650	Vacuum
CNT impregnated	CNT	1000	1650	Vacuum

3.3 Experiments about the Effect of Matrix Reactivity on the LSI Process Efficiency

In order to understand the mechanism and kinetics associated with SiC formation by LSI process, different alternative matrix materials in powder form was infiltrated with liquid silicon at 1650 °C and in vacuum. Experimental studies have been carried with carbons derived from phenolic resin and from mixture of phenolic resin and microcrystalline cellulose. Moreover, in order to examine the effects of nanoparticle addition to pyrolyzed phenolic resin on transformation of SiC, mixtures of carbon derived from phenolic resin- nano-SiC powder and carbon derived from phenolic resin and CNT were applied to LSI process.

Firstly, for all of the experimental studies phenolic resin was converted to carbon by applying pyrolysis at 1000 °C under flowing nitrogen atmosphere for 2 h. Furthermore, carbon derived from microcrystalline cellulose was also obtained by pyrolysis of microcrystalline powder at 1000 °C, under flowing nitrogen atmosphere for 3 h. After that, carbon derived from phenolic resin was mixed with other precursors in predetermined weight percentages (Table 3.2). Preparation of CNT and carbon derived from phenolic resin mixture had different process than other precursors due to hydrophobic nature of the CNT. Because of having hydrophobic nature, carbon nanotubes tend to agglomerate and prevent formation of homogenous CNT-carbon mixture. Therefore, in order to overcome this problem, firstly 95:5 wt % carbon derived from phenolic resin, CNT, respectively, and 5 ml propanol were mixed and kept in an ultrasonic disperser for 15 minutes. Next, equal moles of powder silicon and the carbon derived from phenolic resin mixture was added to the suspension and it was kept in an ultrasonic disperser for 15 minutes. Finally the suspension containing silicon powder, carbon and CNT was placed to a furnace kept at 60°C for 1 day to remove the propanol.

Table 3. 2 Classification of liquid silicon infiltration carbon preforms based on precursor type.

Sample Name	**Precursor type**
PR	Carbon derived from phenolic resin
PR-MC	60:40 wt % carbon derived from phenolic resin and carbon derived microcrystalline cellulose
PR-nanoSiC	95:5 wt % carbon derived from phenolic resin and nano-SiC
PR-CNT	95:5 wt % carbon derived from phenolic resin and CNT

3.4 Characterization Studies

3.4.1 Microstructural characterization

Microstructural characterizations of the pyrolyzed CFRP and silicon infiltrated composites were conducted using scanning electron microscope (SEM) (FEI Nova Nano SEM 430) equipped with an energy dispersive X-ray spectroscopy (EDS) analyzer. All of the samples were examined after grinding and polishing the surfaces with 800-1000 grit size SiC papers and diamond (1 μm and 0.5 μm) suspended solutions, respectively. Observations were done at an accelerating voltage of 10 kV.

3.4.2 Density Measurement

Density and open porosity contents of the samples were measured by the Archimedes' Principle using xylol ($CH_3C_6H_4CH_3$) using PRECISA XB220A balance equipped with a density determination kit. After weighing the samples in dry condition, the samples were inserted into xylol solution and held in desiccators for 1 h. In order to achieve successful penetration of xylol into the pores vacuum was also applied to the desiccators. Then, the samples were put in a beaker filled with xylol on the balance and the weights of the samples were measured when they were in the solution. Finally, after taking the samples out of xylol, weight of xylol impregnated samples were also measured in air to determine the amount of impregnated xylol into pores.

During the density and open porosity calculations, density of xylol (ρ_{xylol}) was taken as 0.861 g/cm^3. Volume and density of each sample were calculated by use of Eqs. (3.1-3.2)

$$V_{sample} = \frac{M_{a,x} - M_{x,x}}{\rho_{xylol}} \tag{3.1}$$

$$\rho_{sample} = \frac{M_a}{V_{sample}} \tag{3.2}$$

where,

M_a = mass of the sample in air

$M_{a,x}$ = mass of xylol impregnated sample in air

$M_{x,x}$ = mass of xylol impregnated sample in xylol

Percentages of open porosities were determined by equation (3.3);

$$P_{open}(\%) = \frac{(M_{a,x} - M_a)/\rho_{xylol}}{(M_{a,x} - M_{x,x})/\rho_{xylol}} x100 \qquad (3.3)$$

3.4.3 Structural Analysis by X-ray Diffraction (XRD)

X-ray diffraction (XRD) characterization using Rigaku D/MAX2200/PC was performed for structural examination of phenolic resins, C/C preforms after pyrolysis at various temperatures and silicon infiltrated C/C-SiC composites. The source was Cu Kα containing both wavelengths $K\alpha_1$ = 1.54056 Å and $K\alpha_2$=1.5444 Å. Scans were done in the 2θ angle range of 5-110° with a rate of 2°/min.

Interlayer spacing, d (Å), for the (002) peak of turbostratic carbon structure was investigated by Bragg's Equation, Eq 3.4;

$$n\lambda = 2d\sin\theta \qquad (3.4)$$

The crystallite sizes were calculated using Scherrer Equation, Eq (3.5);

$$L = \frac{K\lambda}{\beta\cos\theta} \qquad (3.5)$$

where,

K: shape factor which has a range of values. In calculations crystallite size, Lc which was measured from (002) peak and value of 0.9 was used,

λ: wavelength of the X-ray (1.54056 Å),

B: intrinsic breadth,

Θ: Bragg angle.

Rietveld Analysis was done by GSAS (General Structure Analysis System, (developed by R.B. von Dreele and A.C. Larson, University of California, 2001) for the calculation the weight percentages of the phases. The parameters used for the refinement are tabulated in Table 3.3.

Table 3. 3 Initial Rietveld Fitting parameters and constant parameters.

Crystal Structure	Si	Diamond
	SiC	Zinc Blende Cubic
	C	HCP
Space Group	Si	Fd-3m
	SiC	Td/F43m
	C	P63/mmc
Instrumental Broadening	GU	0.08
	GV	-2.87
	GW	13.76
Lattice Parameters	Si	a = b = c =5.4309 Å
	SiC	a = b = c =4.3480 Å
	C	a = b = 2.4664 Å, c= 6.7110 Å

3.4.4 Thermogravimetric Analysis and Fourier Transform Infrared Spectroscopy (TGA + FTIR)

Perkin Elmer Pyris STA 600 Thermogravimetric Analysis & Spectrum FT-IR Spectrum (TGFT) was used to determine types of gases evolved during the each pyrolysis step. During the thermogravimetric analysis evolved gases are transferred to

FTIR device to define the gases. Approximately 8 mg cured phenolic resin in powder form was used for each measurement.

3.4.5 Thermogravimetric Analysis (TGA)

The weight loss behaviors of the phenolic resin were analyzed by thermogravimetric analysis (TGA) with an EXSTAR TG/DTA 7300 to measure the mass change in a controlled atmosphere. Structure of the device is illustrated in Figure 3.8. Left crucible is used for reference samples whereas the right crucible is for actual samples. Right crucible was loaded with approximately 8 mg powder form of cured phenolic resin. Thermogravimetric measurements were performed between 30 ºC and 900 ºC by employing a heating rate of 10 ºC/min under N_2 atmosphere.

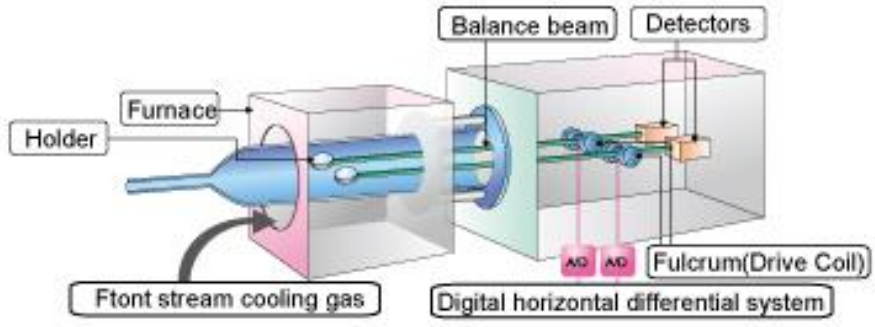

Figure 3. 8 Structure of EXSTAR TG/DTA 7300.

3.4.6 Three Point Bending Test

Flexural strength and strain of the composites were determined by three-point bending tests. Length, width and thickness of the three-point bending test specimens were 15, 3 and 3 mm, respectively. Tests were applied at a cross-head speed of 0.4 mm/min using a screw-driven type test machine (Instron 5565A) with a span length of 16 mm. Flexural strength, and strain values were calculated using equations (3.6) and (3.7),

respectively, via load vs deflection data. Fracture surfaces of the three-point bending test specimens were examined using SEM.

$$\sigma_f = \frac{3PS}{2bd^2} \tag{3.6}$$

$$\varepsilon_f = \frac{6Dd}{S^2} \tag{3.7}$$

where ;

P:load at a given point on the load deflection curve, N,

D: maximum deflection of the center of the specimen, mm,

S: support span, mm,

b: width of the specimen, mm,

d: thickness of the specimen, mm.

CHAPTER 4

RESULTS AND DISCUSSION

Liquid silicon infiltration (LSI) is a complex process where key variables play a distinguishable role on the effectiveness of densification. LSI progress is mainly controlled by preform characteristics governed by pyrolysis temperature, density, porosity content and reactivity of the carbon as well as experimental variables such as temperature and atmosphere. Therefore, considering these parameters understanding their effects on the densification behavior and optimum liquid silicon infiltration parameters are crucial.

This chapter contains four main parts. In the first part of the study, in order to understand the transformation of the polymer matrix into carbon during pyrolysis, the pyrolysis behavior of the phenolic resin was investigated. Furthermore, the effect of different pyrolysis temperatures on the microstructure and resulting properties of the C/C preforms obtained from the initial CFRP was also investigated. The second part of the study was aimed to discuss the optimum liquid silicon infiltration parameters. Thirdly, results and discussions on the effect of both nano-SiC powder and carbon nanotube (CNT) usage as matrix additives into the C/C preforms on the silicon infiltration behavior was presented. Finally, effect of using alternative matrix combinations such as microcrystalline cellulose, carbon nanotube, and nano-SiC on the reaction and C/C-SiC composite formation kinetics has been discussed.

4.1 Pyrolysis of the phenolic resin

As mentioned in Chapter 2 processing of C/C-SiC composites via liquid silicon infiltration (LSI) or reactive melt infiltration (RMI) can be divided into three separate process steps:

i) Manufacturing of carbon fiber reinforced polymer matrix (CFRP) preform by autoclave technology,

i) Conversion of the polymeric matrix into carbon by pyrolysis under inert atmosphere thus forming a carbon/carbon preform,

iii) Converting carbon matrix into SiC matrix by melt infiltration of liquid silicon and formation of the ceramic composite end product termed as C/C-SiC composite.

In the third step, liquid silicon infiltrates into the preform via capillary forces, therefore, microstructures and properties of CFRP and matrix material have an important effect on the infiltration process. As a result, the aim of this part is to investigate the effect of varying pyrolysis temperature on the microstructure and resulting properties of the carbon matrix material of the C/C preform.

As the matrix material of the CFRP resol-type phenol formaldehyde supplied by ROKETSAN was used. Phenolic resin is a thermoset material, and it consists of 3D network structure in as-cured condition having amorphous and glassy structure with a high crosslink density.

4.1.1 Thermogravimetric Analysis (TGA) of the Phenolic Resin

Thermogravimetric analysis (TGA) was applied to the initial CFRP from 30 to 900°C. In the thermogravimetric analysis result, according to the recorded mass change three different regions are observed (Figure 4.1). From 30 to 400°C, mass change occurs slightly. Between 400 and 700°C, mass change shows sudden decrease, while from 700 to 900°C it is seen that there is a slight variation is in the mass.

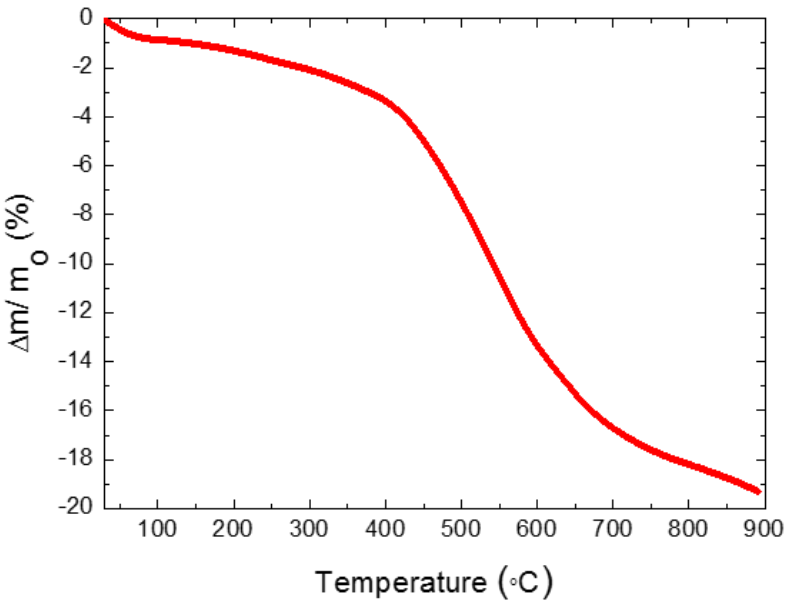

Figure 4. 1 Thermogravimetric Analysis of as-cured phenolic resin.

In order to examine whether thermogravimetric analysis result is reliable or not, weight loss values obtained at different pyrolysis temperatures and weight loss values obtained from thermogravimetric analysis results were compared. It was seen that weight loss values at different temperatures obtained by two different methods are consistent with each other (Table 4.1).

Comparison of TGA data with gas evolution-FTIR analysis results revealed that, pyrolysis contains three major reactions between room temperature and 900 °C, where by each step different gases evolve. These steps are called post curing, main pyrolysis and dehydrogenization [57]. In order to identify which gases evolve during each step FTIR analyses was applied to the forming gases during pyrolysis (Figure 4.2).

Table 4. 1 Comparison of weight loss values obtained at varying pyrolysis temperatures and weight loss values obtained from thermogravimetric analysis result.

Temperature (°C)	**Weight loss (%) (according to TGA)**	**Weight loss (%) (after pyrolysis of different temperatures)**
100	0.85	0.72
200	1.30	1.25
300	2.08	2.11
400	3.35	3.45
500	7.40	6.52
600	13.19	14.90
700	16.79	15.04
800	18.26	16.65
900	19.26	17.84

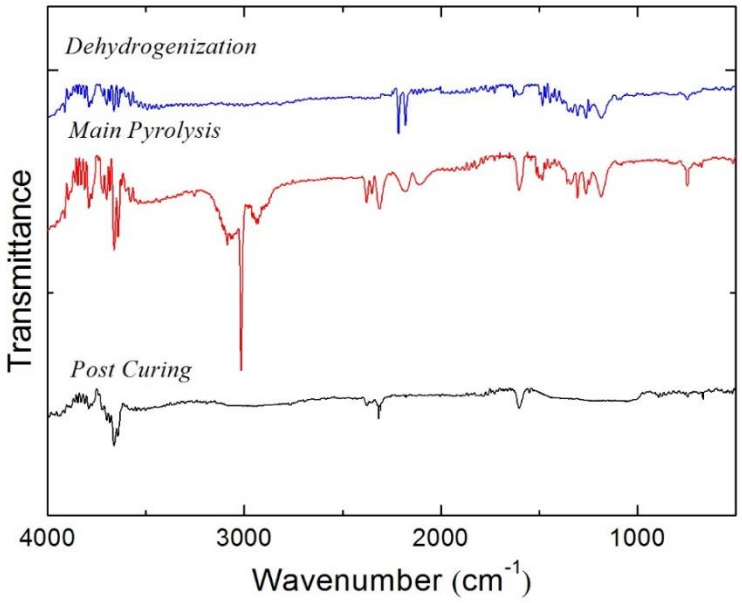

Figure 4. 2 FTIR analysis of gases evolved during pyrolysis.

As mentioned in Chapter 2, the matrix material is a phenolic resin, which is a thermoset. The matrix is primarily composed of methylene bridge phenolic unit and during post curing according to the FTIR analysis, H_2O and CO_2 are generated. Asymmetric, symmetric and bending stretch peaks of the O-H band exist correspondingly at 3756, 3657 and 1595 cm^{-1}. Since additional crosslinking occurs at this step and these crosslinks are formed as a result of two condensation reactions between functional groups of cured phenolic resin, H_20 is expected to be evolved gas. According to Parker [58], depending on the location of the separation of the chain phenol and cresol occurs. Then, first condensation reaction involves two phenol groups and results in ether crosslink. Second condensation reaction takes place between methylene group and a phenol group and forms C-H crosslink (Figure 4.3). Asymmetric and bending peaks of CO_2 correspondingly at 2349 and 667 cm^{-1} can be observed in the spectrum. However, as the symmetric stretch is infrared inactive, i.e., there is no change in dipole moment during the symmetric stretch vibration, 1340 cm^{-1} bond is not observed in the spectrum. Although pyrolysis takes place in an inert atmosphere, during decomposition of the phenolic resin oxidation/combustion reactions may be observed in the system. In other words, oxygen radicals may be generated which will cause combustion at the end of which H_2O and CO_2 may be produced as a product. Moreover, obtaining low molecular weight gases at this step is consistent with the TGA results and the corresponding weight loss data.

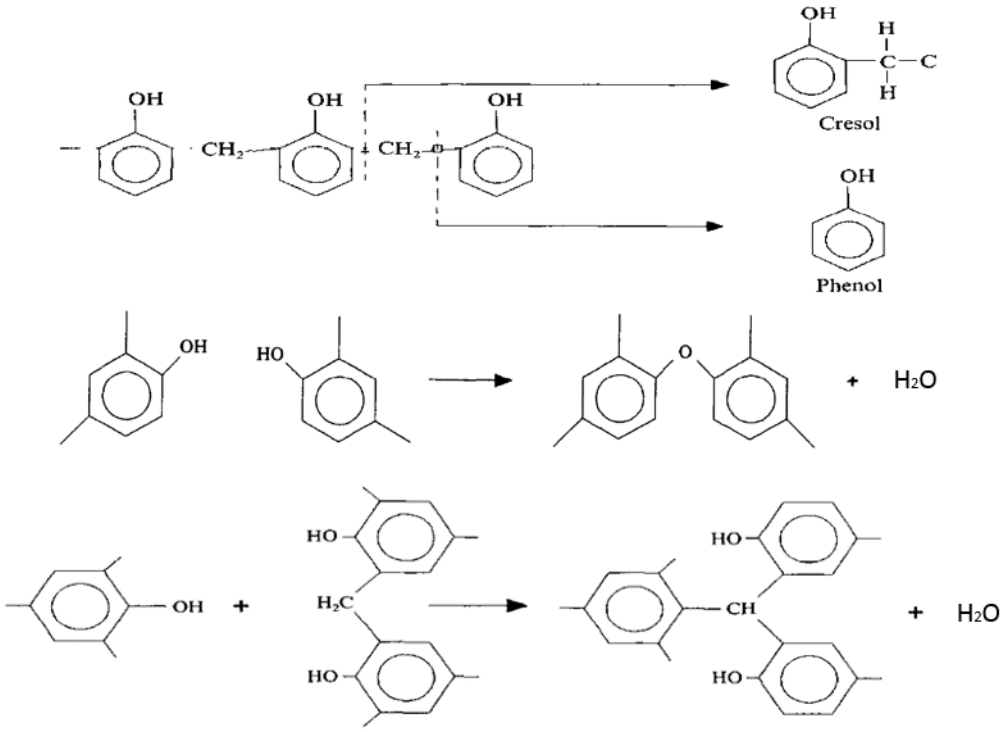

Figure 4. 3 Possible reactions taking place during post curing step.

According to the FTIR analysis in main the pyrolysis part, H_2O, CO, CO_2, CH_4, C_2H_6 gases are generated (Figure 4.2). Increase in the number of evolving gaseous species was expected, because the mass change shows sudden decrease in this region according to TGA and weight loss analysis. Since the polymeric matrix is converted to carbon by breaking the ether crosslink and C-H crosslink, which are produced during post curing step, char with aromatic carbon and hydrogen gas are produced. Evolution of the CH_4 can be explained by the possible reaction between the produced hydrogen gas and Methylene Bridge (Figure 4.4).

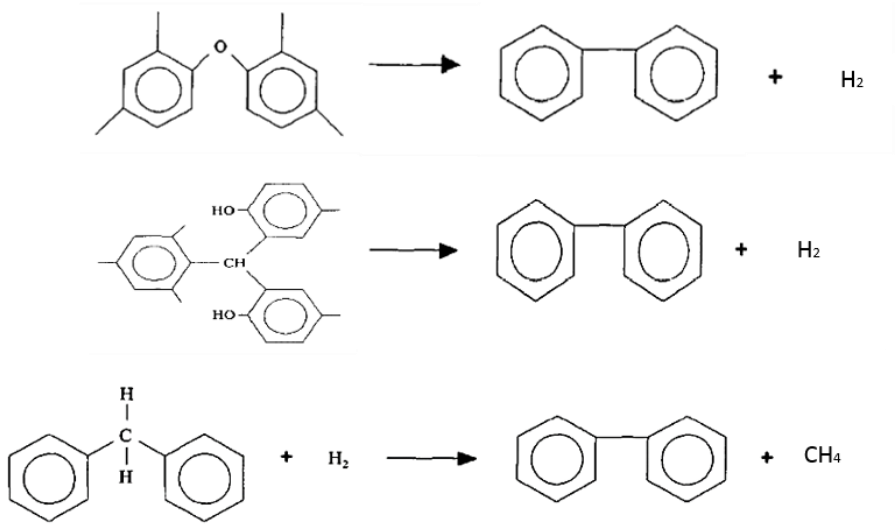

Figure 4. 4 Possible reactions taking place during main pyrolysis step.

In dehydrogenization step, according to literature remaining hydrogen atoms are removed from the ring structure and hydrogen gas is expected to evolve (Figure 4.5) [59]. At the end of the process, turbostratic carbon structure is obtained. According to the FTIR analysis of generated gas, in dehydrogenization step CO and H_2O were produced. Although H_2 is expected to be generated, it is not observed in the FTIR spectrum because of the infrared inactive characteristics of the H-H band. (Figure 4.2).

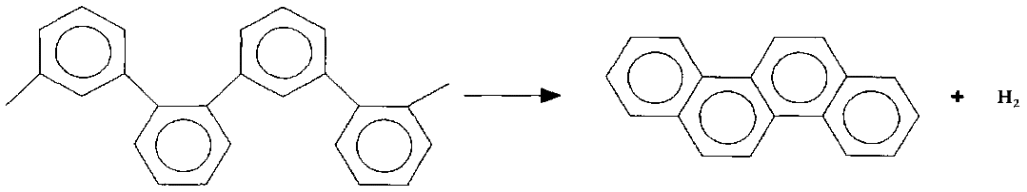

Figure 4. 5 Possible reaction during the dehydrogenization step.

There is no CO_2 formation in dehydrogenization step, because all of the the oxygen formed during earlier stages of pyrolysis is dissipated. Therefore, due to the absence of combustion reaction CO_2 formation does not exist.

4.1.2. Phase Evolution of the Phenolic Resin during Pyrolysis

The aim of the pyrolysis step is to convert the phenolic polymer matrix into carbon. In order to monitor the occurrence of this conversion, X-ray diffraction analysis results of as-received phenolic resin and phenolic resin pyrolyzed at 1000 °C were compared. As shown in Figure 4.6, the diffraction pattern of as-received phenolic resin points out to the presence of an amorphous structure with a broad peak at $2\Theta = 18.5°$, which is due to adjacent chains of the linear polymer [59]. Pyrolysis of the phenolic resin at 1000 °C resulted in glassy carbon formation. Its diffraction pattern shows two broad peaks corresponding to the (002) and (102) planes of turbostratic carbon structure (Figure 4.6(b)) [57].

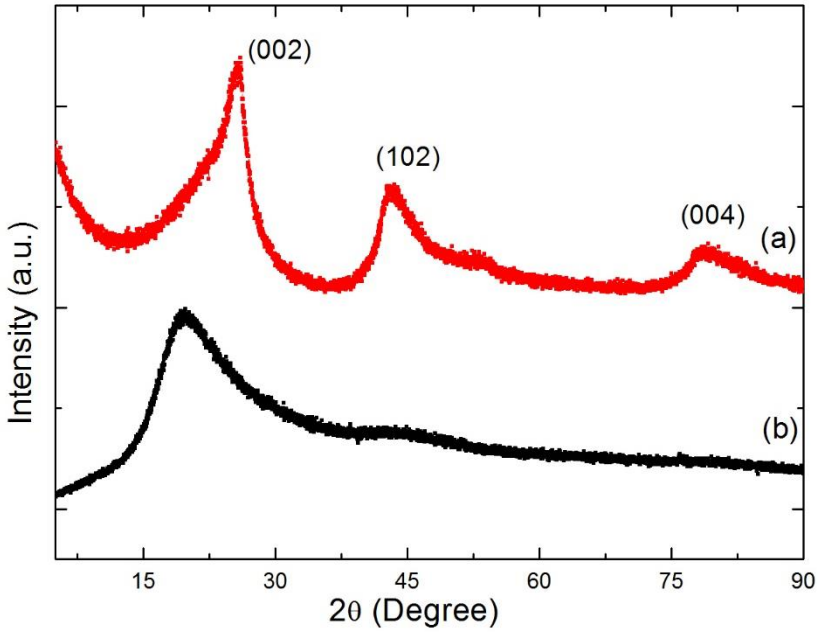

Figure 4. 6 XRD patterns of (a) the as-received phenolic resin, (b) phenolic resin pyrolyzed at 1000 °C.

It is important to investigate the effect of varying pyrolysis temperature on the carbonization process. Therefore, variation of XRD pattern in post curing step at different pyrolysis temperatures (100, 200, 300, 400 °C) were studied. It is seen in Figure 4.7 that diffraction pattern of non-pyrolyzed phenolic resin and those post cured at different temperatures have similar character of scattering showing a broad and asymmetric peak at approximately 18.5°. TGA and FTIR analysis also indicated that the chemical structure of the phenolic resin does not change significantly. Only additional crosslinks occurs during post curing step, and chemical structure still has 3D network being amorphous and glassy with higher crosslink density. Therefore, observing similar XRD patterns up to the pyrolysis temperature of 400 °C is meaningful (Figure 4.7).

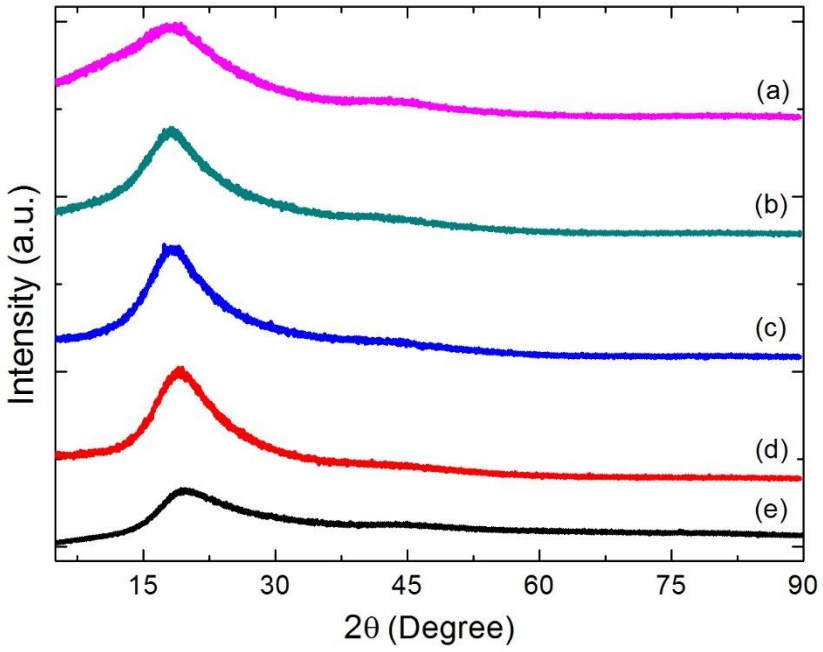

Figure 4. 7 XRD patters of pyrolyzed phenolic resin at different post curing temperatures at (a) 400, (b) 300, (c) 200, (d) 100 °C and (e) as-received phenolic resin.

After the main pyrolysis and dehydrogenization step it is observed that with increasing heat treatment temperature (002) peak shifts to the right, and also this peak gets sharper (Figure 4.8). Moreover, (102) and (004) peaks become more visible. As the peak shifts to the right, diffraction angle increases which is related to the decrease in the interlayer spacing between the ribbons with increasing pyrolysis temperature.

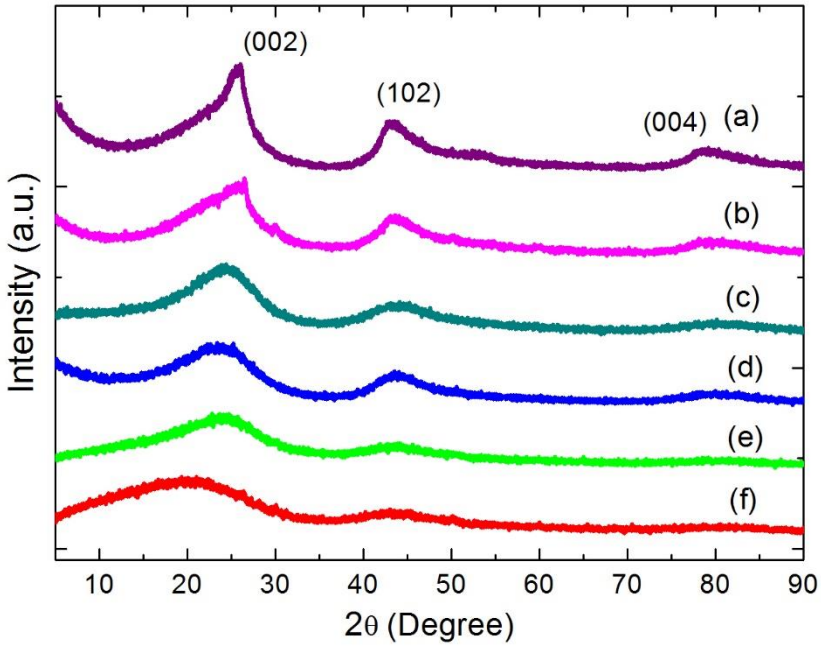

Figure 4. 8 XRD patterns of the phenolic resin pyrolyzed at different temperatures at (a) 1000, (b) 900, (c) 800, (d) 700, (e) 600, (f) 500 °C leading to main pyrolysis and dehydrogenization.

For 500°C pyrolysis condition, interlayer spacing between ribbons is 4.60 Å, and 3.46 Å at 1000°C (Table 4.2). Since in the literature interlayer spacing of turbostratic carbon structure has been reported as 3.44 Å [57], it can be said that with increasing pyrolysis temperature interlayer spacing of ribbons gets closer to the theoretical value. This can be explained by the tangled and coiled structure of the material pyrolyzed at 500 °C

containing aromatic molecules and methylene bridges, i.e. 3D network structure. During the main pyrolysis and dehydrogenization step, due to the elimination of the aromatic molecules and removal of hydrogen internal strain energy between the ribbons is gradually released.

Table 4. 2 Variation of the crystal parameters with pyrolysis temperature.

Pyrolysis Temperature (°C)	**d (002) (Å)**	**Lc (Å)**
500	4.60	10
600	3.90	11
700	3.80	12
800	3.65	12
900	3.52	13
1000	3.46	13

Moreover, crystallite size (Lc) of the pyrolyzed resin was calculated using Scherrer equation. Although these crystallite sizes do not give the exact value of the observed layer diameter of stacking, it is a commonly applied method in order to obtain relative values [61]. Smaller crystallite size means that 3D ordering does not take place. Moreover, with increasing pyrolysis temperature, it does not reach to higher values because, in turbostratic carbons there is no 3D ordering as in graphite (Figure 4.9).

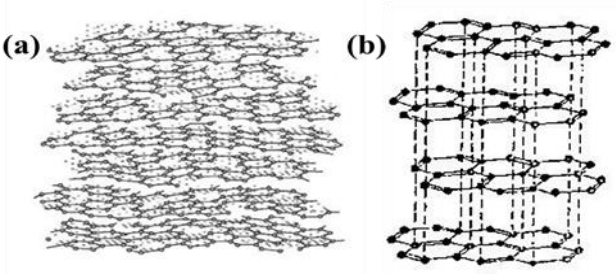

Figure 4. 9 Schematic representation of of (a) turbostratic carbon and (b) graphite structures [62].

4.2. Pyrolysis of CFRP

4.2.1 Open Porosity and Density of the C/C Preform

Open porosity and density are important control parameters for the C/C preform which were measured after every processing step. They were used for fundamental materials characterization serving as a quantitative parameter to assure quality. Morphology, size, type and content of the pores are critical parameters strongly affecting the densification behavior during the subsequent LSI process.

As it is clearly seen in Figure 4.10 and 4.11, respectively, with the increasing pyrolysis temperature, density of the C/C preform decreases while its open porosity is vice versa. At this point, it is important to note that the higher the density of the C/C preforms the more difficult is silicon infiltration during the following LSI process. In the lower density condition, content of the pores is higher leading to a higher probability of having available interface between the free carbon and the infiltrated Si. Therefore, the fraction of SiC formation, i.e. density of the resulting C-C/ SiC composite, is expected to increase with decreasing density of C/C preform.

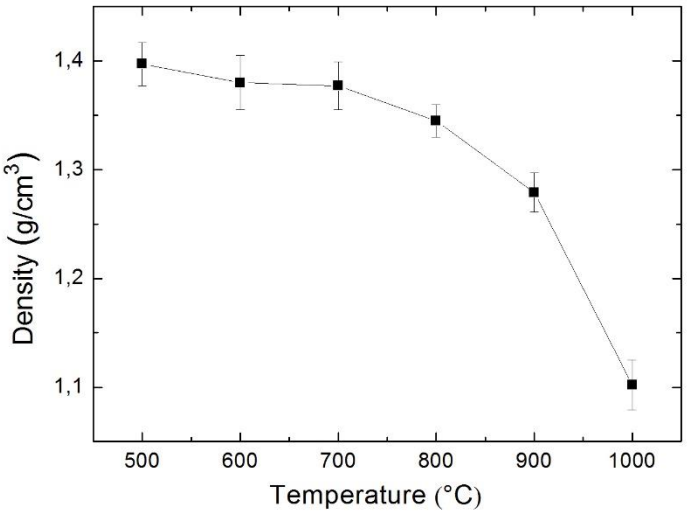

Figure 4. 10 Density of CFRP composites after pyrolysis at different temperatures.

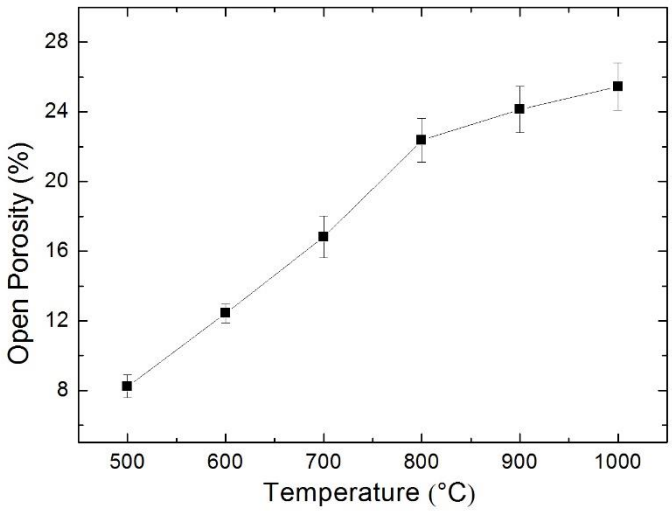

Figure 4. 11 Porosity of CFRP composites after pyrolysis at different temperatures.

4.2.2 Crack Pattern of the C/C Preform

Crack pattern is an important issue, because when the liquid silicon infiltrates into the carbon matrix of the C/C preform with capillary forces, it flows through these channels like cracks. Therefore, in order to achieve effective silicon infiltration, cracks must have optimum opening and distribution. If the opening of the crack is too small, SiC formed at the interface may act like an obstacle for the liquid silicon infiltration and hence it may make the infiltration of silicon into the inner parts difficult (Figure 4.12(a)). On the other hand, if the density of these cracks are too high, there is a possibility of having reaction between fibers and the liquid silicon. This high temperature reaction with liquid silicon may be detrimental for the reinforcement behavior of the fibers. Moreover, there must be no reaction between the reinforcement and the matrix material in composite materials, therefore, if liquid silicon reacts with carbon fibers, there will be no composite behavior remaining in the system. Therefore, crack pattern directly affects the mechanical properties of the resulting C/C-SiC composites [60].

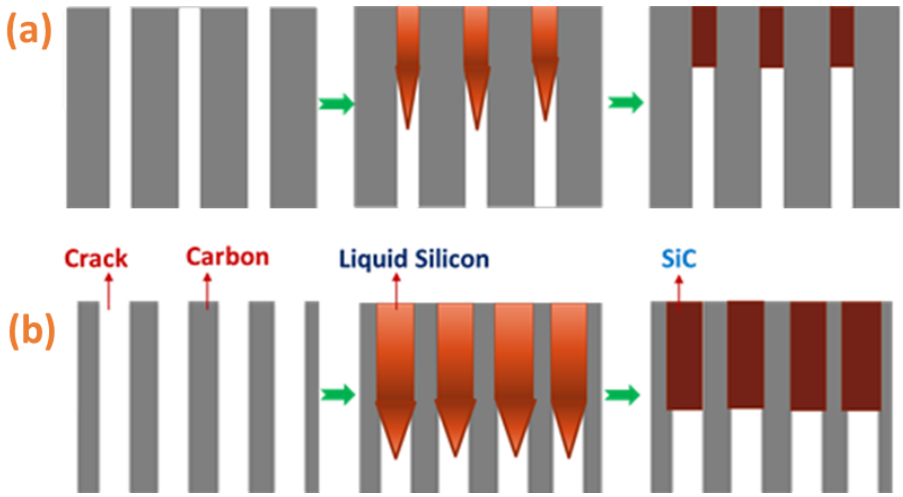

Figure 4. 12 Different silicon infiltration models for a) low porosity, high density and b) high porosity, low density C/C preform condition.

In order to investigate the effect of the pyrolysis temperature on the properties of the CFRP composites, different pyrolysis temperatures were used throughout this study. When the SEM micrographs of the pyrolyzed preforms are compared, it is seen that non-pyrolyzed condition does not contain any crack and pore initially, Figure 4.14(a). After pyrolysis at 500 °C, some pores started to be observed in the matrix, Figure 4.14(b). Formation of these pores can be attributed to the evolution of different gases (solvent, monomer, steam etc) during extended curing, which are trapped in the matrix [61]. Furthermore, at the beginning of pyrolysis huge amount gases also evolve from the converting matrix which are also entrapped in the structure. This may cause the formation of new pores and enlarge existing ones [62]. It is seen that, pyrolysis at 600 °C results in debonding at the fiber and matrix interface (Figure 4.14(c)). Weak fiber-matrix interface due to Wan-der-Waals interactions along with the pores and pore channels frequently existing at the interface may have caused debonding at this temperature [63]. During this process chemical or secondary bonds between the fibers and matrix material are broken. Moreover, at the fiber and matrix interface existence of normal and shear stresses may cause decrease in the strength of the matrix [64].

Despite the presence of this type of cracks, reinforcement material is still strong, while the interface and the matrix is becoming weaker. At 700°C, partial delamination and microcracks are observed in the matrix, Figure 4.14(d). At 800 and 900°C, transversal cracks are observed in the matrix, Figure 4.14(e) and (f). These cracks are developed due to interconnection mechanism in which the present crack is developing by interacting with the debonding initiation, propagation and interconnection the minimizing the energy [65]. Crack opening of the specimens were tried to be determined using SEM micrographs (Figure 4.13). As mentioned prior crack formation is started at approximately 600 °C, in the range of main pyrolysis region. It is seen that with increasing pyrolysis temperature crack opening increases, and from 800 °C it shows nearly linear behavior. This phenomenon is important for the effectiveness of the liquid silicon infiltration process.

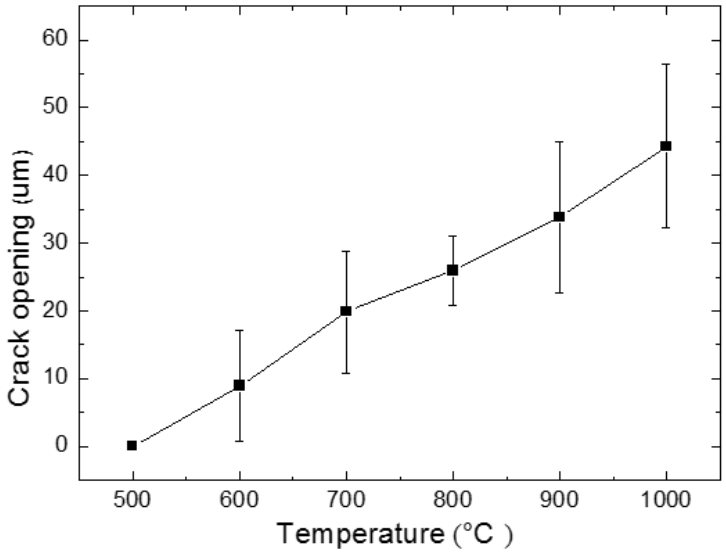

Figure 4. 13 Crack opening of C/C preforms after different pyrolysis temperatures.

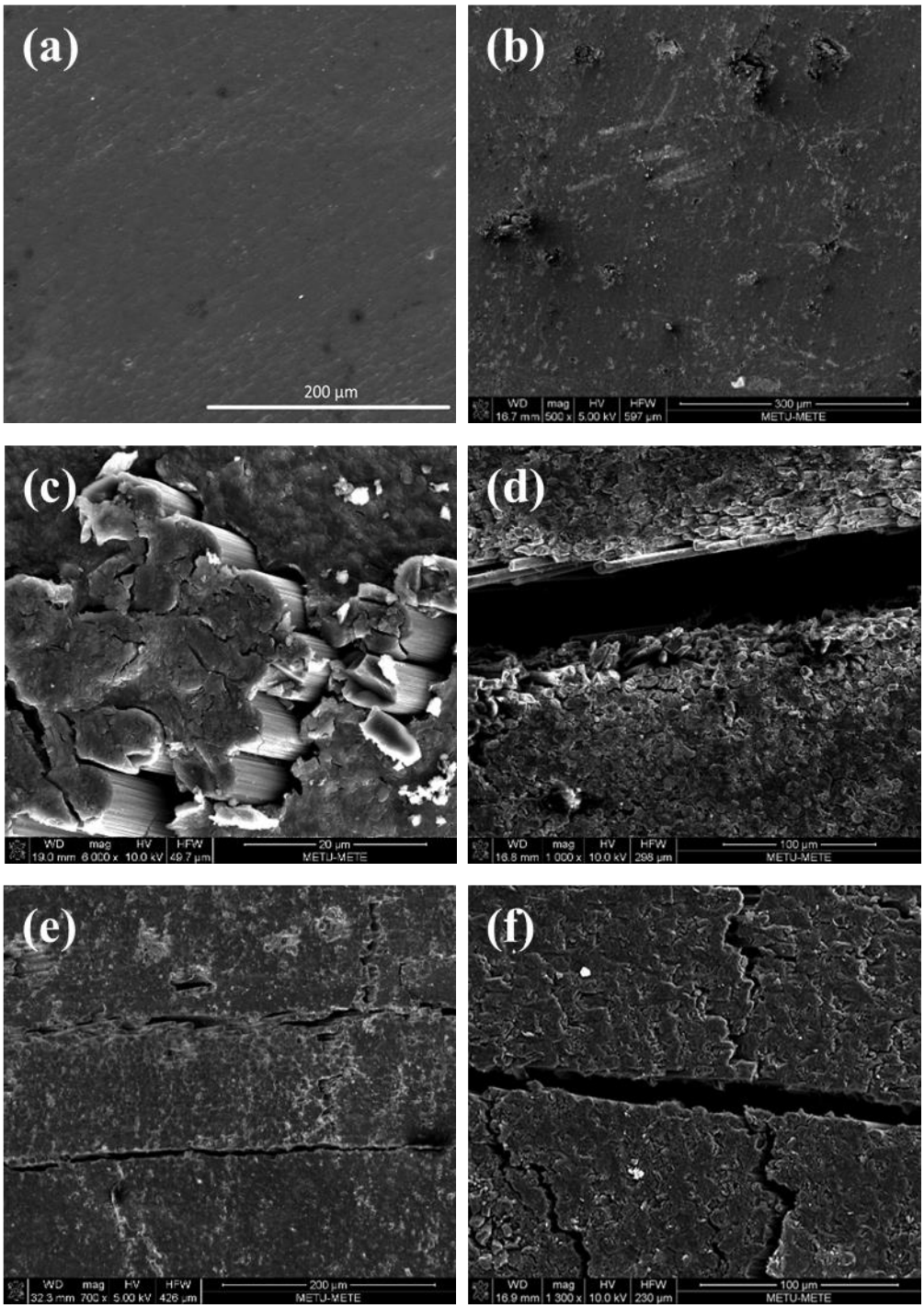

Figure 4. 14 SEM micrographs of CFRP composites pyrolyzed at different temperatures: (a) non-pyrolyzed, (b) 500 °C, (c) 600 °C, (d) 700 °C, (e) 800 °C and (f) 900 °C.

4.2.3 Effect of Pyrolysis on the Mechanical Behavior of the C/C Preforms

Mechanical properties and fracture behavior of the C/C preforms pyrolyzed at different temperatures were studied using three point bending test. As it is seen in Figure 4.15, pyrolysis affects the mechanical strength of the initial CFRP composite and the C/C preforms, which change significantly with the pyrolysis temperature. Expectedly, with increasing pyrolysis temperature, flexural strength of the CFRP composite and that of the C/C preforms degrade. While converting the phenolic polymer matrix into free carbon via pyrolysis, the composite behavior of the CFRP diminishes. This is caused by the lack of load transfer from the matrix to the fibers which lose their contact at the vanishing interface. Consequently, fracture in the C/C preforms occurs at lower strains.

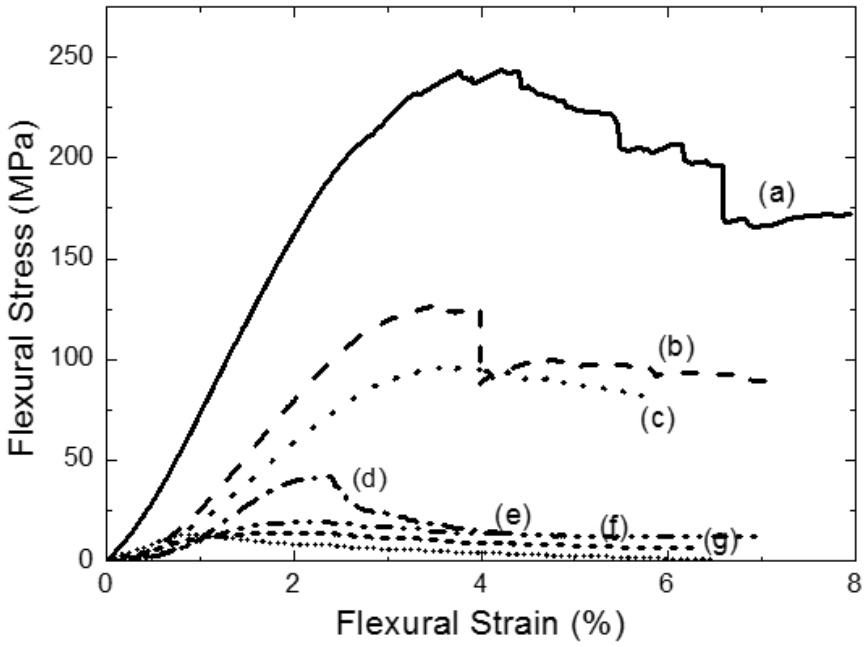

Figure 4. 15 Flexural stress vs Flexural strain curves of CFRP composites pyrolysed at different temperatures: (a) non-pyrolyzed, (b) 500, (c) 600, (d) 700, (e) 800, (f) 900 and (g) 1000 °C.

4.3. Determination of the Optimum Liquid Silicon Infiltration Process Parameters

4.3.1. Effect of Pyrolysis Temperature on the LSI Process

In this part of the study, the influence of pyrolysis temperature on the densification behavior of liquid silicon infiltration process is presented. C/C preforms pyrolyzed at various temperatures were silicon infiltrated at 1550 °C under argon atmosphere.

Table 4. 3 Density and porosity of the C/C preforms pyrolyzed of 700, 800, 900, 1000°C and C/C-SiC composites silicon infiltrated at 1550 °C under argon atmosphere.

	C/C Preform			**C/C-SiC Composite**	
	Average Crack Opening (μm)	**Density (g/cm^3)**	**Open Porosity (%)**	**Density (g/cm^3)**	**Open Porosity (%)**
700P	19.85 ± 9.80	1.37	16.8	1.23	24.1
800P	25.92 ± 5.08	1.34	22.3	1.32	21.4
900P	33.80 ± 11.20	1.27	24.1	1.44	20.9
1000P	44.04 ± 12.32	1.10	25.4	1.47	16.1

As stated in Table 4.3, with increasing pyrolysis temperature density of the C/C preform decreases, while their porosity is vice versa. After the application of the silicon infiltration process it is expected that the density of the resulting composite must increase, because forming silicon carbide (3.21 g/cm^3) has higher density than the initial amorphous carbon (1.8 g/cm^3). Improvement in the final composite density was obtained for 800, 900 and 1000 °C pyrolysis conditions. Although for the 700 °C pyrolysis case, density of the preform decreases and porosity of the preform increases after the infiltration. As mentioned 700 °C pyrolysis case belongs to main pyrolysis

where the dehydrogenization part of the pyrolysis has not been completed, and the preforms still contain some compounds which can evolve at higher pyrolysis temperatures. During the infiltration, rest of the pyrolysis may occur and evolving gases may prevent the infiltration of the liquid silicon. Moreover, rapid temperature change may also produce extra crack formation. As shown in Figure 4.16(b), after the silicon infiltration composite material has higher crack width. Calculated average crack width 48 μm after infiltration verifies the occurrence of this extended pyrolysis.

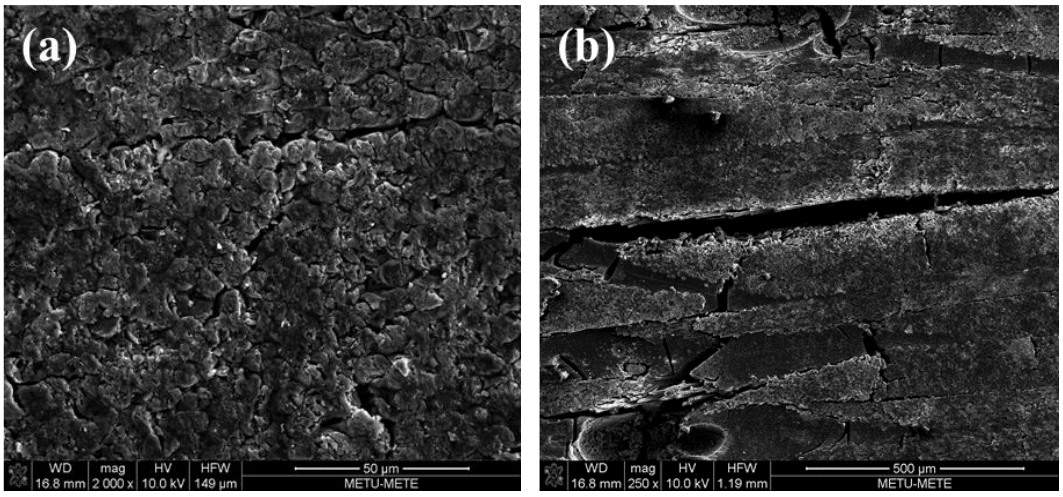

Figure 4. 16 SEM micrographs of C/C preform after (a) pyrolysis at 700 °C, (b) silicon infiltration at 1550 °C.

Besides, if the polymeric matrix material is not completely converted to turbostratic carbon and contains excess polymeric compounds, additional oxidation products evolve. SEM micrographs (Figure 4.17) and EDS analysis results (Figure 4.18) show that SiO_2 and unreacted Si are present in the microstructure. Residual Si may react with the oxygen in the furnace at relatively low temperatures (900-1200 °C) and a thin film of amorphous silicon dioxide may form [66]. Even though this is the case, XRD analysis (Figure 4.19) of silicon infiltrated C/C-SiC composite does not reveal any

SiO_2 peak, because of its amount should be lower than % 5 in the residual powder. This shows that there is some oxygen present in the controlled atmosphere of the furnace during the experiments.

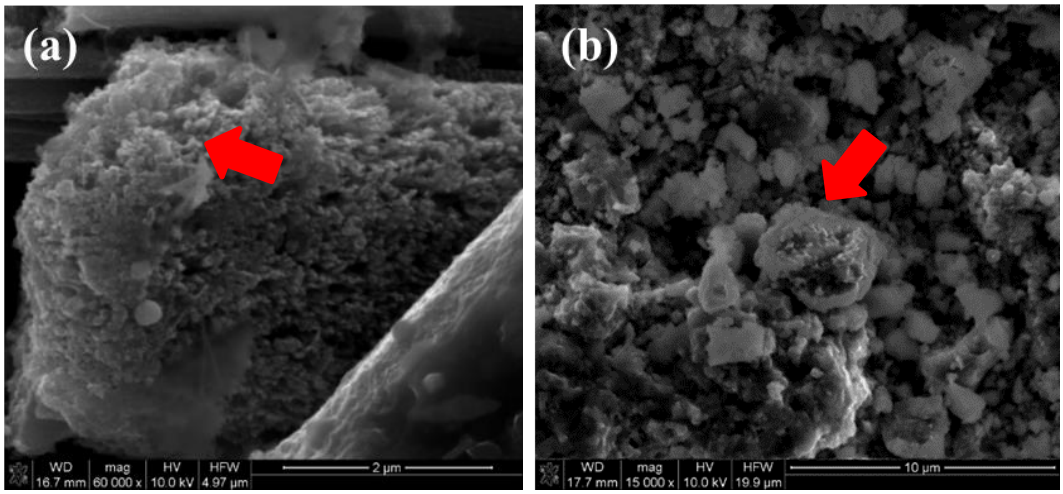

Figure 4. 17 SEM images of (a) SiO_2 formation (b) residual silicon present in the microstructure of 700P C/C preform silicon infiltrated at 1550 °C.

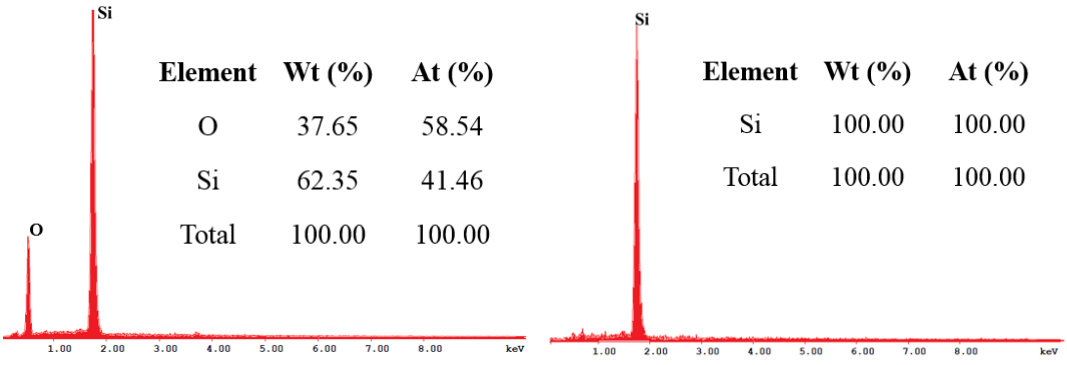

Figure 4. 18 EDS results of 700P C/C preform silicon infiltrated at 1550 °C consisting (a) SiO_2 and (b) residual silicon.

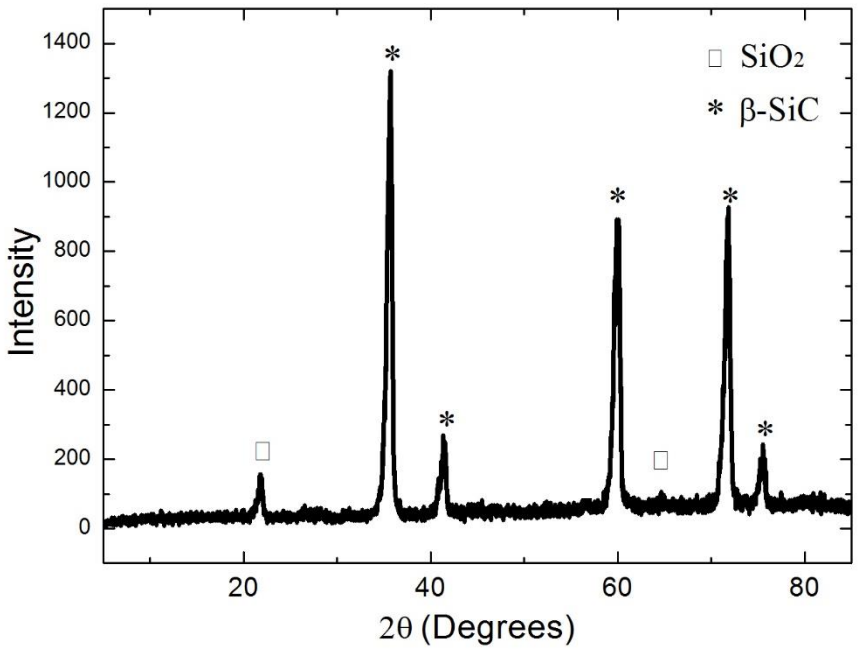

Figure 4. 19 XRD diffractogram of residual powder obtained after silicon infiltration of 700P C/C preform at 1550 °C.

As it is shown both in Table 4.3 and Figure 4.21, with decreasing C/C preform density, density of the final C-C/SiC composite increases. As previously discussed in Section 4.2, increasing of pyrolysis temperature results in C/C preforms with lower density, higher porosity and higher crack opening leading to improved densification of silicon infiltrated composites. However, densification by silicon infiltration has been obtained in C/C preforms pyrolyzed at temperatures above 800 °C. For all pyrolysis temperatures after silicon infiltration outer and inner parts of the resulting C/C-SiC composites reveal different microstructures. This is because, liquid silicon is not able to reach to the inner parts of the C/C preform. Only at the outer regions of the C/C preform SiC formation was observed while inner parts of the composite still contain untransformed carbon matrix. Figure 4.20 (d), (e), (f) represent microstructures from

the outer parts of the silicon infiltrated composite which contain carbon fibers and SiC matrix. In the case of the inner regions of the silicon infiltrated composites shown in Figure 4.20 (a), (b) and (c) SiC does not exist and, carbon fibers seem to be damaged due to high temperature treatment during silicon infiltration.

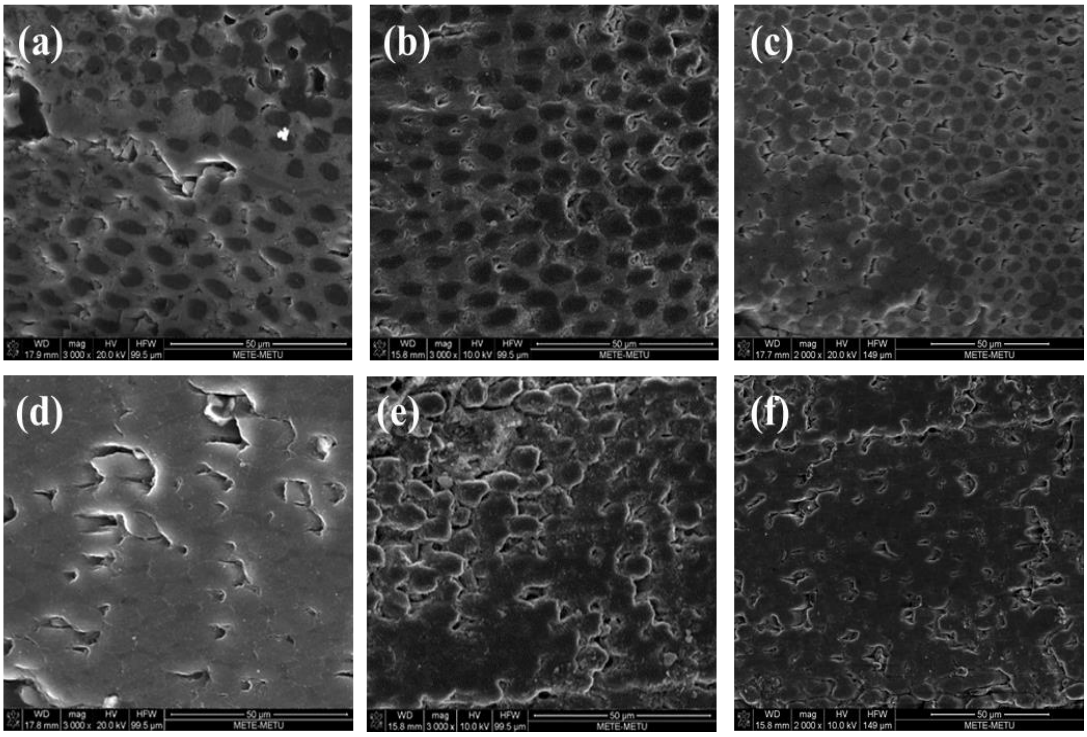

Figure 4. 20 SEM micrographs of silicon infiltrated preforms pyrolyzed at a,d) 800, b,e) 900 and c,f) 1000 °C where a,b,c are taken from the inner regions and d,e,f from the outer regions of the composite cross-sections.

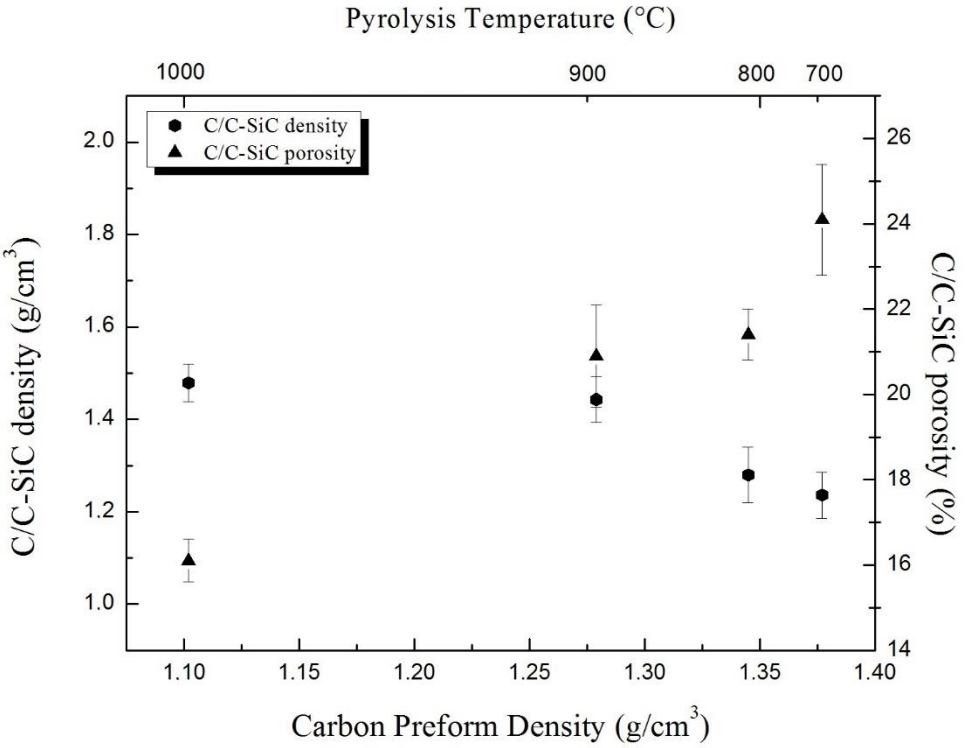

Figure 4. 21 Relationship between C/C preform density and C/C-SiC composite density/open porosity.

XRD analysis of C/C-SiC composites obtained by silicon infiltrating the C/C preforms pyrolyzed at 800, 900 and 1000 °C in which relatively high densification is achieved was conducted on their cross sections, Figure 4.22. For all of the samples, existing phases are carbon which has a wide peak around 26 ° and beta silicon carbide with the corresponding diffraction peaks. Carbon has a wide peak because it contains both turbostratic carbon existing in the matrix and the carbon fibers existing at the cross section of the specimen. Silicon and SiO_2 peaks are not observed in the diffraction data, therefore, it can be said that all of the silicon infiltrated into the C/C preform has reacted with the carbon matrix and has formed silicon carbide. Moreover, for all of the silicon infiltrated composites it can be said that pyrolysis steps are completed successfully at 800, 900 and 1000 °C. In order words polymeric matrix has been

converted to turbostratic carbon completely and matrix did not contain any non-carbon species which may have produced oxidation products like CO_2, CO or H_2O during the infiltration process.

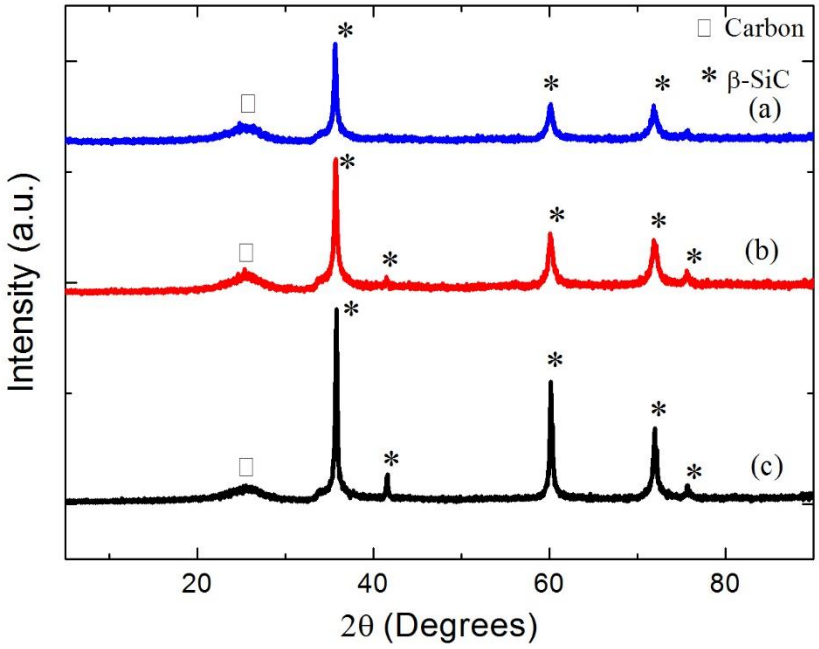

Figure 4. 22 XRD results of C/C-SiC composites obtained from C/C preforms pyrolyzed at (a) 800, (b) 900, (c) 1000 °C.

In order to get information about the weight percentages of the phases which exist in the XRD analysis, "Rietveld Analysis" was conducted. Although this method is not commonly applied to bulk materials containing oriented fibers, it can be useful for having relative information about the weight fraction of the phases. In Table 4.4, it can be seen that with increasing pyrolysis temperature amount of SiC formed increases. This is because with increasing pyrolysis temperature crack width and porosity increases in the C/C prefrom and more effective silicon infiltration is obtained.

Table 4. 4 Rietveld Analysis of C/C-SiC composites that silicon infiltrated under argon atmosphere.

	SiC (Wt. Frac.)	**C (Wt.Frac.)**
800P1550LSI-A	0.11	0.89
900P1550LSI-A	0.33	0.67
1000P1550LSI-A	0.37	0.53

In order to observe the effect of pyrolysis temperature of the C/C preforms on silicon infiltration depth, resulting C/C-SiC composites were cut and their central cross sections were examined using EDS line analysis (Figure 4.23) and SEM micrographs. SEM micrographs were taken for all pyrolysis temperatures from the outer and inner regions of the composites to get information about the microstructural variations. Calculated average silicon infiltration depth values are given in Table 4.5. C/C preform that pyrolyzed at 700 °C is not included during this investigation because of XRD analysis and SEM micrographs after infiltration did not reveal any evidence about SiC formation for this pyrolysis temperature. Results obtained from both EDS analysis and SEM examination are consistent with each other such that with increasing pyrolysis temperature, (increase in crack opening and porosity content of the preforms) silicon infiltration depth increases.

Table 4. 5 Infiltration depth values of liquid silicon in C/C-SiC composites.

Specimen	**Infiltration depth (µm)**
700P	N.A
800P	112.1±65.1
900P	285.6± 86.3
1000P	409.6 ± 124.9

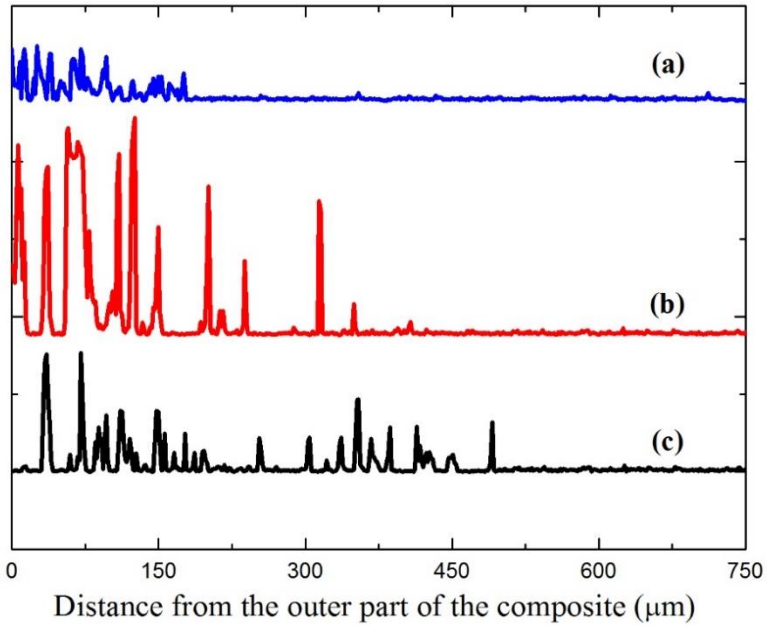

Figure 4. 23 EDS line analysis of silicon in the C/C-SiC composites from the outer surface for C/C preforms pyrolyzed at (a) 800, (b) 900, (c) 1000 °C.

C/C preforms pyrolyzed at different temperatures were not successfully infiltrated under argon atmosphere, where spontaneous wetting is the only driving force, which gives rise to infiltration of the liquid silicon into the micro cracks and pore channels of the preform [67]. All of the specimens were exposed to so called choking-off of the pores and cracks. The ideal C/C preform for effective liquid silicon-carbon reaction should have sufficient amount of porosity and cracks to allow efficient infiltration of liquid silicon. Proper crack sizes and a narrow crack size distribution are also important for liquid silicon infiltration [68]. The cracks must be large enough to allow capillary force to overcome liquid silicon viscosity to achieve total crack filling by the SiC formation. However, if the cracks are too large, the silicon carbide formed would not effectively fill in the cracks, therefore, unreacted silicon may exist inside the cracks. Considering XRD analysis and SEM micrographs indicating that silicon does not exist

in the microstructure, it can be said that calculated average crack size values are not too large for efficient infiltration. On the contrary, for all of the preforms, crack openings seem to be too small that capillary forces cannot overcome the viscosity of the liquid silicon correspondingly compared to insufficient crack sizes reduce infiltration rate [67]. Having lower infiltration rate than reaction rate gives rise to crack choking by the silicon carbide formation early in the reaction at the outer regions of the C/C preforms obtained from preforms pyrolyzed at temperatures higher than 700 °C. Therefore, choking blocks further flow of the liquid silicon into the inner parts of the C/C preform and terminates the reaction inside the preform (Figure 4.24) [69]. Consequently, cracks in the C/C preform must have an optimum value for the silicon to react with the interior regions of the preform by having higher infiltration rate than reaction rate to allow complete conversion of silicon carbide.

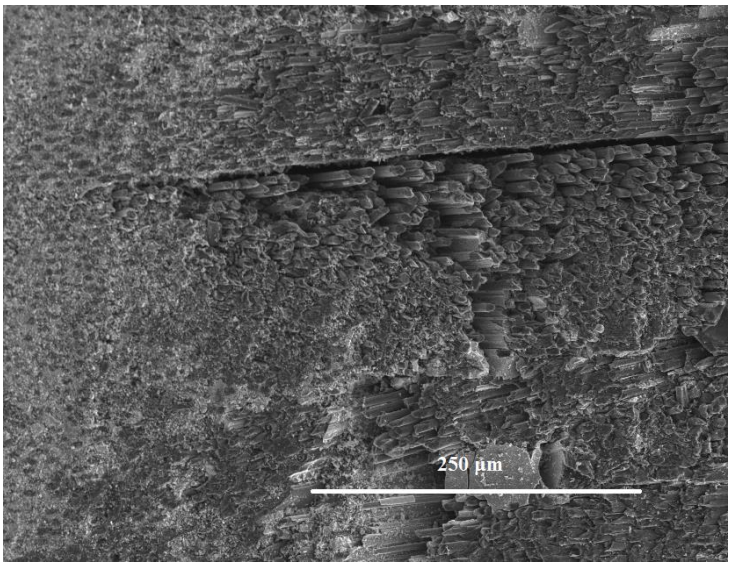

Figure 4. 24 SEM micrographs representing the choking-off crack of the preform pyrolyzed at 900 °C and then silicon infiltrated at 1550 °C.

As mentioned in Section 4.2, increasing pyrolysis temperature leads to preforms with lower density, higher porosity and higher crack opening resulting in improved densification of the C/C-SiC composites by providing high infiltration rates. This is to say that C/C preforms having higher average crack sizes provide higher infiltration rate and hence higher possibility to have reaction between liquid silicon and carbon matrix to form denser SiC phase.

4.3.2. Effect of Pressure vs. Vacuum on the Efficiency of LSI Process

In order to investigate the effect of vacuum and pressure in the controlled atmosphere on the efficiency of liquid silicon infiltration, C/C preforms pyrolyzed at 1000 °C (1000P), which have nearly same amount of porosity, density and crack width, were silicon infiltrated at 1550 °C under argon atmosphere (1000P1550LSI-A) or in vacuum (1000P1550LSI-V).

Table 4. 6 Density and open porosity comparisons of silicon infiltrated preforms under argon atmosphere and vacuum.

Property	**1000P**	**1000P1550LSI-V**	**1000P1550LSI-A**
Density (g/cm^3)	1.10	1.58	1.48
Open Porosity (%)	25.46	8.89	16.13

As it is seen in Table 4.6, C/C preform pyrolyzed at 1000 °C has a density of 1.10 g/cm^3 and porosity content of 25.46 %. After the infiltration at different atmospheric conditions, for both of the cases due to the chemical reaction at the interface of carbon and liquid silicon, some amount of SiC was formed in the matrix, therefore, density of the preform has increased as opposed to its porosity content. The increase in the density of the preform infiltrated in vacuum is higher than that of the one infiltrated under argon atmosphere. Porosity reduction compared to just pyrolyzed preform, is 65.08% and 36.65% after silicon infiltration in vacuum and under argon, respectively.

Although both preforms have same crack opening, in the case of infiltration in vacuum cracks were not chokked-off, consequently liquid silicon was infiltrated to the inner regions of the material. SEM micrographs (Figure 4.25), EDS mapping (Figure 4.26) EDS line analysis (Figure 4.27) represent that not only the outer regions but also the inner regions of the composite reveal SiC formation. Even though, SiC formation has been achieved during silicon infiltration at 1550 °C in vacuum in the inner parts of the preforms pyrolyzed at 1000 °C, still the existing cracks could have not been filled entirely (Figure 4.25(b)), despite the supporting effect of the accompanying volume expansion due to SiC formation [70].

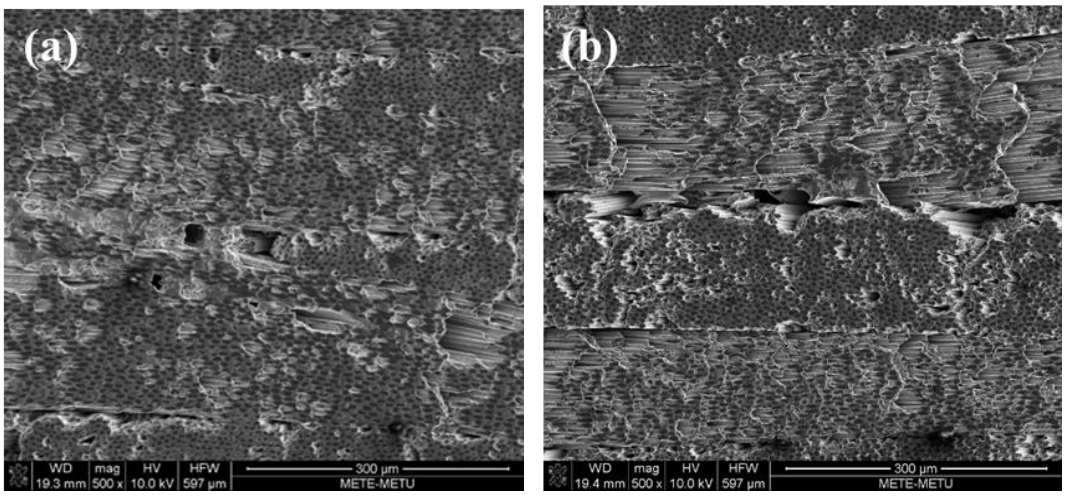

Figure 4. 25 SEM micrographs of 1000P1550LSI-V C/C-SiC composite containing micro cracks and pores in the (a) outer regions, (b) inner regions.

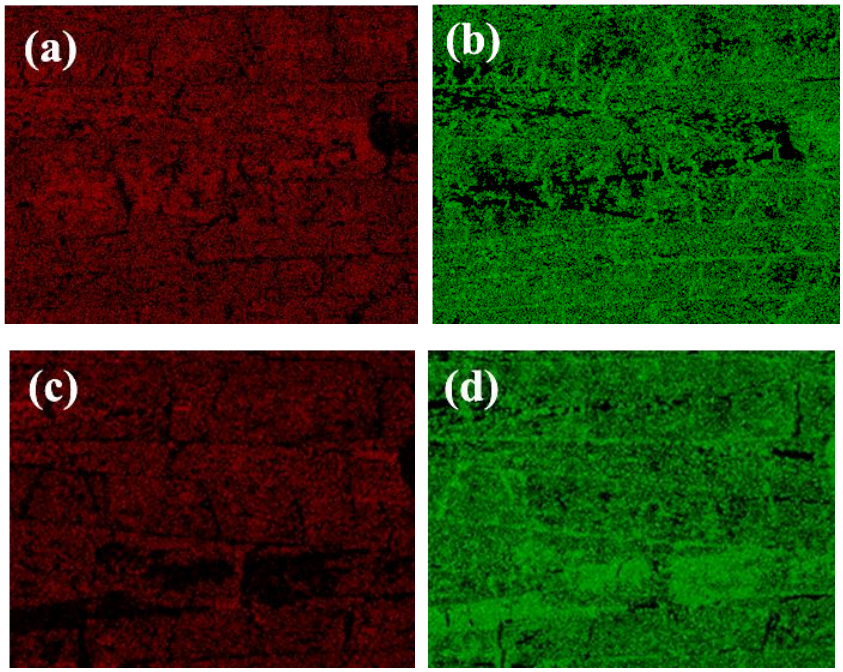

Figure 4. 26 (a) Carbon mapping at 200 μm (b) Silicon mapping at 200 μm (c) Carbon mapping at 700 and (d) Silicon mapping at 700 μm from the outer surface.

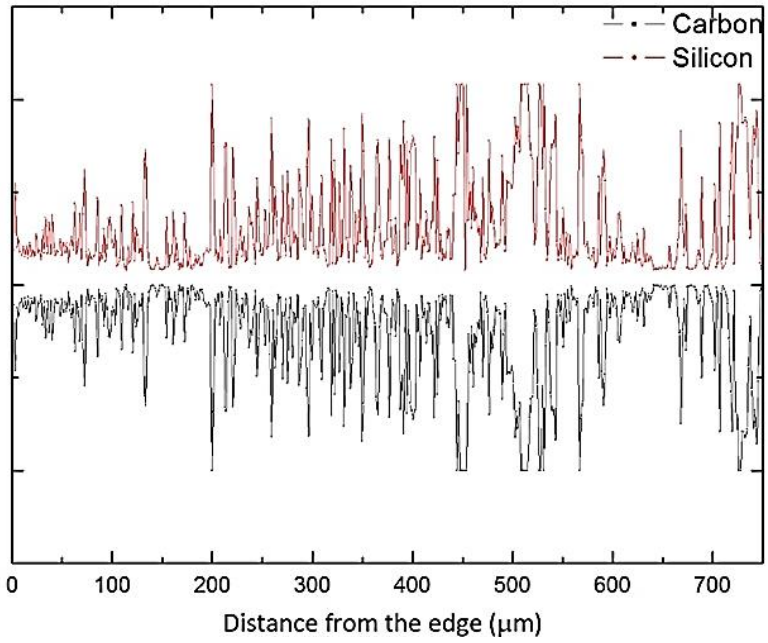

Figure 4. 27 EDS silicon and carbon line analysis of the C/C-SiC composite from its outer surface.

The XRD patterns of composites silicon infiltrated in different atmospheres are shown in Figure 4.28. It is clear that both composites are composed of carbon and β-SiC. No residual silicon exists in the resulting composites, indicating that all of the infiltrated silicon has reacted with carbon. Intensities of the corresponding peaks are different, even (200) peak of β-SiC does not exist under argon condition. These different diffraction intensities at the same 2Θ angles reveal information about the quantitative phase analysis. Rietveld analysis was applied to obtain information about the relative weight fractions of the phases. According to this analysis while for argon atmosphere weight fraction of SiC and carbon are 0.37 and 0.53 respectively, those for vacuum are 0.54 and 0.46, respectively (Table 4.7). Carbon weight fractions include the carbon from both the matrix and the fibers in the composite.

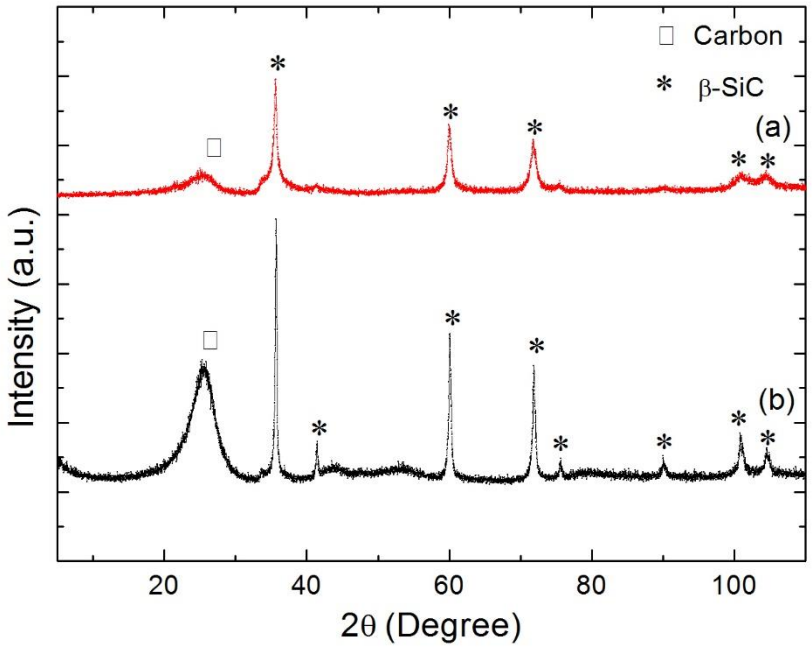

Figure 4. 28 XRD analysis of C/C-SiC composites silicon infiltrated under (a) argon atmosphere and (b) in vacuum.

Table 4. 7 Rietveld analysis of the C/C-SiC Composites silicon infiltrated at 1550 °C and under different atmosphere conditions.

	SiC (Wt. Frac.)	**C (Wt.Frac.)**
1000P1550LSI-A	0.37	0.53
1000P1550LSI-V	0.54	0.46

As it is seen, containing the same amount of porosity, density and crack width composites silicon infiltrated at the same temperature, reveal different infiltration depths under different controlled atmospheres. In vacuum, infiltration depth increases and with a high degree of SiC formation. Although XRD diffractograms of the composites does not show any SiO_2 peaks, surface oxidation of silicon under argon atmosphere is more possible than in vacuum. As a result, SiO_2 formed because of oxidation may have prevented the effective wetting of the carbon matrix. According to Ellingham diagram an oxygen partial pressure in the order of 10^{-6} atm is sufficient to oxidize the silicon surface. Vacuum atmosphere may prevent formation of volatile SiO_2, therefore, it can help deoxidation of the surface.

The more possible reason is that driving force for SiC formation is capillary effect. Capillary infiltration depends on the equilibrium between 3 phases: solid-liquid-gas. If the one component changes (vacuum versus ambient atmosphere), capillary effect also changes [71]. For infiltration process surface tension is constant for vacuum and atmosphere condition and radii of curvature depends on the pressure difference in the atmosphere. Under argon atmosphere condition, penetration of liquid silicon is hindered by the pressure barrier, and hence, liquid silicon has lower radius of curvature. On the contrary, under vacuum the radius of the curvature will be high due to the absence of pressure barrier. Therefore, it may be stated that the presence of a gas phase at Ar-Si-C triple line should hinder the penetration of the liquid phase, in other words, the reduction of argon pressure at Ar-Si-C triple line leads to enhanced silicon infiltration.

4.3.3 Effect of Infiltration Temperature on the LSI Process

In order to study the effect of the liquid silicon infiltration temperature on the identical densification properties of the resulting composites, C/C preforms pyrolyzed with similar processing variables were silicon infiltrated under vacuum at 1550 and 1650 °C. It is seen in Table 4.8 that, there is an increase in C/C-SiC composite density with increasing infiltration temperature where amount of pore filling by formed silicon carbide formation is higher. Moreover, comparing the SEM micrographs (Figure 4.29), it is seen that crack and pore contents are less in samples infiltrated at higher temperatures.

Table 4. 8 Density and porosity comparison of C/C-SiC composites silicon infiltrated at two different temperatures.

Property	**1000P**	**1000P1550LSI(V)**	**1000P1650LSI(V)**
Density (g/cm^3)	1.10	1.58	1.68
Open Porosity (%)	25.45	8.89	6.32

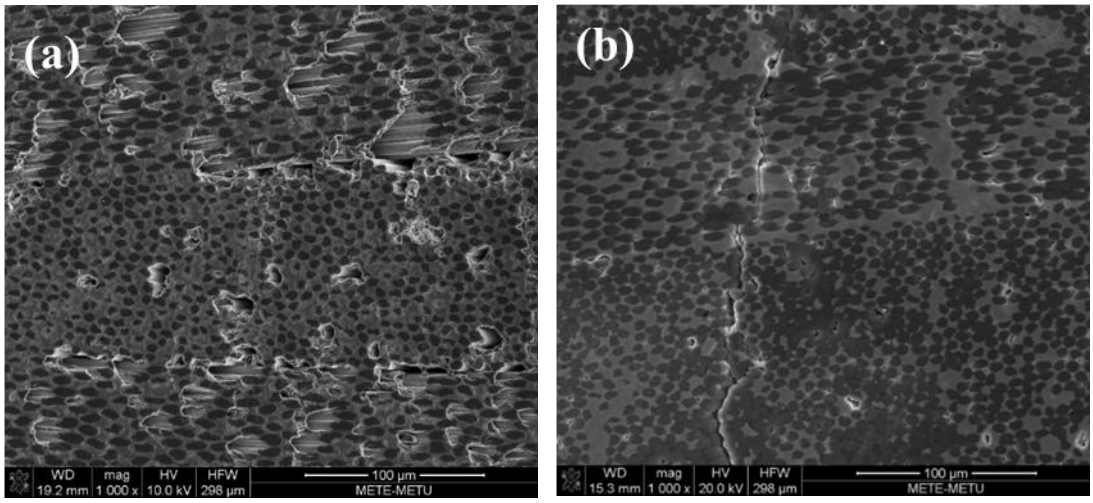

Figure 4. 29 SEM micrographs of the C/C-SiC composites silicon infiltrated at different temperatures of (a) 1550 °C and (b) 1650 °C.

The XRD patterns of composites 1000P1550LSI(V) and 1000P1650LSI(V) are presented in Figure 4.30. As is clear from their diffractograms, composites are composed of carbon and β-SiC, and diffraction peaks of silicon and silicon dioxide do not exist. As at the higher infiltration temperature composite have more ability to fill the cracks by silicon carbide formation, higher amount of SiC weight fraction was observed in the composite infiltrated at higher temperatures as expected, Table 4.9.

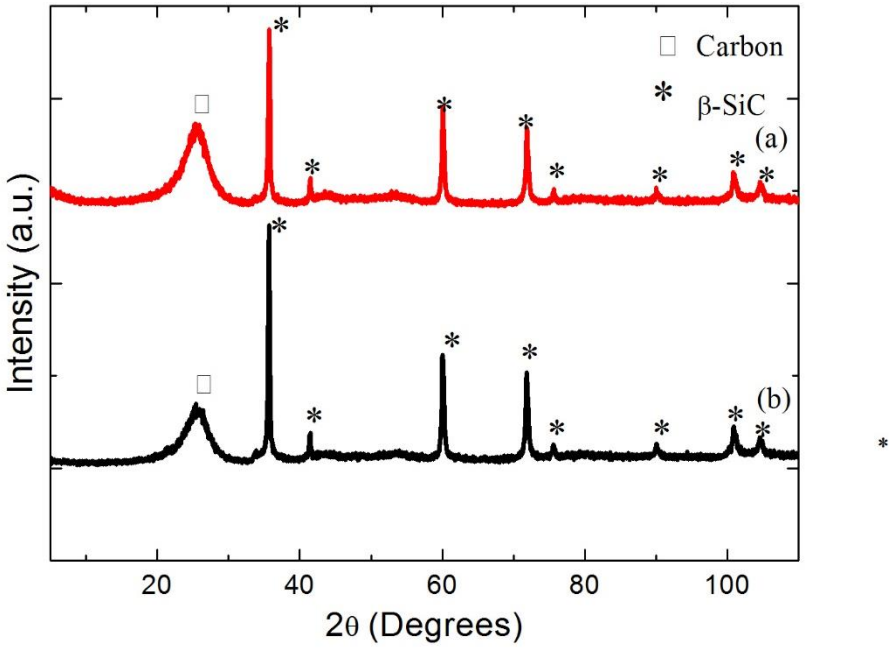

Figure 4. 30 XRD analysis of C/C-SiC composites silicon infiltrated at different temperatures of (a) 1550 °C and (b) 1650 °C

Table 4. 9 Rietveld Analysis results of C/C-SiC composites silicon infiltrated at different temperatures (a) 1550 and (b) 1650 °C.

	SiC (Wt. Frac.)	**C (Wt.Frac.)**
1000P1650LSI-V	0.71	0.29
1000P1550LSI-V	0.54	0.46

Achieving better densification characteristics via sufficient filling of the cracks and pores at higher silicon infiltration temperature can be attributed to the higher infiltration rate obtained. At the higher temperature, lower viscosity liquid silicon is expected to flow faster through the cracks and pores in the preform. According to literature viscosity of liquid silicon changes between 5.10 x 10^{-4} - 7.65 x 10^{-4} Pa.s at 1550 °C and 4.59 x 10^{-4} - 6.38 x 10^{-4} Pa.s at 1650 °C, respectively [72].

Furthermore, dynamic contact angle which directly affects the wetting ability of liquid silicon on the carbon surface was found to increase with increasing viscosity. Viscous forces tend to oppose wetting by working against wetting slowing down the reaction rate which wetting line approaches to its equilibrium position [73].

Moreover, effects of viscosity on the liquid silicon infiltration rate may be expressed by Darcy equation [74] [75].

$$x^2 = \left[\frac{2K}{\mu(1-V_f)} \Delta P \right]^2 t^2$$

where x = infiltration depth, K= permeability of the preform, V_f= fiber amount of the preform, ΔP= pressure difference, μ= viscosity of the liquid silicon and t= infiltration time. According to this equation it may be stated that under constant permeability of the preform and pressure conditions, infiltration depth increases with decreasing viscosity of the liquid under consideration. Therefore, in the current case higher infiltration depth at constant process time achieved at higher temperature, in other words higher rate of infiltration, gave rise to more efficient filling of the cracks and pores in the C/C preform.

4.2.4 Optimum Liquid Silicon Infiltration parameters

To sum up, taking into consideration of all parameters that directly affect the efficiency of the liquid silicon infiltration process, in order to obtain better densification pyrolysis must be applied at 1000 °C and following, silicon infiltration of the C/C preforms must be conducted at 1650 °C in vacuum atmosphere.

As mentioned in Chapter 2, LSI process is composed of three main stages. The first stage is CFRP production where as-received CFRP microstructure is shown in Figure 4.31(a) that contains no cracks and pores. Density of the as-received CFRP was measured as 1.35 g/cm^3 (Table 4.10). The second stage is pyrolysis of CFRP where the polymeric matrix is converted to turbostratic carbon. As discussed earlier in this study optimum pyrolysis temperature resulting in efficient silicon infiltration was determined as 1000 °C in order to achieve optimum crack size, density, porosity parameters which directly affects the progress of LSI. After pyrolysis at 1000 °C, C/C preform microstructure contains microcracks (Figure 4.31(b)) and, it has a density of 1.12 g/cm^3 (Table 4.10). At the final stage, liquid silicon infiltration of the C/C preform is applied using the determined optimum parameters through this study. Resulting the microstructure of the C/C-SiC composite contains carbon fibers and SiC matrix (Figure 4.31(c)), where its density of the composite increases to 1.68 g/ cm^3.

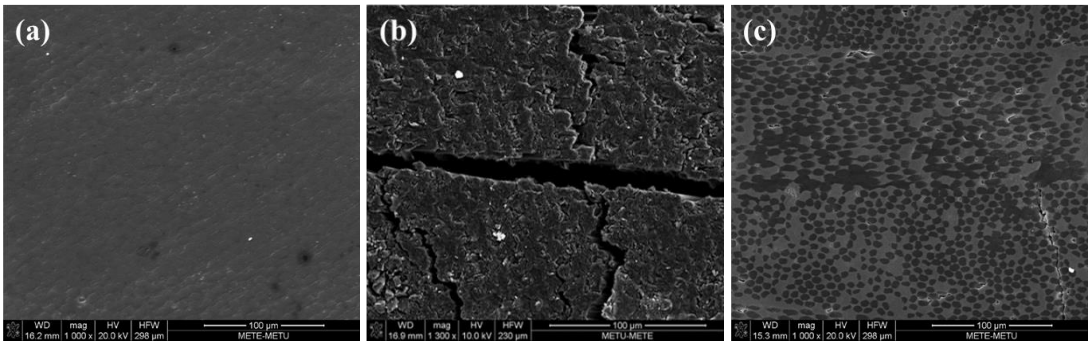

Figure 4. 31 SEM micrographs that showing the microstructural changes during composite processing, (a) as-received CFRP, (b) C/C preform pyrolyzed at 1000 °C and, (c) C/C-SiC composite fabricated using above mentioned optimum liquid silicon infiltration parameters.

Table 4. 10 Density change from the initial to the final composites during liquid silicon infiltration at each process stage.

Property	**As-received CFRP**	**C/C Preform**	**C/C-SiC Composite**
Density (g/cm^3)	1.35	1.10	1.68

Furthermore, three point bending test were applied to the corresponding composites after each stage of the liquid silicon infiltration process. As-received CFRP containing no pores and cracks in its structure showed a flexural strength of nearly 230 MPa, Figure 4.32(a). After pyrolysis at 1000 °C, as mentioned in Section 4.2 cracks were created in the structure. As a result of this crack formation, applied load could not be transferred from matrix to carbon fibers in the C/C preform leading to a considerable strength decrease (10 MPa), Figure 4.32(c). Following liquid silicon infiltration where carbon matrix was converted to silicon carbide, and some of the existing cracks were filled with silicon carbide. As the capability of load transfer from the silicon carbide matrix to carbon fibers increased flexural strength of the resulting C/C-SiC composite increased to 90 MPa, Figure 4.32(b).

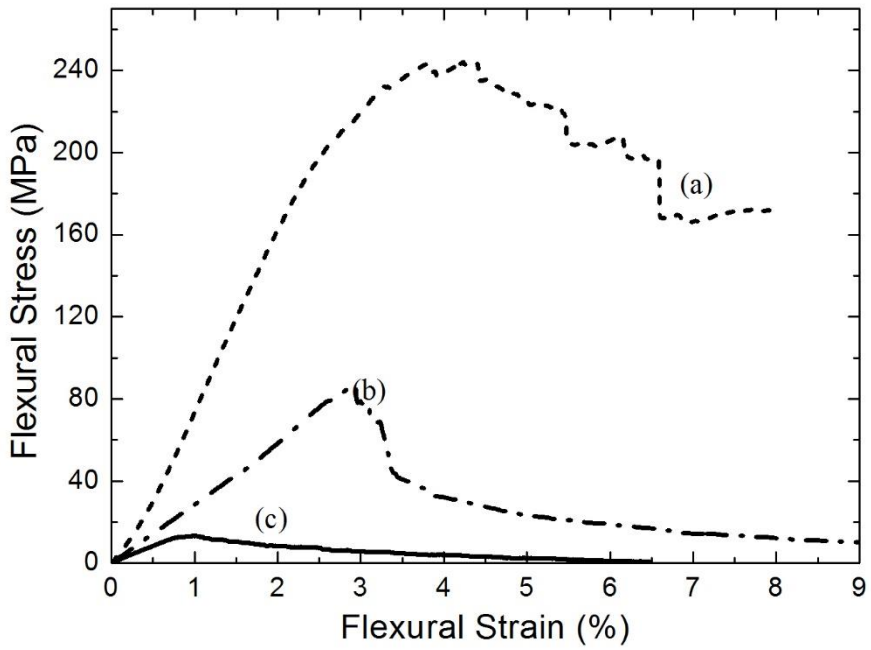

Figure 4. 32 Flexural stress-strain curves of (a) As received CFRP, (b) C/C -SiC Composite, (c) C/C preform pyrolyzed at 1000 °C.

4.4 Effect of Matrix Additives in C/C Preform on the Efficiency of the LSI Process prior to Liquid Silicon Infiltration

Nano-SiC powders and carbon nano tubes (CNT) were impregnated into the C/C preforms as nucleation sites and extra carbon source, respectively, to investigate their effect on the efficiency of LSI process. In Section 4.3 the optimum sequence of the process parameters were identified as pyrolysis at 1000 °C, followed by liquid silicon infiltration at 1650 °C under vacuum. Consequently, in this part of the study these parameters were applied to matrix additive containing C/C preforms during silicon infiltration.

Beginning with C/C preform pyrolyzed at 1000 °C with density and porosity content of 1.10 g/cm^3 and 25.45 %, respectively, it is seen that after liquid silicon infiltration nano-SiC containing C/C-SiC composite has lower density than the no additive containing composite. On the contrary, CNT containing C/C-SiC composite has better densification properties with higher density and lower porosity content (Table 4.11). These different densification properties reveal that infiltration depth in the C/C preforms during liquid silicon infiltration are different for each case. Therefore, SEM micrographs of these three cases were compared as it is seen in Figure 4.33. For the nano-SiC impregnated preform condition Figure 4.33(a) and (b) only at the outer regions of the composite SiC formation was observed, while inner parts of the composite still contain untransformed carbon matrix and carbon fibers which were exposed to degradation due to high temperature treatment during silicon infiltration.

Table 4. 11 Density and porosity comparison of matrix additive containing and not containing C/C preforms after silicon infiltration, and hence C/C-SiC composite formation.

	No-additive	**Nano-SiC**	**CNT**
Density (g/cm^3)	1.68	1.54	1.74
Porosity (%)	6.32	10.02	4.85

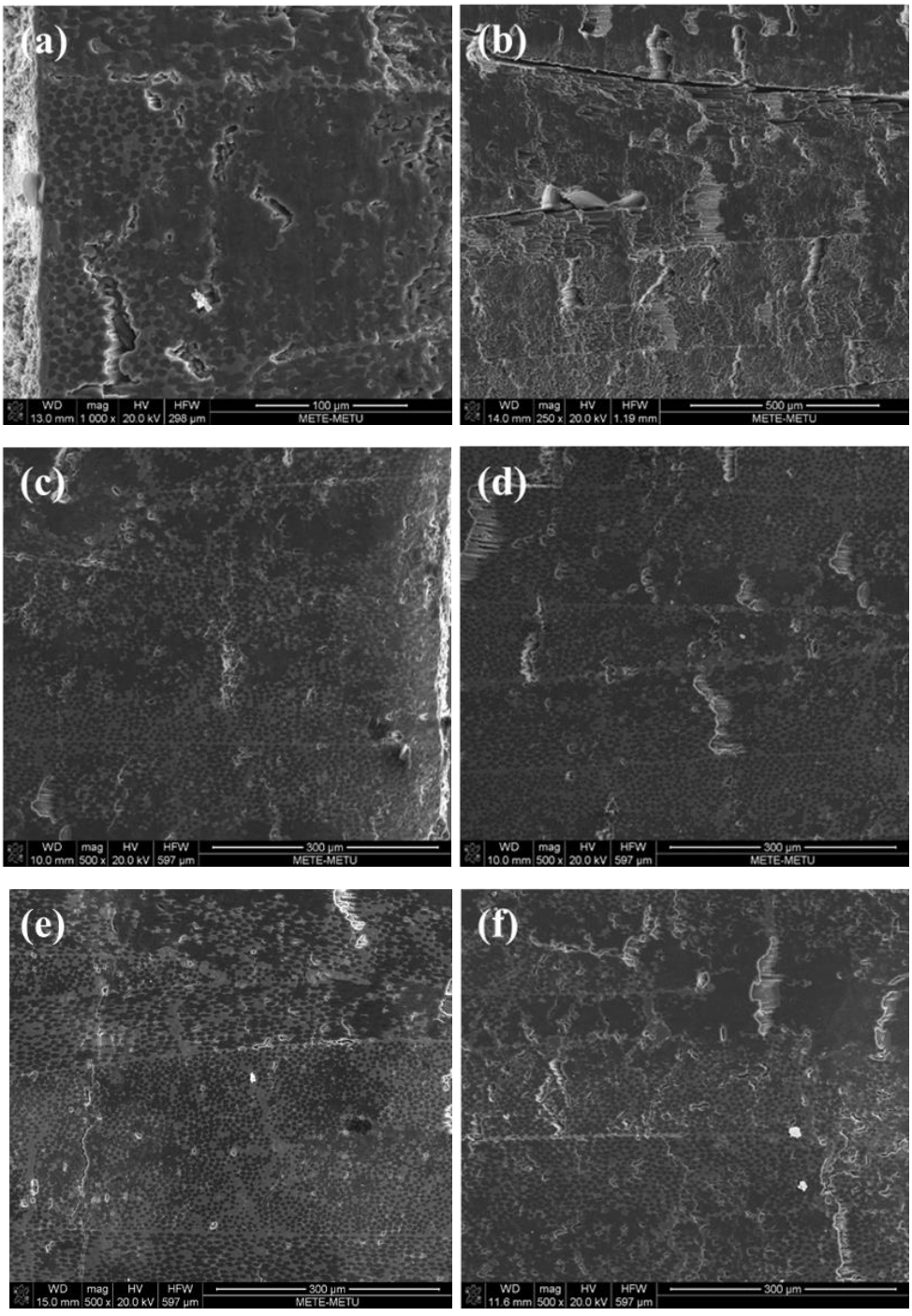

Figure 4. 33 SEM micrographs showing the microstructural changes in (a) nano-SiC impregnated, outer (b) nano-SiC impregnated, inner (c) CNT containing, outer (d) CNT containing, inner, (e) no additive containing, outer and (f) no additive containing, inner C/C composites after liquid silicon infiltration.

Although, conversion of carbon matrix into SiC was not achieved at the inner regions of the nano-SiC impregnated C/C-SiC composite, density increase was observed since impregnated beta-SiC nanopowders have a density of 3.21 g/cm^3. As it is seen in Figure 4.34(b), infiltration depth in nano-SiC impregnated composite is nearly 110 μm. In contrast to nano-SiC containing C/C-SiC composite, CNT impregnated one reveals successful silicon infiltration into the inner regions of the composite, i.e, both in the outer and inner regions of the composite conversion of carbon matrix into SiC was obtained (Figures 34(c) and (d)). This result is consistent with the density increase observed in CNT containing composite.

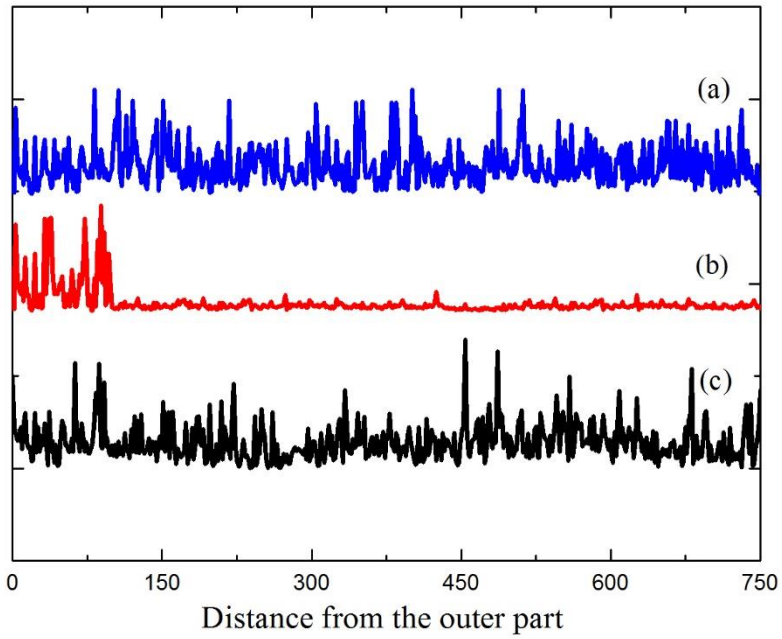

Figure 4. 34 EDS line analysis of silicon in the C/C-SiC composites from the outer surface for C/C preforms (a) as-received, (b) nano-SiC impregnated, (c) CNT impregnated.

The XRD analysis results of the composites are presented in Figure 4.35. As it is seen all of the composites are composed of carbon and β-SiC, while diffraction peaks of

silicon and silicon dioxide do not exist. Based on the different intensities of the peaks in each composite, rietveld analysis was used to identify relative amounts of the existing phases (Table 4.12). It is seen that whereas impregnation of nano-SiC decreases the SiC weight fraction, CNT addition resulted in higher amount of SiC formation.

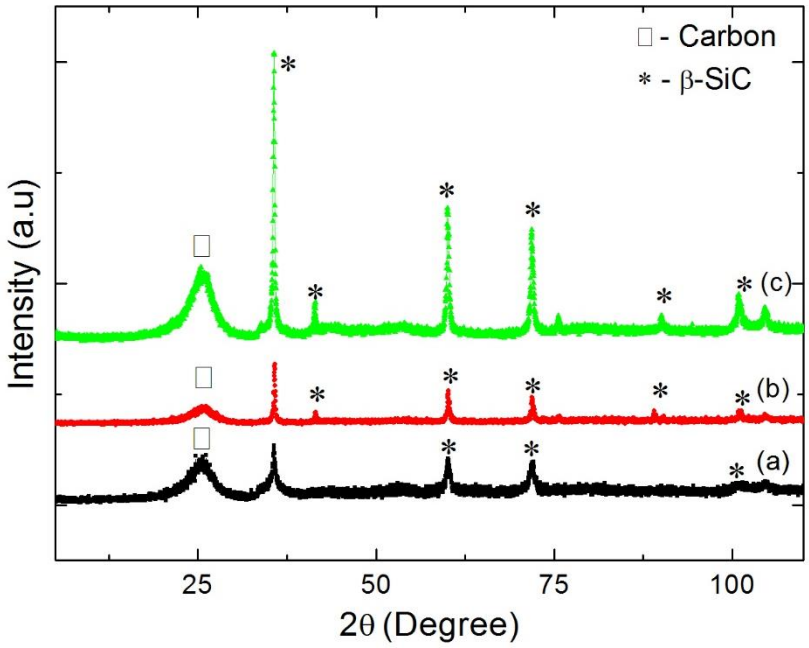

Figure 4. 35 The XRD diffractograms of (a) no additive, (b) nano-SiC and CNT containing C/C-SiC composites.

Table 4. 12 Rietveld analysis result of no additive, nano-SiC and CNT containing C/C-SiC composites after liquid silicon infiltration.

	SiC (Wt. Frac.)	**C (Wt.Frac.)**
As-manufactured	0.71	0.29
Nano-SiC	0.37	0.63
CNT	0.76	0.24

The density of the CNT added composite is higher than that of the no additive containing composite because it contains less cracking. As mentioned in Chapter 2, SiC formation occurs by a two-stage mechanism composed of heterogeneous nucleation and growth of SiC layer. After reaching the melting point of silicon, with the help of the capillary forces liquid silicon infiltrates into the cracks of the C/C preform and by reacting with the carbon matrix it forms SiC [76-77]. Figure 4.36 presents the polycrystalline SiC layer between the carbon fiber and the crack in no additive containig C/C-SiC composite, where existing cracks could have not been filled entirely by the formed SiC layer. Since subsequent growth of the SiC layer occurs by the diffusion of carbon and silicon atoms through this formed layer, in the case of the absence of the carbon atoms, this growth is suppressed and residual unfilled cracks exist in the microstructure. However, when CNT fills the cracks in the C/C preform, cracks contain extra carbon source to maintain the growth of the SiC layer and effective crack filling is obtained.

Carbon reactivity towards liquid silicon plays an important role in silicon carbide formation. The reactivity of carbon affects the rate of carbon dissolution by liquid silicon; and therefore, the rate of silicon carbide formation at the carbon-silicon interface. Furthermore, the surface area of the carbon in contact with the liquid silicon is also effective on the reaction kinetics. Comparing with turbostratic carbon which is in amorphous condition, CNT has higher reaction kinetics because of its higher surface area. As a result, carbon atoms can be more readily dissolved in liquid Si. Therefore, having higher surface area of CNT compared to turbostratic carbon enhances the SiC formation rate.

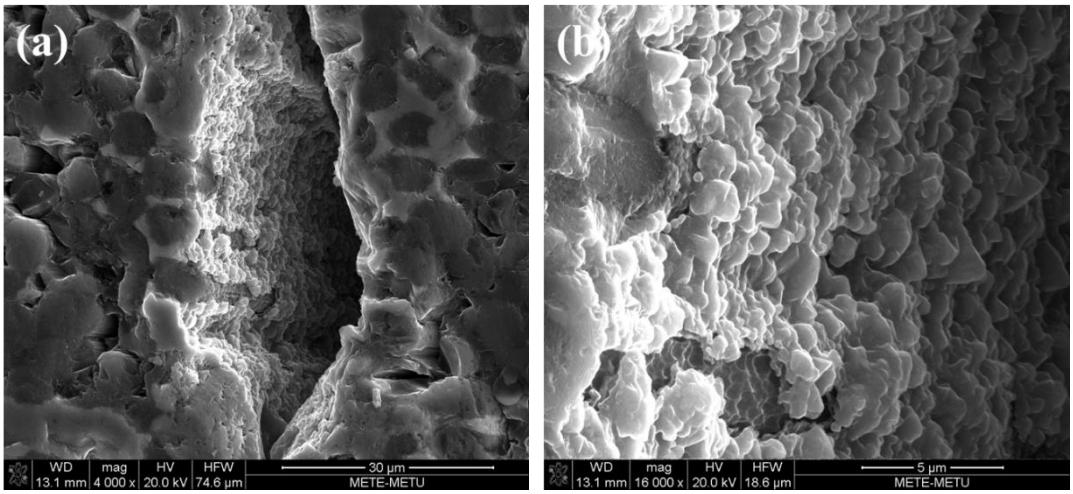

Figure 4. 36 SEM micrographs of SiC layer formed in the crack.

In the case of the nano-SiC containing C/C preform, the aim was to create nucleation sites for heterogeneous nucleation of the SiC, and with increasing the nucleation rate, to improve the rate of the SiC formation within the cracks. SiC powders used in this study as a matrix additive have particle size ranging from 100 to 200 nm being suitable to be impregnated into the cracks of the C/C preforms with an average opening of 44 µm. However, even though this is the case agglomeration of the nano-SiC powders during impregnation hindered their penetration to the inner parts of the C/C preform. Furthermore, these SiC powder agglomerates have blocked the cracks at the outer parts of the C/C preforms hindering the infiltration of liquid silicon to the inner parts of the composite during LSI process. In other words, agglomeration of the nano-SiC powder used as a matrix additive has decreased the permeability of the C/C preforms towards liquid silicon infiltration. This effect is schematically illustrated in Figure 4.37, showing the decrease in the permeability by the nano-SiC powder agglomerates limiting the liquid silicon infiltration, and hence SiC formation in the cracks of the C/C preform.

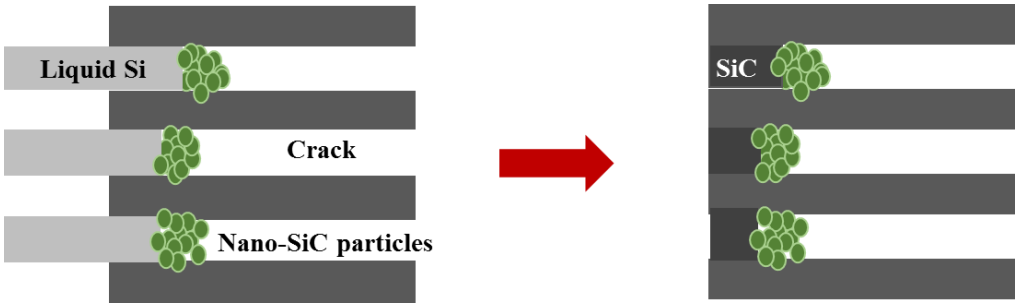

Figure 4. 37 Schematic illustration of agglomerated nano-SiC particles limiting liquid silicon infiltration and SiC formation.

Three point bending tests were utilized to compare the mechanical behavior of no additive containing composites with that of nano-SiC and CNT impregnated composites. Figure 4.38 shows the flexural stress-strain curves of the resulting C/C-SiC composites. As mentioned in section 4.3, no additive containing C/C-SiC composite have a flexural stress value of nearly 85 MPa. This value has decreased after nano-SiC impregnation. This was caused by decreasing the permeability of the C/C preform by agglomeration of the nano SiC powders, as a result of which the carbon matrix was not converted to SiC effectively and fiber degradation has occurred due to the temperature gradient. Cracks existing in the microstructure of the nano-SiC containing C/C-SiC composite prevent the load transfer from the matrix to the fibers leading to lower flexural strength. On the contrary, parallel to the higher density and higher SiC content in the matrix, CNT containing C/C-SiC composite has higher flexural strength compared to no additive containing C/C-SiC composite. Crack free microstructure results in successful load transfer from the SiC matrix to the carbon fibers enhancing flexural strength.

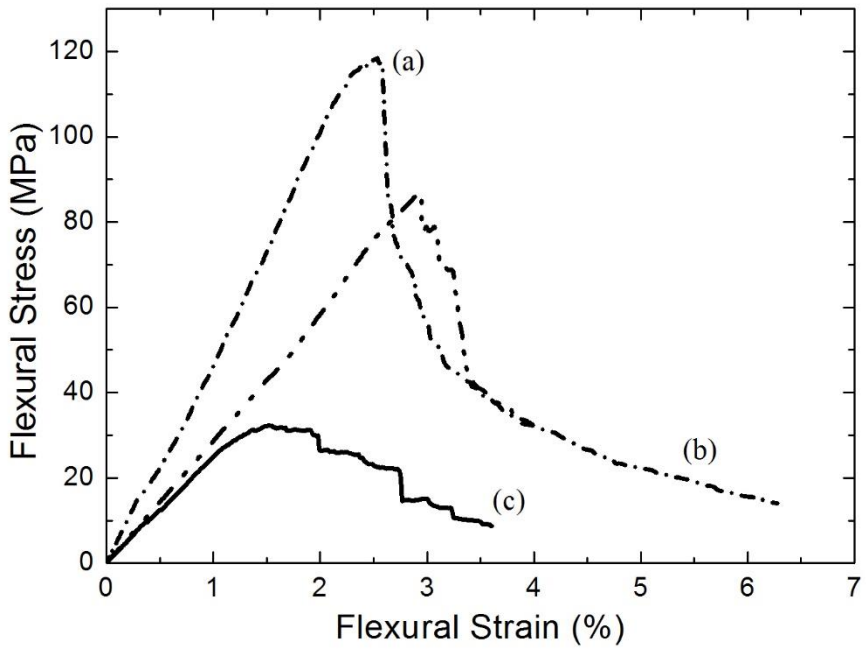

Figure 4. 38 Flexural stress-strain curves of (a) no additive, (b) nano-SiC and (c) CNT containing C/C-SiC composites.

In Figure 4.39 fracture surfaces of C/C-SiC composites is presented. Figure 4.39(a) shows the fracture surface of nano-SiC impregnated C/C-SiC composite containing only degraded carbon fibers without any SiC matrix. On the contrary, no additive and CNT containing C/C-SiC composite fracture surfaces (Figure 39(b) and (c)) represent that both SiC matrix and carbon fibers were exposed to fracture.

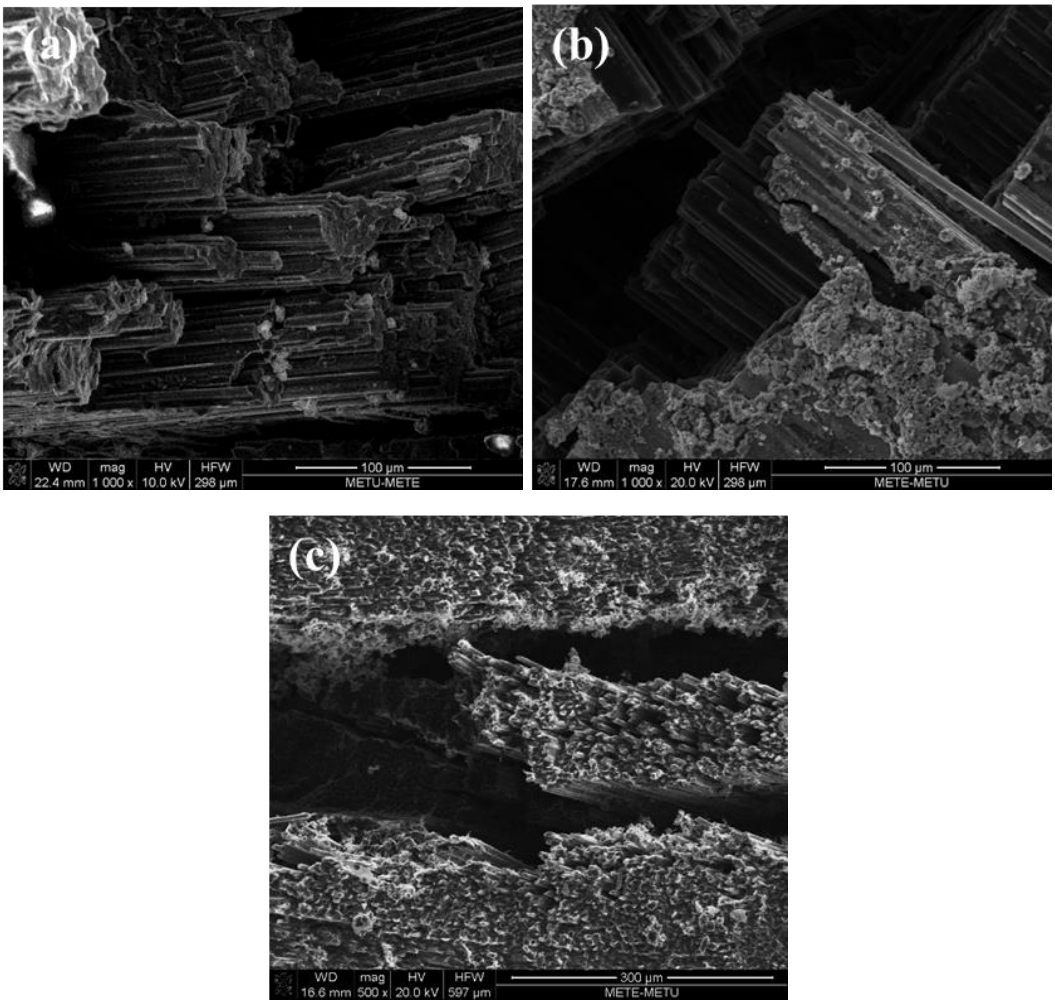

Figure 4. 39 SEM pictures of fracture surfaces of (a) no additive, (b) nano-SiC and (c) CNT containing C/C-SiC composites.

4.5 Investigations on Matrix Reactivity Towards the Efficiency of the LSI Process

The pyrolysis is an important step for controlling the C/C preform characteristics which directly affect the densification during LSI. In spite of the fact that preform characteristics mainly depend on pyrolysis temperature, the matrix reactivity of the preform is not governed by altering the pyrolysis conditions. Efficient and successful transformation of carbon matrix into silicon carbide, strongly depends on the matrix reactivity as well. In order to investigate this alternative matrix materials in powder

form were reacted with liquid silicon using the predetermined optimum LSI parameters defined as 1650 °C in vacuum for 1 h. Experimental studies have been carried out on carbon derived from phenolic resin (PR) and on a mixture of phenolic resin – microcrystalline cellulose (PR-MC). Moreover, in order to point out the effects of matrix additives on the conversion of carbon into SiC, mixtures of carbon derived from phenolic resin with nano-SiC powder (PR- NanoSiC) and carbon derived from phenolic resin with carbon nanotube (PR-CNT) were also let to react liquid silicon using the above mentioned process condition, respectively.

Before mixing with the carbon derived from phenolic resin, in order to ensure that pyrolysis of microcrystalline cellulose gave rise to carbon formation, XRD analysis was conducted on pyrolysed microcrystalline cellulose powders. As it is seen in Figure 40(b)), because of the fact that XRD pattern of pyrolyzed microcrystalline cellulose presents (002), (102) and (004) peaks at the defined diffraction angles of carbon, transformation of organic precursor into carbon was achieved by the applied pyrolysis [78-79].

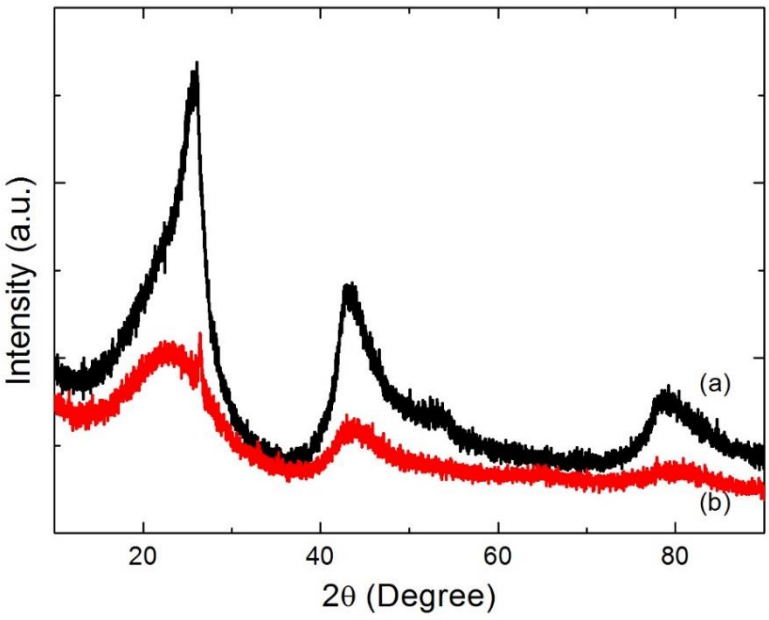

Figure 4. 40 XRD analysis of pyrolyzed (a) phenolic resin and (b) microcrystalline cellulose.

In order to reveal the efficiency of SiC formation in alternative matrix materials amounts of the existing phases after reacting with liquid silicon, Rietveld analysis were conducted (Figure 4.41-4.44). As it is seen in Table 4.13, in all of the matrix materials there is almost no residual silicon remaining. This is because, for all of the cases liquid silicon also reacts with graphite crucible and forms some amount of SiC. Therefore, unreacted silicon may not exist in the graphite crucible after the process.

Table 4. 13 Weight fraction of the phases in alternative matrix materials after reacting with liquid silicon.

Sample Name	SiC (Wt.Frac.)	C (Wt.Frac.)	Si (Wt.Frac.)
PR	0.76	0.24	0
PR-MC	0.98	0.02	0
PR-NanoSiC	0.87	0.13	0.006
PR-CNT	0.99	0.01	0

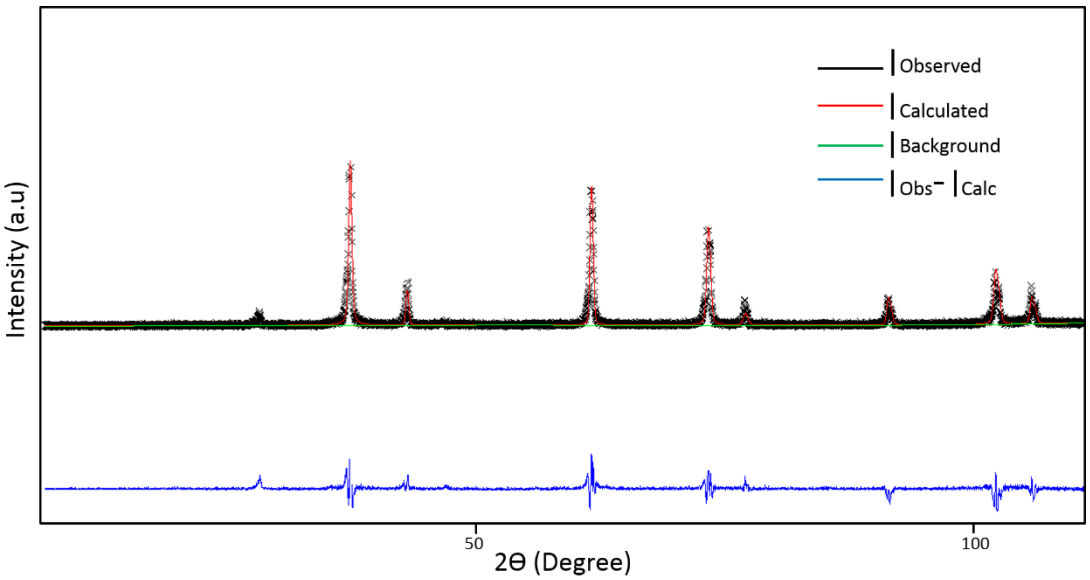

Figure 4. 41 Rietveld fitting of SiC formed using carbon derived from phenolic resin.

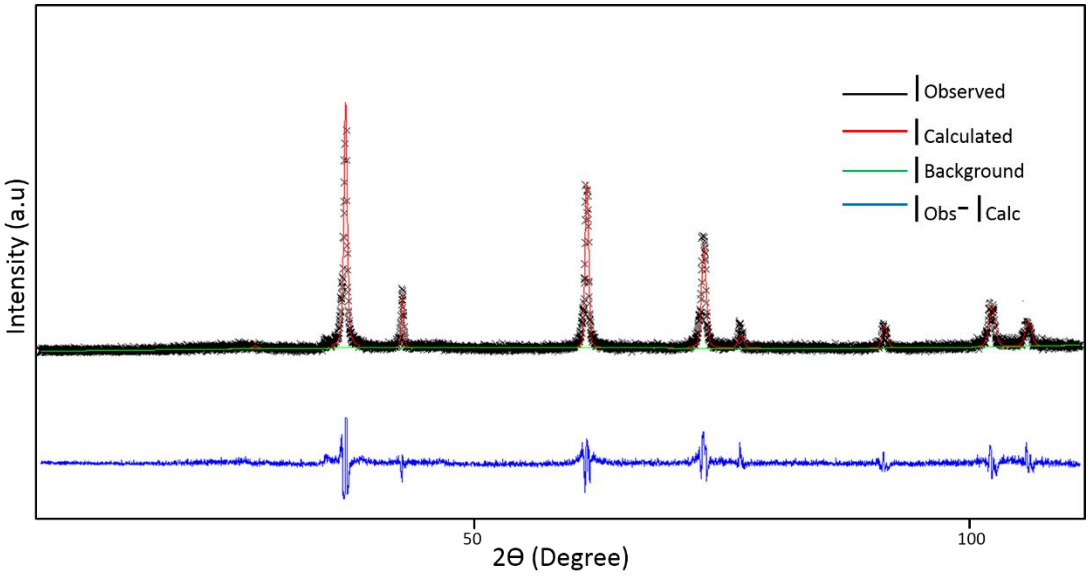

Figure 4. 42 Rietveld fitting of SiC formed using mixture of carbon derived from phenolic resin and microcrystalline cellulose.

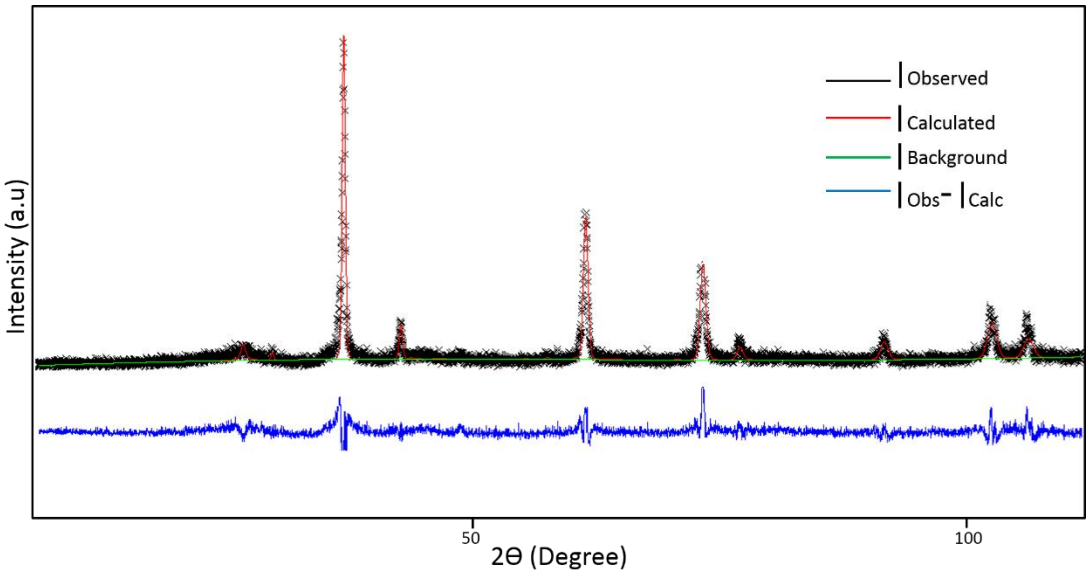

Figure 4. 43 Rietveld fitting of SiC formed using mixture of nano-SiC powder and phenolic resin.

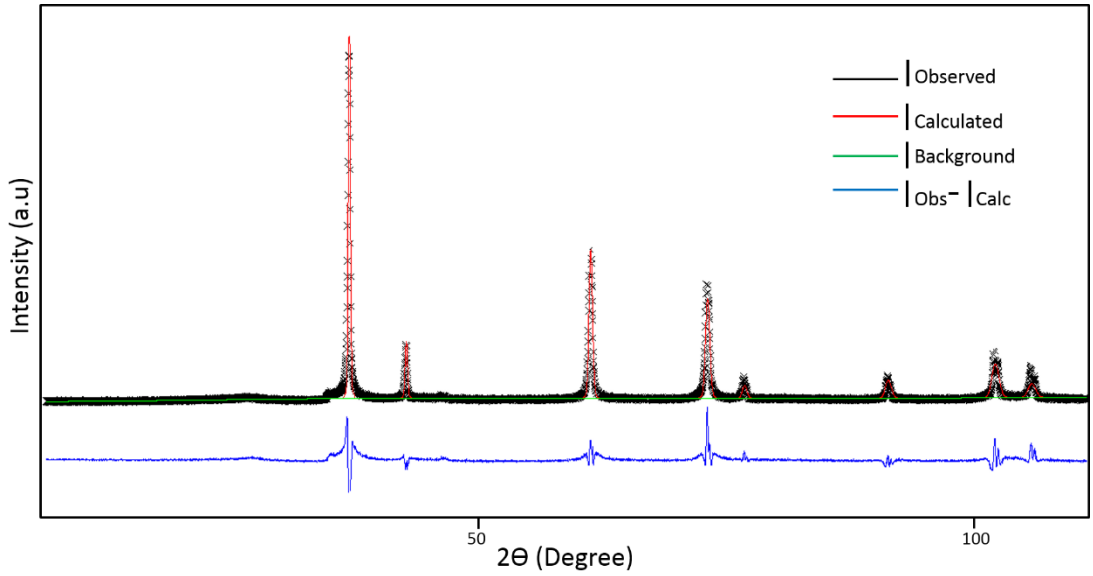

Figure 4. 44 Rietveld fitting of SiC formed using mixture of CNT and carbon derived from phenolic resin.

In spite of the fact that for all of the matrix material combinations equal moles of carbon were mixed with equal moles of silicon, after reacting with liquid silicon, PR-MC type matrix presented higher amount of SiC than PR matrix. Moreover, unreacted carbon amount is comparably lower for PR-MR. Having higher amount of SiC formation with PR-MC mixture can be explained by the differences in the carbon reactivities of the matrix materials after pyrolysis. Pyrolysis of microcrystalline cellulose and phenolic resin gives rise to carbon precursors having different reactivities which directly affect the rate of silicon carbide formation. The degree of atomic ordering in the precursor defines the carbon reactivity. With decreasing carbon atomic ordering, the concentration of available carbon active sites increases, therefore, dissolution of carbon atoms in liquid silicon occurs more easily. As mentioned in Section 1, pyrolysis of phenolic resin results in turbostratic carbon structure. Following the removal of aromatic rings from the structure in dehydrogenization and main pyrolysis steps, small graphene clusters may have been formed. These clusters increase the atomic ordering of the phenolic resin, i.e. decrease the reactivity of the achived

carbon. On the other hand, cellulose molecules do not contain any aromatic rings, and hence, finally formed amorphous carbon does not contain graphene structure (Figure 4.45).

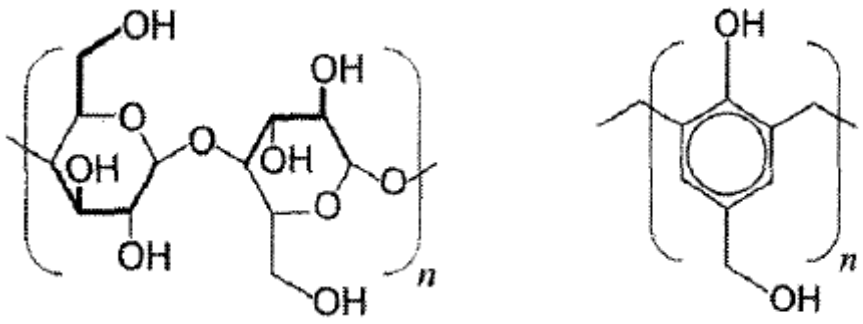

Figure 4. 45 Atomic structure of (a) Microcrystalline Cellulose, (b) Phenolic Resin.

According to Table 4.13, SiC formation is higher in PR-nanoSiC mixture compared to only PR matrix. As mentioned in Chapter 2, reaction formation of SiC is diffusion controlled. This occurs in two stages where firstly a thin SiC layer forms between liquid silicon and carbon precursors, then SiC formation proceeds with the diffusion of the carbon atoms through formed SiC layer and growth of this formed layer. In the PR-NanoSiC mixture nano-SiC particles behave like existing nucleation sites on which liquid silicon can react with carbon precursor, enhancing SiC formation.

The highest amount of SiC formation has been achieved by the reaction of liquid silicon with PR-CNT mixture with trace amount of residual carbon and unreacted silicon. As already known, nano materials have significantly higher amount of surface area compared the bulk materials. High amount of surface area enhances the carbon-liquid silicon interaction resulting in high fraction of SiC formation.

Moreover, representative morphology of formed SiC grains are shown in Figure 4.46. SiC have two polymorphs where α-SiC is formed at temperatures higher than 1700 °C while a hexagonal, β-SiC with a zinc blende crystal structure are formed at temperatures below 1700 °C. Due to the fact that reaction temperature with liquid

silicon was 1650 °C, only β-SiC was observed throughout this study. As mentioned earlier SiC layers get thicker according to diffusion limited silicon carbide formation, where heterogeneous nucleation and growth of SiC occurs by the diffisuion of carbon through the formed SiC layer. Considering this mechanism, presented microstructures were compared in Figure 4.46.

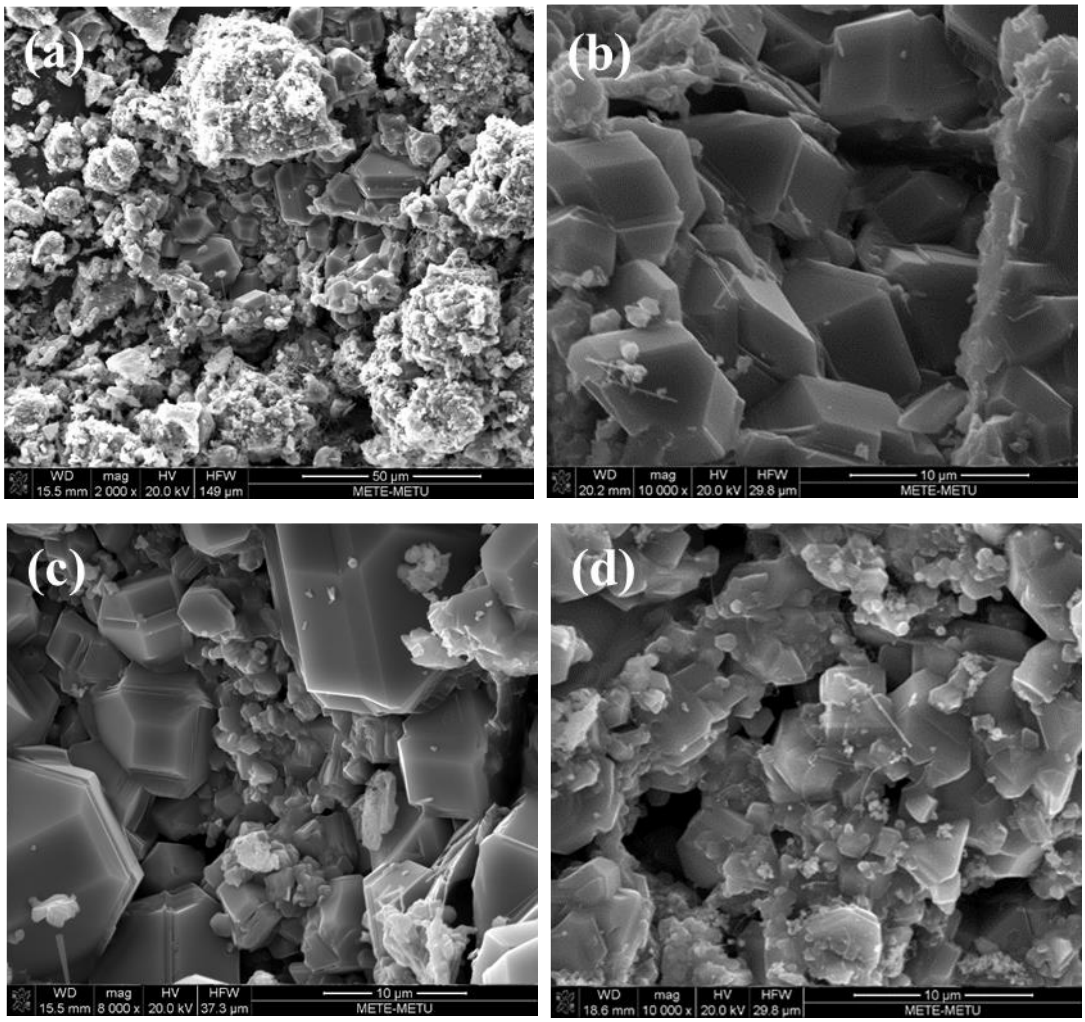

Figure 4. 46 Morphology of β-SiC grains (a) PR precursor, (b) PR-MC, (c) PR-NanoSiC and (d) PR-CNT.

SiC morphology formed in PR only differs from those of the others, due to the fact that it does not only contain SiC grains but also unreacted carbon in its microstructure.

Both PR-CNT and PR-MC mixtures present nearly uniform and small sized SiC grains associated with the initial formation of SiC at presented carbon sources. Higher amount of carbon sources with finer morphologies resulted in higher degree of nucleation rate, and hence high number of fine SiC grains have formed. PR-Nano-SiC mixture microstructure reveals varying grains sizes, mainly due to varying time [79]. Growth of large twin crystals may be explained by nucleation of SiC grains at the surface of already formed SiC grains.

CHAPTER 5

CONCLUSION

Liquid silicon infiltration (LSI) is a complex process where key variables have a distinguishable role on the effectiveness of the densification and properties of the resulting ceramic composites. The most important findings and conclusions of the current study are listed as follows;

- The evolution of microstructure and changes in the properties of the CFRP during pyrolysis at different temperatures has been investigated. It was shown that phenolic resin converts to turbostratic carbon during pyrolysis.

- Pyrolysis of phenolic resin is composed of three main steps called post curing, main pyrolysis and dehydrogenization. In order to achieve turbostratic carbon structure, each step must be completed and polymeric matrix must be completely converted to turbostratic carbon for effective subsequent liquid silicon infiltration.

- Morphology and content of the pores as well as density of the C/C preforms resulting from the pyrolysis process are critical parameters strongly affecting the densification behavior during the LSI process.

- Applied pyrolysis temperature plays an important role on the densification behavior observed during the LSI process. Increasing pyrolysis temperature results in C/C preforms with lower density, higher porosity and higher crack opening leading to improved densification of silicon infiltrated composites.

Proper crack opening and a narrow crack opening distribution are important, in light of the fact that the liquid silicon to react with the interior regions of the preform infiltration rate should be higher than reaction rate to allow complete conversion to silicon carbide. In other words C/C preforms with higher average crack opening have higher possibility to promote reaction between the liquid silicon and the carbon matrix.

- Effect of infiltration atmosphere on the infiltration depth was investigated. Presence of a gas phase at the Ar-Si-C triple line hinders the penetration of the liquid silicon into the C/C preform, i.e. reduction in Ar pressure at the Ar-Si-C line leads to enhanced liquid silicon infiltration flux.

- Under constant permeability of the C/C preform, higher silicon infiltration temperature results in more efficient filling of the cracks and pores in the C/C preform, as lower viscosity accelerates the infiltration rate.

- Taking into consideration of all of the parameters which directly affect the efficiency of the LSI process, in order to obtain denser and mechanically strength C/C-SiC composites, pyrolysis should be conducted at 1000 °C and following liquid silicon infiltration should be applied at 1650 °C under vacuum.

- Nano-SiC powder impregnated as a matrix additives to the C/C preform does not improve the efficiency of the liquid silicon infiltration because of the agglomeration of the nano-SiC powders within the existing cracks. Agglomeration of the nano-SiC powder used as matrix additive has decreased the permeability of the C/C preforms towards liquid silicon infiltration, and hence limited the SiC formation in the inner parts of the preform.

- ❖ Usage of CNT as a matrix additive in the C/C preform enhanced the efficiency of the LSI process leading to C/C-SiC composites having higher density and flexural strength compared to no additive containing ones. High surface area of CNT in contact with liquid silicon has enhanced the reaction kinetics of SiC formation compared to no additive containing case leading to improved densification.

In order to enhance the process and performance of the C/C-SiC composites and the efficiency of the liquid silicon infiltration method, the followings remarks are suggested for future studies:

- Besides the C/C preform characteristics, properties of the initial material, CFRP, also effects the silicon infiltration process. Therefore, it would be notable to control characteristics of the CFRP including fiber volume fraction, woven type and matrix content etc.

- In addition to matrix reactivity studies, effect of the matrix additives on LSI process should be further investigated by impregnating these materials in different amounts during the CFRP production. By this way, it would be possible to understand the effect of matrix additives on the LSI process more clearly.
- In this study it was revealed that morphology and content of the pores and density of the C/C preform are critical parameters, therefore, detailed study on the effect of generating agents incorporated into the CFRP on the progress of the LSI process may be conducted.

REFERENCES

[1] K.K.Chawla, Ceramic Matrix Composites, Malta: Chapman & Hall, 1993.

[2] F. C. Chapbell, Manufacturing Technology for Aerospace Structural Materials, UK: Elsevier Science, 2006.

[3] L. Zhuan and P. Xiao, "Preparation and tribological properties of C fibre reinforced C/SiC dual matrix compossites fabrication by LSI," *Solid State Sciences,* vol. 16, pp. 6-12, 2013.

[4] Y. Zhang, "Effect of pyrocarbon content in C/C preforms on microstructure and mechanical properties of the C/C-SiC composites," *Material Science and Engineering,* vol. A, no. 500, pp. 64-69, 2009.

[5] P. Narotham and J. Lamon, Ceramic Matrix Composites, New Jersey: John Wiley & Sons, 2014.

[6] G. A. Evans, W. F. Zok and T. J. Mackin, High Temperature Mechanical Behavior of Ceramic Composites, Boston: Butterworth-Heinemann, 1995.

[7] J. W. Hutchinson and H. M. Jensen, "Models of fiber debonding and pullout in brittle composites with friction.," *Mech. Mater. 9,,* p. 139–163, 1990.

[8] D. Desnoyer, A. Lacombe and J. M. Rouges, "Large thin composite structural parts," ESA, Nordwijk, The Netherlands, 1991.

[9] F. Christin, "CMC materials for space and aeronautical application," in *Ceramic Matrix Composites*, Weinheim, Wiley- VCH Verlag,, 2008, pp. 357-359.

[10] R. Weiss, "Carbon fibre reinforced CMCs: manufacture, properties, oxidation protection," in *High Temperature Ceramic Matrix Composites*, Weinheim, Wiley-VCH, 2001, pp. 440-456.

[11] R. Weiss, "Carbon/carbons and their industrial applications," in *Ceramic Matrix Composites*, Weinheim, Wiley-VCH Verlag, 2008, pp. 69-108.

[12] H. Moissan., "Nouvelles recherches sur la m´et´eorite de canon diabolo.," *Comptes rendus,* p. 773–786, 1904.

[13] A. W. Weimer, Carbide, Nitride and Boride Materials Synthesis and Processing, London: Chapman & Hall, London, 1997.

[14] M. Birot and J. Pillot, "Comprehensive chemistry of polycarbosilanes, polysilazanes and polycarbosilazanes as precursors for ceramics," *Chemical Rewievs,* pp. 1443-77, 1995.

[15] G. Motz, S. Schmidt and S. Beyer, "The PIP-process: Precursor properties and applications," in *Ceramic Matrix Composites*, Weinheim, Wiley-VCH Verlag, 2008, p. 357–359.

[16] P. Greil, "Polymer derived engineering materials.," *Adv. Eng. Mater., 2,* p. 339–348, 2000.

[17] G. P, "Near net shape manufacturing of polymer derived ceramics," *journal of the european ceramic society,* pp. 1905-14, 1998.

[18] W. Krenkel and F. Berndt, "C/C-SiC composites for space applications and advanced friction systems," *Materials Science and Engineering A 412*, pp. 177-181, 2005.

[19] R. A. Naslain and F. Langais, "CVD Processing of Ceramic-Ceramic Composite Materials," *Material Science Research*, pp. 145-64, 1986.

[20] J. Lipowitz, J. A. Rabe and A. Zangvil, "Structure and properties of Sylramic silicon carbide fiber- a polycrystalline, stoichiometric B-SiC composites," *Ceram. Eng. Sci. Proc*, pp. 147-157, 1997.

[21] K. S. Manish Patel, "High temperature C/C-SiC composite by liquid silicon infiltration: a literature review," *Bull. Mater.Sci.*, pp. 63-73, 2012.

[22] C. C. Evans, A. C. Parmee and R. W. Rainbow, "Silicon treatment of carbon fiber-carbon composites.," in *Proceedings of 4th London International Carbon and Graphite Conference*, London, 1974.

[23] X. Peng, L. Zhuan and X. Xiang, "The morphology and mechanism of formation of SiC in C/C-SiC composites fabricated by liquid silicon infiltration," *Journal of Ceramic Processing Research*, pp. 335-340, 2010.

[24] C. Zuber, T. Reimer and K. Stubicar, "Manufacturing of the CMC nose cap for the EXPERT spacecraft.," in *34th International Conference and Exposition on Advanced Ceramics and Composites*, Daytona Beach, FL, 2010.

[25] F. M. Foley and T. Gutowski, "The Effect of Process Variables on Permeability in the Flexible Resin Transfer Molding (FRTM) Process," in *In 23rd International SAMPE Technical Conference*, Kiamesha Lake, USA, 1991.

[26] P.Greil, "Polymer derived engineering materials," *Adv. Eng. Mater.*, pp. 339-348, 2000.

[27] C. Zuber and B. Heidenreich, "Development of a net shape manufacturing method for ventilated brake discs in single piece," *Ceramic Forum International,* pp. 16-22, 2005.

[28] F. Raether, J. Meinhardt and A. Kienzle, "Oxidation behaviour of carbon short fibre reinforced C/SiC composites.," *J. Eur. Ceram.*, p. 1217–1221, 2007.

[29] M. Freiss, M. Scheifele and W. Zanki, "Development, manufacture and characterization of C/C-SiC components," in *High Temperature Ceramic Matrix Composites*, Berlin, 2010, pp. 92-97.

[30] S. T. Peters, "Filament winding," in *Composites Engineering Handbook*, Newyork, Marcel Dekker, 1997, pp. 515-548.

[31] B. W. D. Wielage, "Thermo-mechanical Monitoring of Composite Materials during the Pyrolysis of C/C Composites," *Key Engineering Materials,* pp. 95-105, 2010.

[32] K. A. Trick and T. E. Saliba, "Mechanisms of the pyrolysis of phenolic resin in a carbon/phenolic composite," *Carbon,* pp. 1509-15, 1995.

[33] K. A. Trick and T. E. Saliba, "A kinetic model of the pyrolysis of phenolic resin in a carbon/phenolic composite," *Carbon,* pp. 393-401, 1997.

[34] G. M. Jenkins and K. Kawamura, Polymeric carbon-carbon fibre, glass and char, Cambridge: Cambride University Press, 1976.

[35] W. Hillig, "Making ceramic composites by melt infiltration," *American Ceramic Society Bulletin,* pp. 56-62, 1994.

[36] F. H. Gern and R. Kochendörfer, "Liquid silicon infiltration: description of infiltration dynamics ans silicon carbide formation," *Composite Part A,* pp. 355-364, 1997.

[37] W. K. F. Gern, "Morphology and infiltration dynamics of liquid siliconized carbon/carbon.," in *Proc. 10th Int. Conf.Compos.Mater.*, Whistler, BC, 1995.

[38] M. W. Elraghy and T. Barsoum, "Synthesis and characterization of a remarkable ceramic: Ti3SiC2,," *Journal of American Ceramic Society,79,* pp. 1953-6, 1996.

[39] H. Pierson, Handbook of Refractory Carbides and Nitrides, Westwood, NJ: Noyes Publications, 1996.

[40] A. Favre, H. Fuzellier and J. Suptil, "An original way to investigate the siliconizing of carbon materials," *Ceram. Int., 29,* p. 2003, 235-43.

[41] H. Singh and R. N. Zhou, "Kinetics Model for the Growth of Silicon-Carbide by the Reaction of Liquid Silicon with Carbon," *J Am Ceram Soc,*, pp. 2456-62, 1995.

[42] J. Schulte-Fischedich, M. Friess and W. Krenkel, "The interlaminar shear strength of C/C-SiC Composites," in *Proceedings of HT-CMC 4 Conference*, Munich, 2001.

[43] K. Hauffe, Oxidation of Metals, Newyork: Plenum Press, 1965.

[44] N. Eustathopoulos, "Dynamics of wetting in reactive metal ceramic systems," *Acta Materialia,* pp. 2319-27, 1998.

[45] O. Dezellus, S. Jacques and F. Hodaj, "Wetting and infiltration of carbon by liquid silicon," *J. Mater. Sci., 40,* pp. 2307-11, 2005.

[46] A. Prabhu and G. Kumar, "Review of non-reactive and reactive wetting of liquids on surfaces," *Adv. Colloid Interface Sci., 133,* pp. 61-89, 2007.

[47] O. Dezellus, F. Hodaj and N. Eustathopoulos, "Progress in modelling of chemical reaction limited wetting," *Journal of the European Ceramic Society*, pp. 2797-803, 2003.

[48] H. Weihs, T. Reimer and T. Laux, "Mechanical Architecture and status of the flight unit of the sharp edge flight experiment," in *SHEFEX, IAF Congress*, Vancouver, 2004.

[49] H. Hald, "Development of a nose cap system for X38," in *Proceedings of International Symposium Atmospheric Reentry Vehicles ans Systems*, Arcachon, 1999.

[50] A. Tewari, T. Srinivasulu, A. Ramesh and A. Kumar, "Development of Manufacturing Technology for C-SiC Jet Vanes," in *Procedia Materials Science 5*, 2014.

[51] A. Schöppach, T. Petasch and B. Heidenreich, "Use of ceramic matrix composites in high precision laser communication optics.," in *European Conference on Spacecraft Structures*, Nordwijk,The Netherlands, 2000.

[52] B. Heidenreich, M. Gahr, E. Strassburger and E. Lutz, "Biomorphic SISIC-materials for lightweight armour," in *Proceedşngs of 30th International Conference on Advanced Ceramics & Composites*, Florida,Usa, 2000.

[53] J. Zhang, Y. Xu, L. Zhang and L. Cheng, "Effect of Braking Speed on Friction and Wear Behaviour of C/C - SiC Composites," *International Journal of Applied Ceramic Technology*, p. 463 – 469 ., 2007.

[54] W. Krenkel, "Design of Ceramic Brake Pads and Disks, American Ceramic Society," *Ceramic Engineering and Science Proceedings*, p. 319, 2002.

[55] R. Gadow and M. Speicher, "Manufacturing of Ceramic Matrix Composites for Automotive Applications," *Ceramic Transactions,* pp. Volume 128 , pp.25-41, 2000.

[56] Z. F. Sachs, "Formula Clutch Systems," 2006.

[57] M. Steiner, T. Erb and M. Hölscher, "Innovative Material Usage in the Porsche Carrera GT," in *Proceedings of FISITA,* Barcelona, 2004.

[58] W. Bernhad, "Thermo-Mechanical Monitoring of Composite Materials during the Pyrolysis of C/C Composites," *Key Engineering Materials,* vol. 425, pp. 95-105, 2010.

[59] A. K. Kercher, "Processing and characterization of monolithic carbon structures based on wood fiberboards," *Materials Science and Engineering A,* pp. 36-45, 1996.

[60] J. Schulte-Fischedich, M. Friess, w. Krenkel, R. Kochendörfer and B. Thielicke, "The interlaminar sher strength of C/C-SiC," in *Proceedings of HT-CMC 4 Conference,* Munich, 2001.

[61] J. Schulte-Fischedick, S. Seiz and N. Lützenburger, "The crack development on the micro- and mesoscopic scale during the pyrolysis of carbon fibre reinforced plastics to carbon/carbon composites," *Composites,* pp. 2171-2181, 2007.

[62] J. D. Nam and J. D. Seferis, "Initial polymer degredation as a process in the manufacture of carbon-carbon composites," *Carbon,* pp. 751-761, 1992.

[63] G. Savage, Carbon-Carbon Composites, London: Chapman & Hall, 1993.

[64] L. A. Berglund and P. Gudmundson, "Effects of composite-like stress state on the fracture of epoxies.," *Composites Science and Technology,* pp. 27-37, 1993.

[65] B. A. Sjögren and L. A. Berglung, "The effects of matrix and interface on damage in GRP cross-ply laminates," *Composite Science and Technology,* pp. 9-21, 2000.

[66] V. Lavrenko and A. P. Pomytkin, "High-temperature oxidation of SiC in a glow-discharge oxygen plasma," *Oxidation of Metals,* pp. 10:97-103, 1976.

[67] H. Zhou and S. N. Singh, "Kinetics model for the growth of silicon carbide by the reaction of liquid silicon with carbon," *Journal Amerikan Ceramic Society,* pp. 2456-2462, 1995.

[68] Y. Zhang and Z. Xiao, "Effect of pyrocarbon content in C/C preforms on microstructure and mechanical properties of the C/C-SiC composites," *Material Science and Engineering A,* pp. 64-69, 2009.

[69] J. Margiotta and D. Zhang, "Microstructural evolution during silicon carbide (SiC) formation by liquid silicon infiltration using optical microscopy," *Int. Journal of Refractory Metals & Hard Materials,* pp. 191-197, 2010.

[70] P. Sangsuvan, S. N. Tewari and J. E. Gatica, "Reactive infiltration of silicon melt through microporous amorphous carbon performs," *Metallic Materials Transactions,* pp. 933-944, 1999.

[71] E. O. Einset, "Capillary infiltration rates into porous media with applications to silicon composite processing," *Journal American Ceramic Society,* pp. 333-338, 1996.

[72] S. Kumar, A. Kumar and D. Rohani, "Capillary infiltration studies of liquids 3D-stitched C-C preforms Part B: Kinetics of silicon infiltration," *Journal of the European Ceramic Society,* pp. 2651-2657, 2009.

[73] J. S. Dezellus O, "Wetting and infiltration of carbon by liquid silicon," *Journal of Material Science,* p. 2307 – 2311, 2005.

[74] S. Kumar, A. Kumar and A. Shukla, "Capillary infiltration studies of liquids 3D-stitched C-C preforms Part A: Internal pore characterization by solvent infiltration, mercury porosimetry, and permeability studies," *Journal of the European Ceramic Society,* pp. 2643-2650, 2009.

[75] R. Asthana, "Dynamic wetting effects during infiltration of metals," *Scripta Materials,* pp. 1203-1210, 1998.

[76] M. Y. Chiang, P. R. Messner and D. C. Terwilligner, "Reaction formed Silicon Carbide," *Materials Science and Engineeing A,* vol. 144, no. 1-2, pp. 63-74, 1991.

[77] A. Favre, H. Fuzellier and J. Suptil, "An original way to investigate the siliconizing of carbon materials," *Ceramics International,* vol. 29, no. 235, pp. 235-343, 2003.

[78] C. E. Nagle and D. C. Bynre, "Cellulose derived composites - A new method for material processings," *Materials Research Innovations,* pp. 137-144, 1997.

[79] Z. Yang, X. He, M. Wu and L. Zhang, "Infiltration Mechanism of diamond/SiC composites fabricated by Si-vapor vacuum reactive infiltration process," *Journal of the European Ceramic Society,* pp. 869-878, 2013.

[80] Z.Lausevic and S.Marinkovic, "Carbon 24," p. 575, 1986.

[81] Z. Y., "Effect of pyrocarbon content in C/C preforms on microstructure and mechanical properties of the C/C–SiC composites," *Materials Science and Engineering A,* p. 64–69, 2009.

[82] K. Trick and T. Saliba, "Mechanism of the Pyrolysis of Phenolic Resin in a Carbon/ Phenolic Composite," *Carbon*, pp. 1509-1515, 1995.

[83] J. Schulte-Fischdick and A. Zern, "The crack evolution on the atomic scale during the pyrolysis of carbon fibre reinforced plastics to carbon/carbon composites," *Composites*, pp. 2237-2244, 2007.

[84] F. Schöder, Handbook of Inorganic Chemistry, Newyork: Springer Verlag Berlin, 1986.

[85] K. S and K. A, "Fabrication and Erosion Studies of C-SiC Composites Jet Vanes in solid rocket motor exhaust," *Journal of the Europen Ceramic Society*, pp. 2425-2431, 2011.

[86] M. Patel and K. Saurabh, "High Temperature C/C-SiC Composite by Liquid Silicon Infiltration- a literature review," *Bull. Mater. Sci.*, pp. 63-73, 2012.

[87] J. A. Parker and E. L. Winkler, "NASA TR R-276," Ames Research Center, 1967.

[88] K. Mlungwane, I. Sigales and M. Herrman, "The wetting behaviour and reaction kinetics in diamon-silicon carbide systems," *Ceramics International*, pp. 2435-2441, 2009.

[89] S. Kumar, "Capillary infiltration studies of liquids 3D-stitched C-C preforms Part A: Internal pore characterization by solvent infiltration, mercury porosimetry, and permeability studies," *Journal of the European Ceramic Society*, pp. 2643-2650, 2009.

[90] S. Kumar, "Capillary infiltration studies of liquids 3D-stitched C-C preforms Part B: Kinetics of silicon infiltration," *Journal of the European Ceramic Society*, pp. 2651-2657, 2009.

[91] W. Krenkel, Ceramic Matrix Composites-Fiber Reinforced Ceremics and their Applications, Weinheim: WILEY-VCH Verlag GmbH & Co., 2008.

[92] G. M. Jenkins and K. Kawamura, Polymeric carbons-carbon fibre, glass and char., Cambridge: Cambridge University Press, 1976.

[93] J.Schulte-Fischedick, "The crack evolution on the atomistik scale," *Composites,* pp. 2237-2244, 2007.

[94] M. H. Hon, R. F. Davis and D. E. Newbury, "Self-Diffusion of Si-30 in Polycrystalline Beta-SiC," *J. Mater. Sci., 15,* pp. 2073-80, 1980.

[95] B. Heidenreich, M. Scheiffele and M. Tausendfreund, "C/C-SiC telescope structure for the laser communication terminal in TerraSAR-X," in *High Temperature Ceramic Matrix Composites*, Berlin, 2010, p. 505–512.

[96] C. P. A. a. R. R. Evans, "Silicon Treatment of carbon fiber-carbon composites," in *Proceedings of 4th London Conference on carbon and graphite*, London, 1974.

[97] O. Dezellus and S. Jacques, "Wetting and infiltration of carbon by liquid silicon," *JOURNAL OF MATERIALS SCIENCE,* p. 2307 – 2311, 2005.

[98] M. H. Davis and R. F. Hon, "Self-Diffusion of C-14 in Polycrystalline Beta-Sic,," *J.Mater. Sci., 14,* pp. 2411-21, 1979.

[99] N. P. Bansal and B. P. Narottam, Ceramic Matrix Composites, New Jersey: John Wiley & Sons, Inc, 2015.

[100] Ceramic Matrix Composites, Newyork: Springer, 1942.